MSc Thesis - TU Delft

STABILITY OF STONES ON MILD SLOPES UNDER WAVE ATTACK

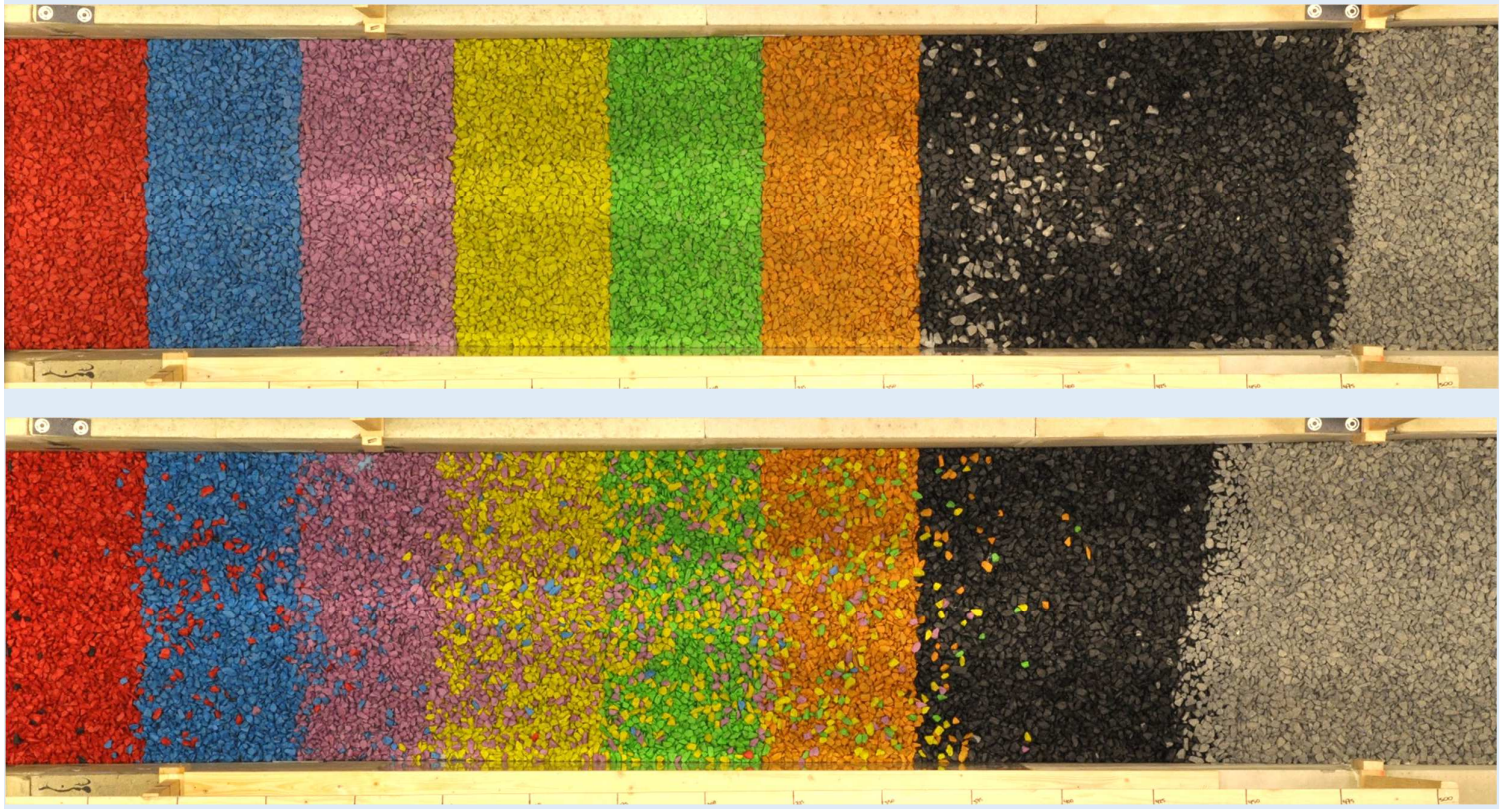

L.A. Mossinkoff

4289005

Technical University of Delft

28 August 2019

TU Delft
Faculty of Civil Engineering
Department of Hydraulic Engineering

de Vries & van de Wiel
Dredging & Environmental Solutions

Deltares
Enabling Delta Life

Graduation committee

Chair member

Dr.ir. B. Hofland
Associate Professor of Coastal Structures
Delft University of Technology

Board members

Ing. C. Kuiper
Guest lecturer of Coastal Engineering
Delft University of Technology

Dr. R.C. Lindenbergh
Associate Professor of Geoscience & Remote Sensing
Delft University of Technology

Dr. M.R.A van Gent
Head of department 'Coastal Structures & Waves'
Deltares

Ir. H.D. Jumelet
Design manager
de Vries & van de Wiel – DEME group
Dredging & Environmental Solutions

Ir. E.A.F Wendt
Tender engineer
de Vries & van de Wiel – DEME group
Dredging & Environmental Solutions

Preface

This report contains the results of the Msc Thesis “Stability of stones on mild slopes under wave attack”. This Msc Thesis is the last fulfilment for graduation of the Msc Hydraulic Engineering at the Delft University of Technology, Faculty of Civil Engineering.

This research is a continuation of the research previously done for de Vries & van de Wiel and the Delft University of Technology, executed by Marieke Wit (2015), Mark Postma (2016), Roy Kramer (2016) and Emiel Wendt (2017). Wit (2015) and Postma (2016) studied the stability of stones on mild slopes with the process-based model XBeach-G. To validate these results, Kramer (2016) carried out physical scale model tests at the TU Delft and Wendt (2017) analysed Kramer’s results in more detail. The results of these research determined the scope of this thesis.

This graduation thesis is performed with the assistance of the Delft University of Technology, the research institute Deltares and the marine contractor de Vries & van de Wiel. From the University I would like to thank my graduation committee for their support during the research and all the advice they have given. Furthermore, many thanks extended to the technicians (Jaap and Sander) of the Fluid Mechanics laboratory during the preparations of the stones. From Deltares I would like to thank Marcel van Gent for his support for this research and the model technicians for their moral support during the testing and the enjoyable lunches. My gratitude goes out to Daan Jumelet and Emiel Wendt from de Vries & van de Wiel for giving me the opportunity to do my Msc Thesis at the company and always be willing to give me advice or answer my questions. Last but not least a huge thank-you to my boyfriend Ruud and my family for always believing in me.

Lieke Mossinkoff
28 August 2019

Abstract

The static stability of stones on mild slopes under wave attack is investigated by this research. First it was checked whether there are any numerical models that could be used to describe the stability of mild slopes. As such, there is no existing model at this moment that can accurately model the stability of mild slopes. To model this correctly, the model has to be able to model plunging and spilling waves, include bed sediment transport and to model the velocity and acceleration due to a breaking wave over multiple layers in depth. The existing models do comply mostly with one of these specifications. To get accurate results, the stability should be modelled with all of the specifications and not one model complied with this. Therefore, it was decided to investigate the stability of stones on mild slopes under wave attack with physical modelling tests at the research institute Deltares.

The physical tests were executed with a constant slope angle of tan α = 1:10 and a constant nominal median stone diameter. The wave steepness (that determines the type of breaking for a constant slope angle), the significant wave height, the number of waves and the layer thickness are varied in between the tests to determine the influences of each parameter on the stability. Of each test an erosion profile is made by photogrammetry from which the profile-related damage parameters can be determined. In the bed strips with coloured stones are laid down to follow the transport of the stones.

According to these erosion profiles three damage parameters were determined. The damage level, S, as is used by Van der Meer (1988) to compare the stability of stones on mild slopes with the formula of Van der Meer (1988) for plunging waves for stones on steep slopes. The Van der Meer (1988) formula is confirmed to be conservative for mild slopes and is preferred not to be used for designing structures with mild slopes. The damage level is concluded not to be representative to describe the damage on mild slopes, because of the definition that uses the erosion area. The erosion profile of mild slopes contains multiple small erosion holes where the damage level uses one average erosion hole as is common for steep slopes. The erosion depth, d_e, is investigated for mild slopes but is not used further. This parameter gives unreliable results for the stability curve and is too sensitive to the removal of a single stone. The damage depth, E_3, is able to accurately describe the damage for mild slopes, is a lot less sensitive to the removal of a single stone and gives reliable results for the stability curve. The range of the damage depth for start of damage to failure is from 0.5 to 2.3. These values are however only applicable for a layer thickness of $2.5d_{n50}$ and a slope angle of tan α = 1:10.

The development of the damage depth is investigated for multiple parameters. The breaker type gives a change in development of the damage depth. For a wave condition with plunging breakers the damage depth development rate is higher per increasing wave height than for a wave condition that includes both plunging and spilling breakers. For the transition zone from plunging to spilling breakers the damage depth increase is very small if the wave height increases. The damage depth is influenced by the number of waves, because after about 11,000 waves the development of the damage depth is still linearly increasing with the number of waves. The damage depth was not stabilized towards a maximum value after this number of waves.

It can be concluded that the transport of the stones is mainly all below the still water level. This also followed from the damage zones. These indicated that the total area of the damage is mostly in between the SWL and $2H_s$ below the SWL. The maximum area location is around $0.8H_s$ below the SWL. The transport is mostly upslope, which is attributed to the mechanism whereby wave forces are strong in upslope direction and where the wave energy is already dissipated before the wave forces go in downslope direction. The location where the most stones are picked up depend on the breaker type, the wave height and the layer thickness. Plunging breakers cause damage more downslope than spilling breakers. Plunging breakers cause more local damage and have a much smaller runup than the

spilling breakers. Per increasing wave height, the location of damage is shifted more downslope due to the increase in breaker depth. The distances that the stones are transported are equal for different breaker types. For an increasing wave height, the transportation distance increased.

Table of Contents

1 Introduction

In this chapter the research is introduced by first giving some background information on the problem in Paragraph 1.1. Following, the problem on which the research is focused is described in detail in the problem description in Paragraph 1.2. In Paragraph 1.3 the research objectives are written down. At last in Paragraph 1.4 the report outline is described.

1.1 Background information

In the past, marine contractors have built many rock protections varying from breakwaters, steep foreshores, pipeline landings to sandy foreshores. For the design of these rock protections the Van der Meer (1988) formula was often prescribed to be used for the determination of the stone diameter. This was also the case for a project executed by de Vries & van de Wiel, a Dutch marine contractor, in the Eastern Scheldt in 2005. They had to install a rock protection on a mild sloped and sandy foreshore. The contract implicitly stated that the Van der Meer (1988) formula had to be used to design a statically stable foreshore for which minor damage was allowed to occur. The designed rock protection for the mild slope was overestimated, because the Van der Meer (1988) formula is validated for steep slopes ($\tan \alpha < 1:6$) only. This resulted in a too expensive design for the rock protection on the foreshore. Due to the non-economic results, de Vries & van de Wiel has started a research path that results in a design method for a statically stable design of stones on mild slopes under wave attack.

For the development of this design method, research have been executed commissioned and supervised by de Vries & van de Wiel to eventually answer the question “How to describe the static stability of stones on mild slopes under wave attack?”. Wit (2015) started the research path by studying the potential of the tool XBeach-G to describe the stability of stones on mild slopes under wave attack. Her research was focused on homogeneous structures. Postma (2016) further elaborated the use of the process-based numerical model XBeach-G by studying the morpho- and hydrodynamics implemented in the tool. In addition to the research of Wit (2015) he studied the modelling potential of XBeach-G for inhomogeneous structures. To validate the results of Wit (2015) and Postma (2016), Kramer (2016) carried out physical model tests on scale to check the stability of stones on mild slopes under wave attack. He performed tests to couple the damage to the irregular wave heights for different slopes. He also executed tests to receive the velocity and acceleration from regular waves near the bed at breaking location for different slopes. The results of these tests are partly elaborated by Kramer (2016) and further elaborated by Wendt (2017). This resulted in a stability parameter to describe the start of motion of the stones on mild slopes. This stability parameter is determined from the local near-bed velocities and accelerations for the start of movement of the stones for the 1:5 slope with regular waves. Wendt (2017) also performed further research on the tool XBeach-G with the conclusion that the output of XBeach-G is incorrect. These results differed from the results obtained from the physical scale model tests done by Kramer (2016), because XBeach-G uses one depth-averaged layer to solve the flow. To get the correct damage the local near-bed flow characteristics have to be used. In this research more physical scale model tests are done to get more data for the stability of stones on mild slopes and to provide in a stability relation.

1.2 Problem description

The static stability of stones on steep slopes under wave attack can be described by the Van der Meer (1988) formulas for plunging and surging waves. These formulas are validated for slopes up to 1:2 for homogeneous structures and up to 1:6 for inhomogeneous structures. The surging formula is only valid for slopes steeper than 1:4, because surging does not occur for milder slopes. To calculate the stability of stones on mild slopes under wave attack the Van der Meer (1988) formula for plunging breakers has been used. The plunging formula appears to be conservative for mild slopes. Schiereck and Fontijn (1996) did physical tests with slopes of 1:10 and 1:25. Following their test results, the stability of stones

on mild slopes appears to be higher than on steep slopes due to the change in breaker type from plunging to spilling.

To describe the stability of stones on mild slopes the process-based numerical model XBeach-G is tested. XBeach-G models the profile response of gravel beaches to storm conditions. This model is tested by Wit (2015), Postma (2016) and Wendt (2017). The results of Wit (2015) are shown against the (extrapolated) Van der Meer (1988) formula in Figure 1.1. The results from the numerical tests for homogeneous structures done in XBeach-G (red stars) are above the extrapolated formula of Van der Meer (1988) (the blue striped line). It can also be concluded from the graph that the Van der Meer (1988) formula cannot be extrapolated in a good way, because the only executed physical tests (black stars) are in area 3. For the mild slopes Wit (2015) performed numerically tests in area 1 and the left side of area 2 (up to an Iribarren number of 1.0). These tests show a clear trend that the stability increases if the Iribarren number decreases and that the Van der Meer (1988) formula is conservative for mild slopes for homogeneous structures.

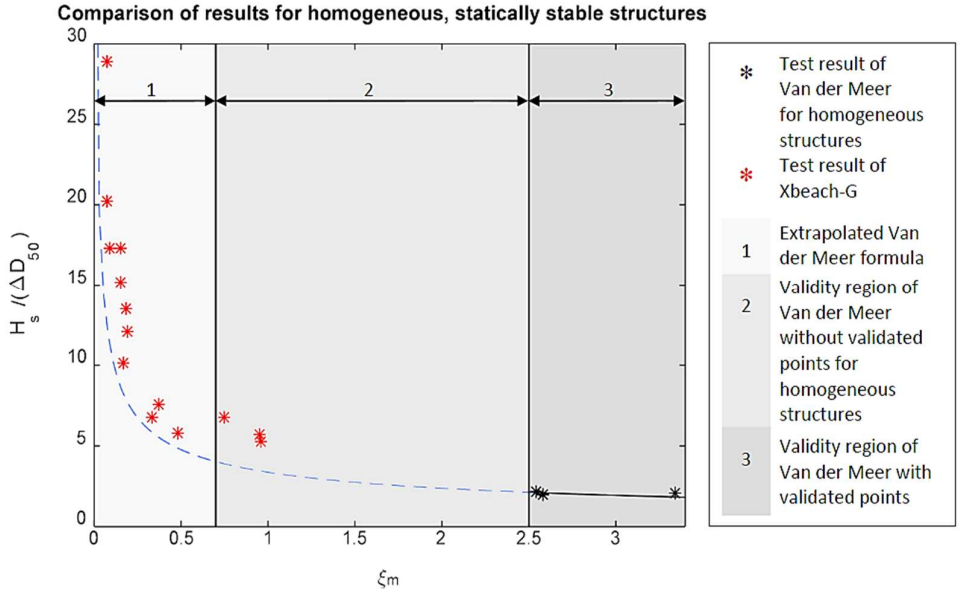

Figure 1.1: XBeach-G results against the van der Meer formula [1988] for plunging breakers (homogeneous structures) (Wit, 2015).

Postma (2016) studied the underlying physics implemented in XBeach-G to model gravel beaches. The model includes two modified bed load transport formulas: Nielsen (2006) and Van Rijn (2007). Postma concluded that the hydrodynamics and the groundwater exchange are correctly implemented in the model. The morphodynamics are implemented by one of the two bedload transport formulas. Both formulas give different results. According to Postma the Nielsen (2006) formula should be applied for slopes milder than 1:6 to describe the stability of stones on mild slopes under wave attack.

Kramer (2016) executed physical model tests to investigate the stability of the stones on mild slopes. The conclusion of Kramer (2016) was that the bed load transport formula of Van Rijn (2007) performs better to describe the stability of stones on mild slopes. This conclusion contradicts to the conclusion made by Postma (2016) that Nielsen (2006) is more accurate.

Wendt (2017) compared the results of Kramer (2016) to the model XBeach-G and came to the conclusion that XBeach-G cannot model the bed load transport accurately for mild slopes. The model is a single-layered, depth-averaged model that caused the local velocity and acceleration near the bed to be too high.

In Figure 1.2 the above mentioned physical and numerical tests results are put together in one graph. The Van Rijn (2007) tests in XBeach-G are more conservative than the conservative extrapolated formula of Van der Meer (1988). The physical tests done by Schiereck and Fontijn (1996) and Kramer (2016) are for the lower Iribarren numbers above the extrapolated formula of Van der Meer (1988) and above the Van der Meer (1988) formula with a slope correction by Wit (2015). The Van der Meer (1988) formula can be concluded to be conservative for mild slopes if compared to the physical tests. To obtain a correct stability formula more physical tests need to be executed to gather more data and determine a correct stability relation.

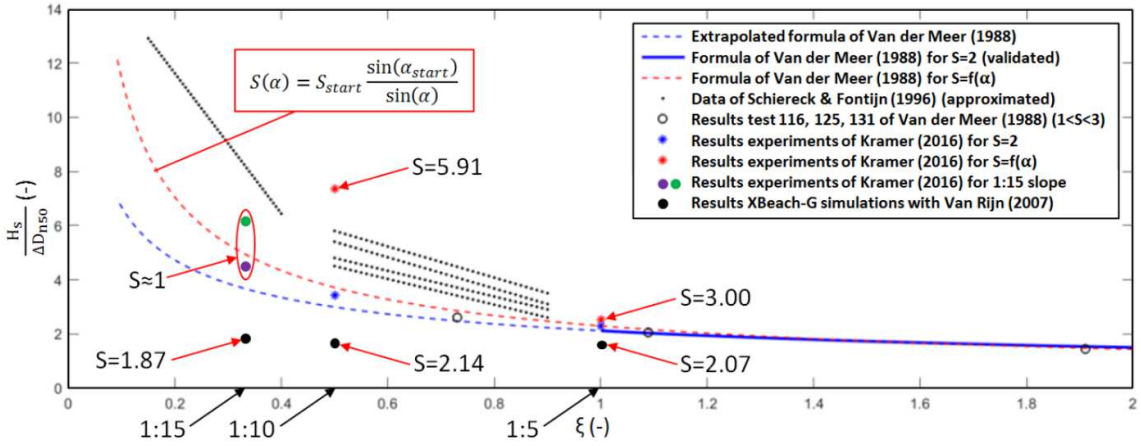

Figure 1.2: The results of the physical tests done by Van der Meer (1988), Schiereck and Fontijn (1996) (black dotted lines) and Kramer (2016). Together with the numerical results of the XBeach-G tests with the Van Rijn (2007) formula by Kramer (2016) .

1.3 Research objective

The research objective follows from the problem description in Paragraph 1.2. In the problem description is stated that there still is no satisfactory design method for the static stability of stones on mild slopes under wave attack. In earlier research is concluded that the design method currently available does not give satisfactory results or is not validated for multiple situations. It is observed that the stability increases for milder slopes. Physical tests are necessary to quantify these observations and to be able to develop a design method for mild slopes. In the physical tests in this research the influence of the different types of wave breaking in combination with increasing wave heights are tested for one mild slope. From these tests a relation follows between the stability, the wave height and the type of wave breaking. This relation is valid for the one slope tested. The research objective is equal to the research objective from the research done before by Kramer (2016) and Wendt (2017), which is to develop a design method for the static stability of stones on mild slopes under wave attack.

The research questions that follow from the above stated objective are elaborated in Paragraph 1.3.1. The research method to answer these questions is explained at the end of this chapter in Paragraph 1.3.2.

1.3.1 Research questions

To reach the objective the main research question is stated as follows:

How to describe the static stability of stones on mild slopes under wave attack?

To be able to answer the main research question, several subquestions are formed.

1. Which damage output parameter fits the static stability description of mild slopes the most?
2. What is the difference in stability for the different types of breaking of the waves?
3. What is the relation between the significant wave height and the stability?
4. How does the stability of the stones on the slope develop with an increasing number of waves?
5. How is the stability of the stones influenced by a different layer thickness of the structure?
6. What is the difference in movement of the stones for the different types of breaking of the waves?
7. How does the stability curve of the physical tests of this research compares to the stability curves of Van der Meer (1988)?

1.3.2 Research method

The main and sub research questions are answered by executing physical tests. These physical tests have a constant slope angle and the wave height, type of wave breaking, the number of waves and the layer thickness vary. From the results of these tests questions 2 to 7 can be answered directly. Question 7 can be answered by comparing the results of the tests to the stability curves of Van der Meer (1988). The first question is answered by determining the different damage parameters from the slope profiles and checking the parameter that fits the static stability description for mild slopes the best.

1.4 Report outline

The report starts with an introduction to the problem and research objectives in Chapter 1. Chapter 2 provides the existing models available to determine the stability of the stones. Chapter 3 focuses on the forces exerted on the stones and the parameters that determine these forces The model set-up to execute physical tests needed for gathering data to determine a new designing method for mild slopes is given in Chapter 4. The results, derived from the gathered data, are shown in Chapter 5. Chapter 6 states conclusions and recommendations based on the results provided in Chapter 5.

2 Literature review of the existing methods to determine the stability

In the past century the stability of stones is researched thoroughly. The research started by physical tests and empirical formulae. These physical tests all had their limitations and the empirically determined stability formulae are only applicable within these limitations. These formulae and their applicability are discussed in Paragraph 2.1. During the rise of the possibilities of numerical modelling several numerical models are developed to model the nearshore processes. At this moment several numerical models can be used to model (a part of) the nearshore processes that are related to the stability of stones. In Paragraph 2.1.10 the numerical models available are presented and their possibilities are discussed for the scope of this research. At the end of each paragraph is concluded if the existing empirical stability formulae or numerical models are able to be used for the scope of this research.

2.1 Statically stability research

To describe the stability of a bed there are a variaty of methods most of whom are still under development. In the past century, research has been done to the stability of stones for a horizontal bed. Izbash (1935) uses the critical uniform velocity acting on a single stone, Shields (1936) the critical friction force caused by the uniform flowing water on the bed and Sleath (1978) the bed shear stress related to oscillating flow (due to non-breaking waves). These stability relations are not applicable to the breaking wave situations on a mild sloping bed in the scope of this research but will be elaborated shortly to show the important developments in the stability research. Iribarren (1938) developed a stability formula for breaking waves, which was generalized by Hudson (1959). In 1988 Van der Meer executed a lot of physical tests from which stability formulae were developed for breaking waves on steep slopes up to tan α < 1:6. Schiereck and Fontijn (1996) did tests on mild slopes and concluded that the Van der Meer (1988) formulae were not applicable for mild slopes, because the stability was higher than the formulae predicted. This conclusion was confirmed by Wit (2015) and Kramer (2016) by their numerical and physical tests. They both concluded that the stability increases for milder slopes.

2.1.1 Izbash

Izbash (1935) stated that there is no stability on a horizontal bed if the forces on the stones aren't in equilibrium. The critical velocity gives the limits of the equilibrium of forces on a stone. The forces on the stone are the flow velocity and its own (submerged) weight. If the critical velocity is exceeded by the flow, the stone starts to move. The stability formula of Izbash is determined for the forces on a single stone and given in Equation 2.1 in which Δ is the relative density [-], d the diameter of the stone [m], u_c the critical velocity [m/s] and g the gravitational acceleration [m/s^2]. The diameter used in the equation is undefined, which gives an uncertainty in its use. Also, the used velocity distribution over the water depth is unknown as is the location where the critical velocity is determined. This limits the formula to be only useful in non-uniform flows where the flow velocity does not depend on an equilibrium between the flow and bed friction force (Schiereck & Verhagen, Introduction to bed, bank and shore protection (2nd edition), 2016).

$$\Delta d = 0.7 \frac{u_c^2}{2g} \qquad 2.1$$

2.1.2 Shields

Shields (1936) investigated the friction force on the bed caused by uniform flowing water. This friction force is generalized and determines the stability of stones on the bed. Only the bed stability can be determined with this theory, not the stability of a single stone. The stability of the bed is described by the critical Shields parameter, ψ_{cr}, which is the critical value for the stability of the bed. If the stability parameter is exceeded, the bed starts to move. The stability parameter is a balance between the bed

shear stress (only valid if the Chèzy-equation is valid) and the particle Reynolds number. The particle Reynolds number indicates if the stone in the bed reaches within the turbulent boundary layer or lies within the viscous sublayer (Schiereck & Verhagen, Introduction to bed, bank and shore protection (2nd edition), 2016). The stability relation is given in Equation 2.2 in which ψ_{cr} is the critical Shields parameter [-], τ_{cr} is the critical bed shear stress [N/m2], u_{*c} is the critical bed shear velocity [m/s] and $Re_*$is the particle Reynolds number [-].

$$\psi_{cr} = \frac{load}{strength} = \frac{\tau_{cr}}{(\rho_s - \rho_w)gd} = \frac{u_{*c}^2}{\Delta g d} = f(Re_*) = f\left(\frac{u_{*c} d}{\nu}\right) \qquad 2.2$$

The critical Shields parameter is displayed in Figure 2.1 where the Shields parameter is set out against the particle Reynolds number. For particle Reynolds numbers higher than 400, the critical Shields parameter becomes constant and equal to 0.055. If the critical Shields parameter is exceeded the bed starts to move and stones are transported.

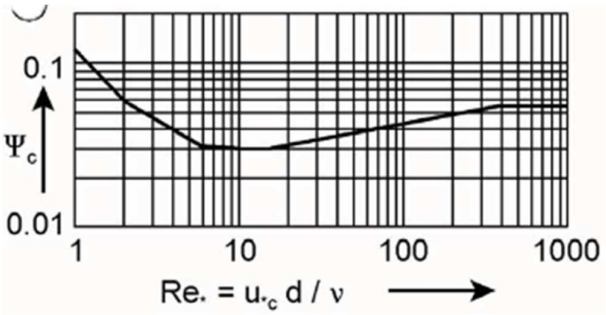

Figure 2.1: The critical shear stress versus the particle Reynolds number (Shields, 1936).

2.1.3 Sleath

Sleath (1978) found the same type of relation as Shields (1936) with the dimensionless shear stress and the dimensionless grain diameter, d_*, by doing tests in oscillatory flow (non-breaking waves) to investigate the movement of the stones. Next to the tests, he analysed tests done by others (e.g. Rance & Warren, 1968) and modified the Shields curve to be applicable on situations with oscillating flow. Both curves, the original and the modified curve, are shown in Figure 2.2. They are made comparable by the dimensionless grain diameter.

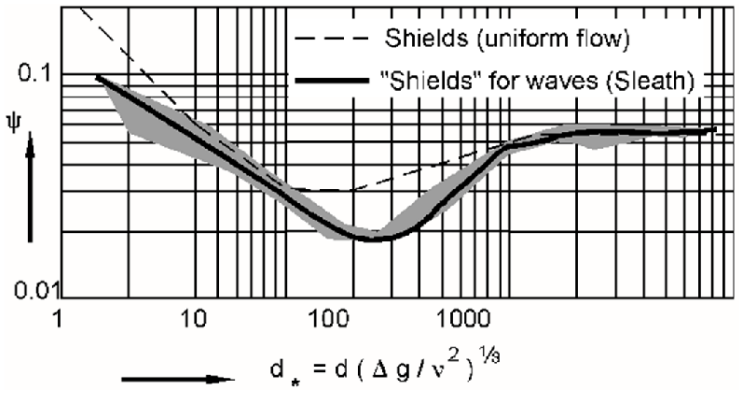

Figure 2.2: The modified Shields-curve by Sleath (1978) and the original Shields-curve (Schiereck & Verhagen, 2016).

The critical shear stress was for large grain diameters found to be also equal to 0.055 for oscillating flow regimes. It is doubtful that the same amount of transport of the stones is to be expected in uniform flow and oscillating flow. Stones in oscillating flow should be more stable due to the changing flow regimes. This means that ψ_{cr} for oscillating flow is probably assumed too low compared to the

threshold for steady flow. The accelerations in the oscillatory flow could also change the threshold, because from accelerating steady flows could be concluded that the critical Shields parameter increases if the bed shear stress increases (Schiereck & Verhagen, Introduction to bed, bank and shore protection (2nd edition), 2016).

2.1.4 Iribarren

Iribarren (1938) has developed a stability formula for stones on breakwaters under the influence of breaking waves. For the effect of the stones lying on a sloped bed Iribarren added a slope correction factor to the stability formula of Shields (1936). The effect of breaking waves on a slope is added by assuming that the velocity is proportional to the celerity in shallow water. The wave height being a representative measure for the water depth: $u \propto \sqrt{gH}$. These correction factors give the stability relation given in Equation 2.3.

$$\underbrace{\rho_w g H d^2}_{load} \propto \underbrace{(\rho_s - \rho_w) g d^2}_{strength} \cdot \underbrace{(\tan\phi \cos\alpha \pm \sin\alpha)}_{slope\ correction\ factor} \qquad 2.3$$

This relation can be rewritten to Equation 2.4 by raising all the terms to the third power and using the following relation: $M \propto \rho_s D_{50}^3$.

$$M \propto \frac{\rho_s H^3}{\Delta^3 (\tan\phi \cos\alpha \pm \sin\alpha)^3} \qquad 2.4$$

2.1.5 Hudson

Hudson (1959) has developed a simplified more general relation for the stability by doing a lot of tests that uses a 'dustbin'-factor, K_D, to include accepted degrees of damage and a simplified slope correction factor compared to the Iribarren (1938) formula. K_D depends on the type of used element. This leads to the relation given in Equation 2.5.

$$M = \frac{\rho_s H_s^3}{K_D \Delta^3 \cot\alpha} \qquad 2.5$$

The Hudson (1959) stability relation has its limitations. The relation can only be used for slopes ranging from $1.5 < \cot\alpha < 4$.

The Iribarren (1938) and Hudson (1959) stability relations both lack by not taking into account several parameters. These are the wave period, the permeability, the number of waves and an unclear definition of the damage.

2.1.6 Van der Meer

Van der Meer (1988) has done physical tests to investigate the stability of stones on steep slopes under breaking waves. The small and large scale tests have been done with irregular waves for slopes ranging from $1.5 < \cot\alpha < 6$. During testing far more parameters have been tested for their influence on stability than Hudson (1959) did. Through these test results tests a curve is fitted, which led to the two equations of Van der Meer (1988), one for plunging and one for surging breakers, shown in Equation 2.6.

$$\frac{H_s}{\Delta d_{n50}} = 6.2\, P^{0.18} \left(\frac{S}{\sqrt{N}}\right)^{0.2} \xi^{-0.5} \qquad \text{(plunging breakers)}$$

$$\frac{H_s}{\Delta d_{n50}} = 1.0\, P^{-0.13} \left(\frac{S}{\sqrt{N}}\right)^{0.2} \xi^{P} \sqrt{\cot\alpha} \qquad \text{(surging breakers)} \qquad 2.6$$

In which: P is the permeability of the structure [-], S the damage level [-], N the number of waves [-], α the slope angle [°], ξ the breaker parameter [-] and $H_s/\Delta d_{n50}$ is the dimensionless stability parameter or Hudson stability parameter [-]. The damage level is explained further in Paragraph 3.4.1 and the breaker parameter in Paragraph 3.2.3.

The Van der Meer (1988) formula is only tested for slopes steeper than 1:6. The formula is extrapolated towards milder slopes by the slope factor in the breaker parameter.

2.1.7 Schiereck & Fontijn

Schiereck & Fontijn (1996) compared the Van der Meer (1988) results with the results of experiments on the stability of stones on mild slopes. These experiments were done by Sistermans (1993) and Ye (1996) on a 1:10 and 1:25 slope with a statically stable structure. In Figure 2.3 the results of the experiments are compared with the Van der Meer (1988) extrapolated formula for plunging breakers. The experiments show that the extrapolated formula of Van der Meer (1988) is conservative for mild slopes, because the results of the experiments (the black dotted lines) lie all above the curve of Van der Meer (1988). The damage was determined by counting the coloured stones from coloured strips of stones in the bed. With this method stones can be traced from their original location during transport to where they end up. This damage measurement is compared to the results of Van der Meer (1988) by assuming that a transportation amount of 0.5 % is equal to a damage level of S = 2 that indicates start of motion.

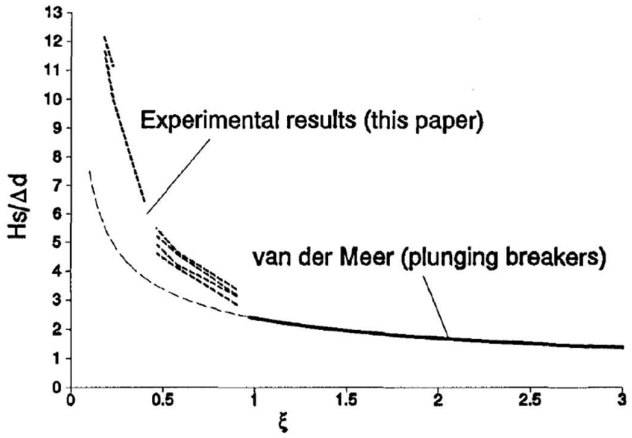

Figure 2.3: The results of physical test by Sistermans (1993) and Ye (1996) compared to the Van der Meer (1988) (extrapolated) formula for plunging breakers.

2.1.8 Wit

Wit (2015) performed tests in the numerical model XBeach-G to investigate the stability of stones on mild slopes. From the tests could be concluded that the stability for mild slopes was higher than the extrapolated formula of Van der Meer (1988) predicted. In Figure 2.4 the results of the numerical tests are compared to the experimental tests of Van der Meer (1988) and the extrapolated formula.

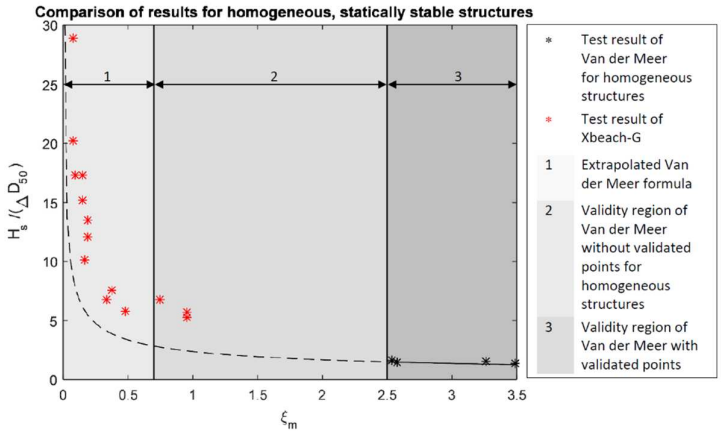

Figure 2.4: The results of the tests done by Wit (2015) compared to the formula of Van der Meer (1988).

All the numerical points lie above the line of the extrapolated formula. While Postma (2016) states that XBeach-G is not able to accurately model the stability of stones on mild slopes due to the fact that amongst other things the morphology is not updated by the hydrodynamics, the results of Wit (2015) give a general confirmation to the overestimation of the extrapolated formula of Van der Meer (1988).

2.1.9 Kramer

Kramer (2016) performed physical tests to research the stability of stones on mild slopes. The tests where done for three slopes (1:5, 1:10 and 1:15) and two wave heights per slope. The results are given in Figure 2.5. The results indicate that the conclusion of Schiereck & Fontijn (1996) and Wit (2015) that the extrapolated formula of Van der Meer (1988) is conservative is correct. The tests done by Kramer (2016) are too few to give a modification to the Van der Meer (1988) formula or give a new stability relation. The results of the tests of Kramer (2016) for the 1:15 slope were unreliable, but they indicate that the stability for lower Iribarren numbers is different than the Van der Meer (1988) formula for plunging predicts.

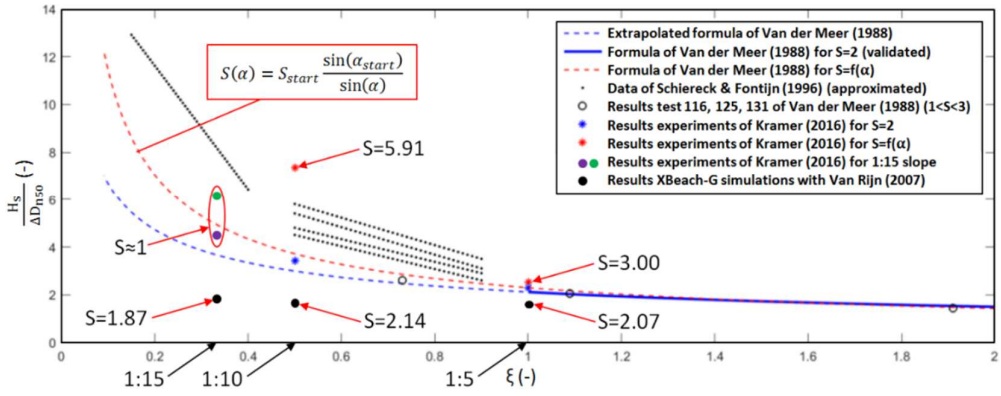

Figure 2.5: Results of tests done by Van der Meer (1988), Schiereck & Fontijn (1996) and Kramer (2016).

2.1.10 Conclusion statically stability research

All the above discussed stability formulae have certain limitations. For the scope of this research, the stability of stones on mild slopes under wave attack, none of the formulae give a correct answer to the stability question.

- Izbash (1935) does not include an equilibrium between the flow and the bed friction force.
- Shields (1936) only determines the stability of the bed and not the stability of a single stone.
- Sleath (1978) include oscillatory flow for non-breaking waves but only for the stability of the bed.
- Iribarren (1938) developed a stability formula for stones on breakwaters under breaking waves. The formulae can only be used for slopes steeper than cot $\alpha < 4$.
- Hudson (1959) simplified this formula and added a correction factor that depends on the element used. The formulae can only be used for slopes steeper than cot $\alpha < 4$.
- Van der Meer (1988) developed a formula for the stability of slopes under breaking waves that includes a lot of parameters. This formula is only applicable to slopes steeper than cot $\alpha < 6$ and not to mild slopes. By later research of Schiereck and Fontijn (1996), Wit (2015) and Kramer (2016) is concluded that the Van der Meer (1988) formula should not be used for designing a mild slope.
- Schiereck and Fontijn (1996) determined the damage of the bed by counting displaced stones. This method is inaccurate to compare to the exact damage parameters like the damage level. These results cannot directly be used to determine an accurate design formula.
- Wit (2015) did tests in the numerical model XBeach-G. From later research by Wendt (2017) follows that XBeach-G overestimates the damage, because the model uses a depth-averaged flow velocity and acceleration.
- Kramer (2016) performed only two tests per slope angle and this is not enough data to develop a new design formula for the stability of mild slopes. Next to this, his results were unreliable.

2.2 Numerical modelling

The stability of stones on mild slopes under wave attack can be modelled by numerical models. For the models to be able to model this correctly, they have to comply with several specifications:

- The waves have to be modelled for storm events with irregular waves, because these are the normative situations for failure of the structure.
- Wave breaking has to be implemented to model the local forces on the stones. The types of wave breaking needed to model are plunging and spilling breakers.
- The flow has to be modelled for multiple layers over the depth to get correct velocities and accelerations near the bed due to the wave breaking.
- Sediment transport has to be modelled correctly to be able to model the stability of the stones correctly and the morphology has to be updated by the hydrodynamics.

There are various types of models to numerically model waves approaching a shoreline. There are conceptual, empirical, parametric and process-based models. Conceptual models only qualitatively describe the process and the situation. Empirical and parametric models are calibrated with existing data. They have no or limited physical basis in their formulas. Process-based models are based on the underlying physics. This is the type of model that is preferred for this research.

Process-based models can be distinguished in wave resolving and wave-averaged models. Wave resolving models model each wave and the response of the model to each wave. They are developed for situations with man-made structures that may not deform. Wave-averaged models average a certain number of waves and then calculate the response of the model. They are based on already existing formulae for sandy beaches (Postma, 2016).

Ten models were examined for their ability to model the stability of the stones. None of the models complied with all the specifications and therefore none could be used for the purpose of the research. Seven of the models were depth-averaged, that are XBeach-G, COBRAS, Coulwave, BeachWin, CSHORE, Shingle-B and CROSMOR-2008. This means that they always overestimate the forces on the stones and give too large profile changes. From the remaining models did SWASH and IH-2VOF not include sediment transport or plunging breakers and OpenFOAM, the most promising model, is too time consuming at this time to model a plunging breaker and can only model an immobile bed. Therefore, it is concluded that no currently available numerical model is able to correctly model the stability of stones on mild slopes under wave attack. The models have to be improved to make them comply with the specifications given above. An elaboration on all the models is given in Appendix A.

3 Literature review of the stone stability parameters

The stability of stones under wave attack can, next to empirical stability formulae, also be expressed with the physical forces that initiate the motion of a stone. These forces are discussed in Paragraph 3.1 together with their influence on the stability of a stone. The momentum balance between these forces determines whether a stone starts to move. The forces on a stone are determined by the hydraulic and structural parameters. The hydraulic parameters are discussed in Paragraph 3.2 and the stone parameters in Paragraph 3.3 together with their (theoretical) influence on the stability of a stone. The hydraulic parameters include the wave parameters, the storm duration and the breaker parameter. The structural parameters include the stone parameters and the notional permeability.

3.1 Forces on a single stone

The initiation of motion of a stone is influenced by different forces. The active forces cause the stone to move and the passive forces keep the stone from moving. The active forces consist of the drag, lift and shear force. The passive forces consist of the gravity and the friction force. Next to these forces, also the position and the orientation of the stones do play a role for the stability, but their effects are kept out of this research (Hofland, 2005).

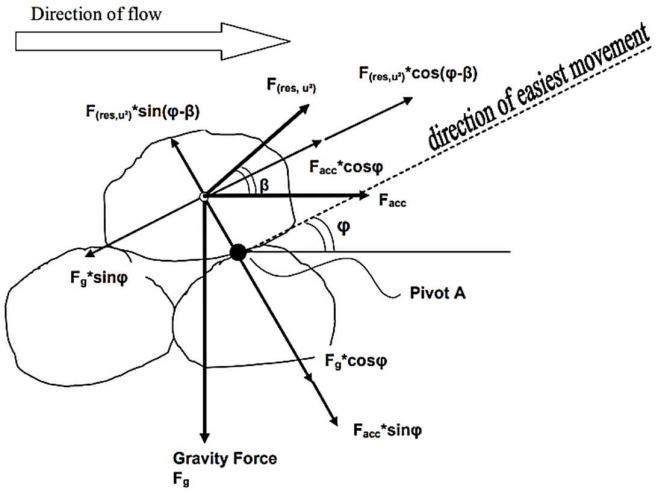

Figure 3.1: Forces acting on a stone in flowing water (Tromp, 2004).

The forces on a stone are explained below and shown in Figure 3.1 with the direction in which they act on the stone. The active forces are elaborated first and after this the passive forces are explained. At the end, the momentum of the stone caused by the forces that induces the initiation of motion is discussed.

The active forces exist of the drag, lift and shear force. The drag force, F_D, is caused by protrusion of the stone into the flow. The protrusion causes pressure differences over the stone and viscous skin forces. It acts in the direction of the current. The lift force is caused by the curvature of the flow lines around the upper side of the stone. The curvature causes a pressure difference over the stone, which causes a force perpendicular to the current direction and in upward direction. The shear force is caused by the current that moves along the stone. The force is implicitly included in the drag force, because it is proportional to u_b^2 and in the direction of the current, as is the drag force (Van den Bos, 2006).

All three forces can be expressed by the same formula with other coefficients or in a bulk formula in which all three forces are combined to one resultant force, see Equation 3.1. In which u_b is the flow velocity near the bed [m/s], C_B the bulk coefficient [-], ρ_w the mass density of water [kg/m^3] and A_B the exposed surface area of the stone [m^2].

$$F_B = \frac{1}{2} C_B \rho_w A_B u_b |u_b| \quad 3.1$$

The passive or resisting forces are the gravity and friction force. The gravity force is caused by the mass of the stone reduced by the uplifting force of the water. The force acts perpendicular to the current and in downward direction. The gravity force is given in Equation 3.2 in which m is the mass [kg], a is the acceleration [m/s^2], ρ_s and ρ_w are the mass densities of the stone and the water respectively [kg/m^3], g is the gravitational acceleration [m/s^2] and V is the volume of the stone [m^3].

$$F_G = ma = (\rho_s - \rho_w) g V \quad 3.2$$

The friction force is caused by the stones itself. The stones interlock with each other and therefore cause friction if a stone wants to move. The friction force is given in Equation 3.3 in which the parameters stand for the same as in Equation 3.2, except for C_F, which is the friction coefficient [-].

$$F_F = C_F (\rho_s - \rho_w) g V \quad 3.3$$

Previous explained forces are for the case of stationary flow. For the scope of this research, which includes wave attack, it is necessary to take this into account in the forces. Tromp (2004) has researched the effect of wave attack on the forces inducing the initiation of motion. The waves cause an extra force being the acceleration force, A_{acc}. The acceleration force is caused by the waves due to horizontal pressure differences creating a pressure gradient. The force is given in Equation 3.4 in which $\frac{\partial u}{\partial t}$ is the horizontal acceleration [m/s^2] and C_M is the acceleration coefficient [-].

$$F_{acc} = C_M \rho \frac{\delta u}{\delta t} V = C_M \rho a V \quad 3.4$$

Initiation of motion occurs for the moment where the momentum of the stone around point A, the contact point with the next stone (see Figure 3.1), is larger than zero. This means that the momentum induced by the active forces is larger than the momentum induced by the passive forces. The stone starts to move in the direction of the easiest movement (given by cos φ). This direction gives the least friction with its neighbouring stones. The direction of easiest movement isn't equal to the direction of the bulk force, so a direction factor has to be added. This result in the momentum equation in Equation 3.5. In which: φ is the angle between the slope angle and the angle of the easiest movement [°] and β is the angle between the acceleration force and the resulting bulk force [°]. The stone will start to move if the left-hand side with active forces is larger than the right-hand side with passive forces.

$$F_B \cos(\varphi - \beta) + F_{acc} \cos \varphi < F_G \sin \varphi \quad 3.5$$

A stone has to withstand these forces during the up- and downrush of the waves. Sistermans (1993) concluded for his research that the forces on the stone are different for these two situations, see Figure 3.2. The uprush is the most critical for gentle slopes, see Figure 3.3.

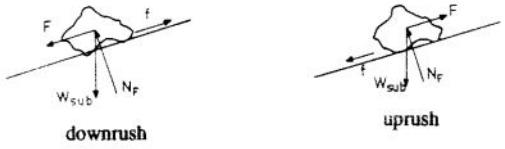

Figure 3.2: Forces on a stone during up and down rush (Sistermans, 1993).

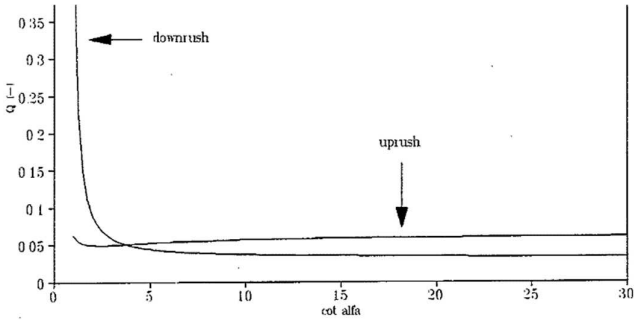

Figure 3.3: Uprush versus down rush for different slope angles. (Sistermans, 1993).

3.2 Hydraulic parameters

The hydraulic parameters influence the stability of the stones, because they determine the active forces on the stones. The hydraulic parameters include the wave parameters (wave spectrum, period and height), the storm duration and the breaker parameter.

3.2.1 Wave parameters

The wave parameters include the wave spectrum, period and height. The spectrum is approached with the JONSWAP spectrum. This spectrum is used for storm sea states that are close to the shore, which means a limited fetch. The sea state is therefore not fully developed before it reaches the shoreline and the structures. The shape of the spectrum is given in Figure 3.4.

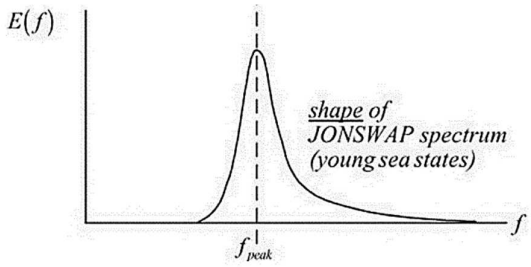

Figure 3.4: The shape of the JONSWAP spectrum (Holthuijsen, 2007).

The JONSWAP spectrum can be described by the peak period and the significant wave height. The peak period, T_p, follows from the peak in the frequency by $f_{peak} = 1/T_p$. The significant wave height, H_s, is the averaged wave height of the highest one-third of the waves, see Equation 3.6.

$$H_s = H_{\frac{1}{3}} = \frac{1}{N/3}\sum_{j=1}^{N/3} H_j \qquad 3.6$$

For shallow water and irregular waves is the maximum wave height determined by: $\frac{H_s}{h} \approx 0.4 - 0.5$ and for deep water by: $H_{max} = 0.14\,L$. The highest one percentage of the waves in deep water can be determined with the significant wave height so $H_{1\%} = 1.5H_s$.

The wave height and the wave period (or deep-water wavelength) together determine the wave steepness by Equation 3.7. The wave steepness influences the stability of the stones. A higher wave steepness increases the stability as can be concluded from model tests performed by Sistermans (1993). The influence of the wave steepness on the stability of the slope is taken into account in the breaker parameter, see Paragraph 3.2.3.

$$s_{0p} = \frac{H_s}{L_0} = \frac{2\pi H_s}{gT_p^2} \qquad 3.7$$

The wave parameters influence the bulk force and the acceleration force on a stone. The bulk force is influenced by the flow velocity near the bed induced by the (non-breaking) waves. The acceleration force is caused by the pressure difference over a stone by the breaking of the waves. Both forces are determined the wave height and the wave period. The acceleration force is mostly influenced by the wave steepness.

3.2.2 Storm duration

The storm duration is determined by the number of waves times the mean wave period. The number of waves influences the damage level until the damage becomes stable after about 15,000 waves. This was tested by Thompson and Shuttler (1975) with long duration tests with up to 15,000 waves for steep slopes up to tan α = 1:6. The results are displayed in Figure 3.5. Before the stabilization of the damage the relation between the damage level and the number of waves appears to be approachable with $S \sim \sqrt{N}$.

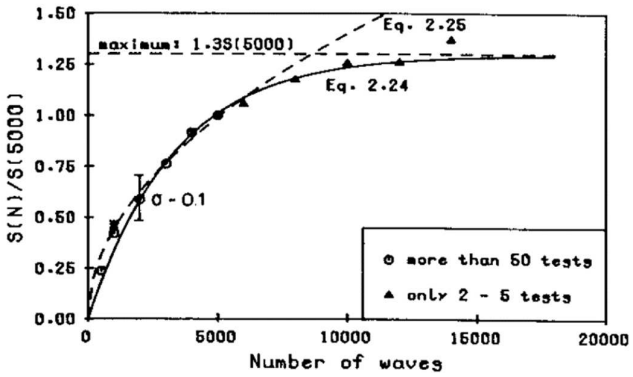

Figure 3.5: The test results of Thompson and Shuttler (1975) of their long duration tests for the stability of a slope.

3.2.3 Breaker parameter

Iribarren (1938) introduced the breaker parameter for processes like wave run-up on structures (also known as dimensionless Iribarren number or surf similarity parameter), ξ, being defined in Equation 3.8. The breaker parameter is defined as the ratio between the slope angle and the wave steepness (with local wave height and deep-water wavelength). The wave height is the significant wave height and the period used by Battjes (1974) for the wavelength is the mean period. The mean period relates to the peak period by $T_p = 1.25T_m$ (Schiereck & Verhagen, Introduction to bed, bank and shore protection (2nd edition), 2016). This means that $\xi_p = 1.25\xi_m$.

$$\xi = \frac{\tan \alpha}{\sqrt{H_s/L_0}} \qquad 3.8$$

The Iribarren number characterizes ranges for the different types of breaking waves on a slope. The existing types are surging, collapsing, plunging and spilling waves. For milder slopes two types of wave breaking are present being the plunging and spilling waves, see Figure 3.6.

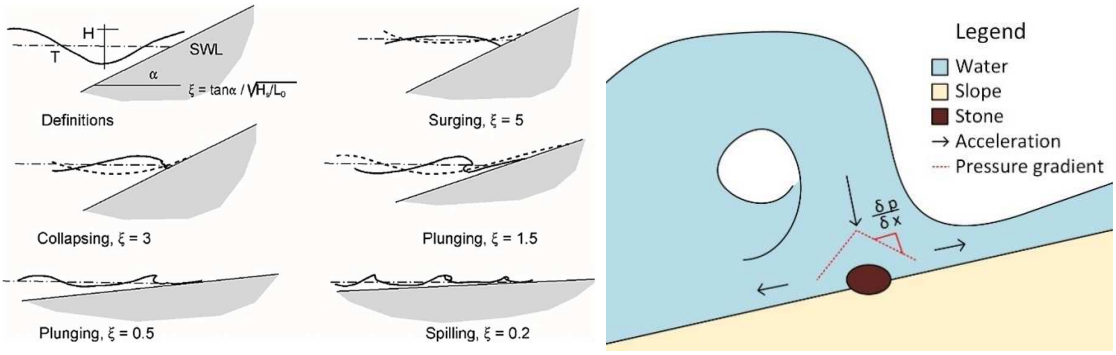

Figure 3.6: Left: The types of breaking with their Iribarren number (Schiereck & Verhagen, 2016). Right: The plunging breaker exerting its force on a stone. Resulting in a pressure difference and accelerations of the flow.

The plunging breaker occurs if ξ_p is in between 0.3 and 1.6. A plunging breaker is very asymmetric and the overturning part of the wave reaches the underlying small water layer with a jet-like force, see Figure 3.6. A lot of energy dissipates into turbulence and a small part progresses into shallower water. A lot of the wave energy is dissipated in the region between the breaking point and the still water level. The concentration of the energy is mostly focussed around the breaker point, so the stability of the stones is more endangered in this area. The run-up of the wave is low, because most energy is already dissipated due to the breaking of the wave. Plunging breakers occur for steeper slopes than the spilling breakers.

The spilling breaker occurs mostly on very flat beaches for $\xi_p < 0.3$. The waves break farther offshore and have a small amount of reflection. The wave height increases when the waves approach the shore due to shoaling. If the wave steepness becomes too large, the waves start to break and the wave height decreases. The jet-like force is a lot smaller for spilling waves and the waves break in a larger water layer compared to the plunging waves. The crest of the spilling wave slides down the face of the wave as it breaks on shore. The energy dissipation is distributed over a long distance when the waves approach the shore. Less energy is dissipated by wave breaking and this results in a higher run-up than plunging waves and does relatively more damage to the slope.

The plunging breakers cause more local damage to a slope than the spilling breakers. This can be explained by the difference in the spreading of the dissipation of the energy on the slope, see Figure 3.7. The plunging breaker has a more centred and local energy dissipation than the spilling breaker. This is due to the jet-like force of the breaking wave. The spilling breaker energy dissipation is more spread over the slope, because the wave breaking is less turbulent and jet-like.

The breaker parameter determines the accelerations force and the pressure difference over a stone. The pressure difference is determined by the difference in energy dissipation over a slope.

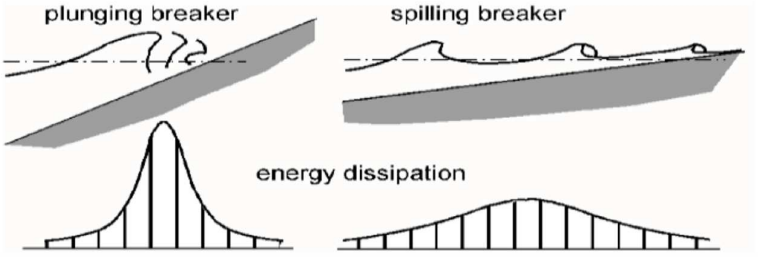

Figure 3.7: The difference in the spreading of the energy dissipation on a slope between the plunging and the spilling breaker (Schiereck & Verhagen, 2016).

3.3 Structural parameters

The structural parameters are important for the stability, because they are the passive/resisting load against the transport of the stones. The structural parameters include the stone parameters (the diameter and the density) and the notional permeability.

3.3.1 Stone parameters

The stone stability is strongly influenced by the stone diameter. For gravel stone batches the nominal median diameter, d_{n50}, is used, because all the stones will have a slightly different size and shape. The nominal diameter, d_n, is the diameter of an equivalent cube with the same weight and volume as the stone. For design purposes with a gravel stone batch the median is taken from all the nominal diameters. The nominal median diameter is determined with the median stone mass and the stone density, see Equation 3.9.

$$d_{n50} = \left(\frac{M_{50}}{\rho_s}\right)^{\frac{1}{3}} \quad 3.9$$

The median mass, M_{50}, is determined from the grading curve of the mass distribution. From the grading curve of the diameter distribution the grading is determined. The grading is given by d_{85}/d_{15}. The classification of the gradation width is given in Table 3.1.

Table 3.1: Grading width classification (CIRIA, CUR, & CETMEF, 2007).

Grading width	d_{85}/d_{15}
Narrow or single-sized gradation	Less than 1.5
Wide gradation	1.5-2.5
Very wide or *quarry run* gradation	2.5-5.0

A (very) wide gradation exists of relatively large to relatively small stones compared to the d_{50}. For a breakwater with steep slopes that needs to be dynamically stable the influence of the fines on the stability is negligible. The fines cause an increase in the water surface tension in between the stones, which results in a more cohesive steep slope (Van der Plas, Van der Meer, Ripoll Dominguez, & Bijl, 2017). For a statically stable slope the fines are transported for smaller design parameters compared to the larger stones. This has a negative effect on the static stability of the slope. For mild slopes a narrow gradation is therefore more stable.

The relative density, also known as the submerged weight, Δ, is determined with the stone and the water density, see Equation 3.10.

$$\Delta = \frac{\rho_s - \rho_w}{\rho_w} \quad 3.10$$

The structural parameters influence the gravity and the friction force. These forces are partly determined by the density of the stones and the volume. Next to these, the friction force is also determined by the grading and shape of the stones that determines how well the stones interlock with each other.

3.3.2 Notional permeability

The notional permeability, P, is introduced by Van der Meer (1988) and is a fictious parameter that describes influence of the armour layer, the filter layer and the core of the structure on the permeability, see Figure 3.8. The notional permeability is only determined for the four types of structures given in Figure 3.8 and has no further physical basis. From Figure 3.8 can be concluded that if the thickness of the layers increases, the notional permeability also increases.

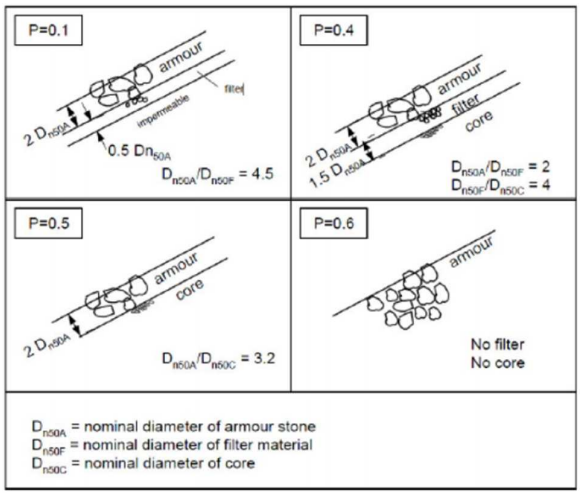

Figure 3.8: Permeability of the bed for different structure compositions (Van der Meer, 1988).

According to Van der Meer (1988) the stability of the stones increases for a more permeable core, as can be seen in Figure 3.9. These tests were done for a slope angle of tan α = 1:2. The water forces that reach the bottom of the armour layer need to be distributed. For an impermeable core the forces cannot enter the core and dissipate their energy in that direction. Instead the waves flow down in between the underlayer and the core. The run-down forces decrease the stability of the stones. For a more permeable core the forces can dissipate into the core and the run-down forces are less.

The datapoints in Figure 3.9 are all calculated points from the damage curves of the physical tests done by Van der Meer (1988). Out of all the datapoints from the physical tests an average damage curve is drawn in between the points for each different test. For fixed amounts of damage (e.g. S=3) and Iribarren numbers, the stability numbers have been calculated from the curves. These stability numbers are set out against the Iribarren numbers in a graph for a fixed damage level and slope angle. The curves in Figure 3.9 are lines drawn between the calculated points for the different core structures. The overall trend from these graphs from Van der Meer (1988) is that the impermeable cores are the least stable, the permeable cores are more stable and the homogeneous structures are the most stable.

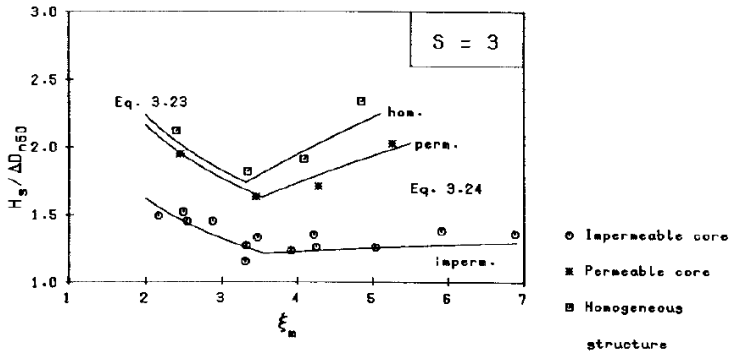

Figure 3.9: Stability of the stones versus different core types for a slope angle of tan α of 1:2 (Van der Meer, 1988).

3.4 Damage parameters

There are two types of stability, static and dynamic. In the case of static stability, there is no or very little damage allowed under design conditions. Damage is defined here as the displacement of stones. For dynamic stability, there is displacement allowed of the stones. These stones form an equilibrium profile that fits the present conditions. After the equilibrium profile is reached, the profile will not change anymore if the conditions stay constant, but there will still be movement of the stones along the profile (Koster, 1990). In this research the focus is on static stability, because the structures in the scope of this research always have to protect the underlying filter layers and therefore the stones are not allowed to move much. To describe the damage of a sloped bed several damage parameters have been developed over the years. These are described in the next paragraphs with their applicability to mild slopes.

3.4.1 Damage level

Van der Meer (1988) used the dimensionless damage level ,S, defined by Broderick and Ahrens (1982). The damage level is determined with the erosion area (defined in Figure 3.10) divided by the nominal median diameter squared, see Equation 3.11. This gives an indication of the total number of displaced stones for a width of one stone diameter.

$$S = \frac{A_e}{d_{n50}^2} \qquad 3.11$$

In which: S is the damage level parameter [-], A_e is the cross-sectional erosion area [m^2] and d_{n50} is the nominal median diameter [m]. Van der Meer (1988) defined that for steep slopes a bed is statically stable if the damage level is smaller than 2. Failure is indicated with a damage level around 10. For mild slopes the damage level values are allowed to be higher according to the conclusions of Schiereck and Fontijn (1996), Wit (2015) and Kramer (2016).

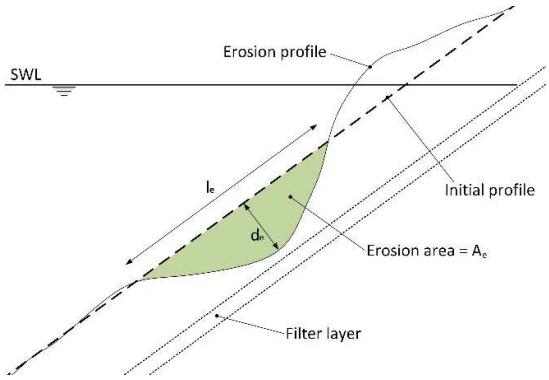

Figure 3.10: The definition of the erosion area (Schiereck & Verhagen, 2016). With A_e is the erosion area [m2], d_e the erosion depth [m] and l_e the erosion length [m].

The damage level gives no information about the shape of the erosion hole. This could differ between a very shallow and wide erosion hole or a deep and small erosion hole. Therefore, the damage level can vary widely before the filter layer is exposed. The damage level can be a very high value and because the erosion hole is shallow the filter layer can still be protected. But the damage level can also be relatively low, but because the erosion hole is very deep the filter layer can be exposed already. For this reason, the damage level is not very useful to determine if the filter layer is protected.

3.4.2 Erosion depth

The simplest measurable damage parameter is the erosion depth, d_e, which is the difference between the initial profile and the eroded profile, see Figure 3.10. This damage parameter is only useful if the stone diameter and the layer thickness are known.

3.4.3 Damage depth

For gravel there is developed another damage parameter by Melby and Kobayashi (1998) being the dimensionless damage depth, E_m. The damage depth is the erosion depth averaged over a circle with a diameter of multiple times the d_{n50} divided by the d_{n50}, see Equation 3.12. In which: $E_{3D,m}$ is the dimensionless damage depth averaged over a circle of m stone diameters [-], d_e the erosion depth (the difference between the initial profile and the eroded profile) [m], d_{n50} the nominal median diameter [m], z_0 the initial profile height [m], z the eroded profile height [m] and α the slope angle [-].

$$E_{3D,m} = \frac{\langle d_e \rangle_{md_{n50}}}{d_{n50}} = \frac{\langle z - z_0 \rangle_{md_{n50}} \cos \alpha}{d_{n50}} \qquad 3.12$$

Hofland et al. (2011) executed a few tests for steep slopes to investigate the damage depth values for the initial damage, intermediate damage and failure. These tests gave the results for the damage depth with d_e averaged over a circle with a diameter of three times the stone diameter given in Table 3.2. These values are an indication for the damage for a layer thickness of two times the stone diameter. A factor for the layer thickness should be included to be able to give a value of failure for all layer thicknesses and slopes. The amount of damage needed for failure for larger layer thicknesses can be approximated with the following formula: $E_3 = (1.5 - 1.6) + (T - 2)$, in which T is the layer thickness (the thickness expressed in T times the d_{n50}). The physical tests of Kramer (2016) confirmed that the damage depth decreases for milder slopes for the same wave conditions, see Figure 3.11. The decrease in E_3 is explained by the wave energy being more spread over a larger area for milder slopes.

Table 3.2: The damage depths as found by Hofland et al. (2011) and De Almeida Sousa et al. (2019) for a layer thickness of $2d_{n50}$.

Amount of damage	Damage depth, E_3*	E_{2D}	$E_{3D,1}$	$E_{3D,5}$
Initial damage	0.2-0.3	0.2	1	0.3
Intermediate damage	0.5-0.6	0.5	1.5	0.7
Failure	1.5-1.6	0.9	2.0	1.1
*For layer thickness of $2d_{n50}$				

De Almeida Sousa et al. (2019) performed physical tests to conclude which type of the damage depth is better. The tests were done with a steep 1:3 slope and a layer thickness of $2d_{n50}$. The damage depth variations tested were E_{2D}, $E_{3D,1}$, $E_{3D,5}$ and S. E_{2D} is the damage depth with the maximum erosion depth averaged over the width of the slope. $E_{3D,m}$ is the damage depth with the maximum erosion depth determined at any location of the slope averaged over a circular area with the diameter equal to m times the d_{n50}. From the tests could be concluded that $E_{3D,5}$ is the better option to describe the damage depth for steep slopes. This was due to a low bias, a low random error and a good distinguishable damage range. The damage ranges for E_{2D}, $E_{3D,1}$ and $E_{3D,5}$ found in the tests are given in Table 3.2. These values are applicable for a layer thickness of $2d_{n50}$.

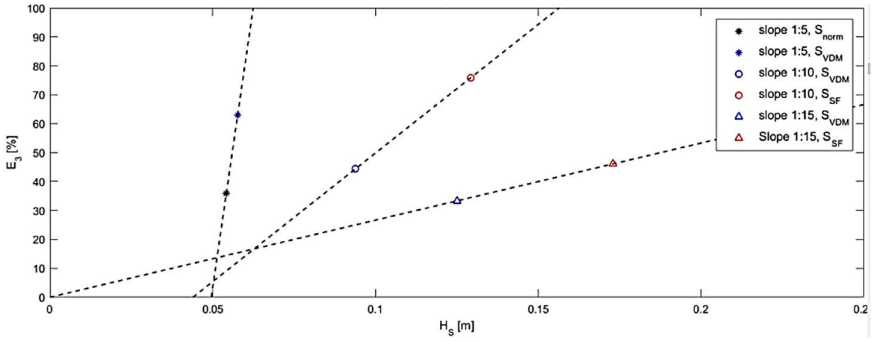

Figure 3.11: The damage depth vs. the wave height for different slopes from the tests of Kramer (2016).

3.4.4 Summary damage parameters

The three discussed damage parameters, the damage level, the erosion depth and the damage depth can all be applied for mild slopes. The values for failure are determined for steep slopes and have yet to be investigated for mild slopes. The diameter and the layer thickness are both parameters of importance to indicate if the values for failure give failure indeed. For instance, a certain erosion depth can result in failure for a small layer thickness and only intermediate damage for a larger layer thickness. The diameter is taken into account for the damage depth, the damage level and the layer thickness only indirectly in the permeability for the damage level. The erosion depth does not include both the diameter and the layer thickness.

The damage parameters also differ in the type of erosion they describe. The damage level describes an area and the other two provide a (relative) depth. The erosion depth and damage depth can stay equal, while the damage level increases. For milder slopes the damage is more spread out across the slope and therefore the damage level can increase before failure is reached. The erosion and damage depth cannot increase, because the depth allowed for failure stays the same for steep and mild slopes. The allowed depth for failure depends on the layer thickness.

3.4.5 Location of damage

The location of damage for irregular waves is spread over the slope. For irregular waves, wave heights differ spectrum wise and the breaking locations also differ over the slope. The higher waves break in deeper water, while the lower waves break in shallower water. In this way the breaking of the waves is spread over the slope and so is the damage. The breaking location of the irregular waves can be estimated by $H_0 = \gamma_b h_b$, with H_0 being the deep-water wave height [m], γ_b the breaker index [-] and h_b the breaker depth [m]. The breaker parameter is determined from the results of some experimental tests and displayed in Figure 3.12 as a function of the Iribarren number (Schiereck & Verhagen, Introduction to bed, bank and shore protection (2nd edition), 2016).

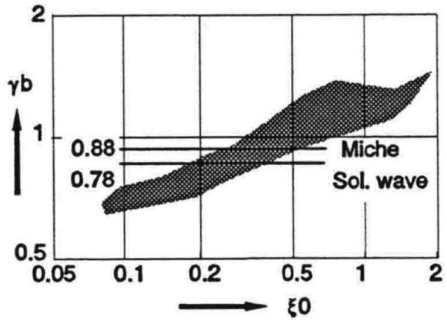

Figure 3.12: The breaker parameter as a function of the Iribarren number (Schiereck & Verhagen, 2016).

The most damage occurs just beyond the point of breaking due to the wave crest falling down and around the SWL due to the wave run-up and run-down velocities. Irregular waves have high run-up velocities due to the irregularities of the waves. If a high wave breaks after a few small waves, the water level is low and this gives a high the run-up velocity high that causes severe damage.

4 Methodology

Concluded in Paragraph 2.2 that no numerical models are available to model the stability of stones on mild slopes under wave attack correctly. This implicates empirical research resulting in data for profile displacement on mild slopes by physical tests. In this paragraph the physical tests are set out with the test set-up, the used constant and variable parameters and the measuring techniques.

4.1 Introduction to the physical tests

The physical tests are executed to gather data. With this data the research questions can be answered. The research questions are answered by three different types of physical tests. Below, the tests are shortly explained together with the research questions they answer. An overview with the different input parameters per test series is given in Table 4.1 and Table 4.2 and an overview of all the tests with the corresponding input parameters can be seen in Appendix B.

In general, all the tests are done with a mild sloped structure on which the stones are laid down. The stones are attacked by waves that reduce the stability of the stones until failure of the structure is reached. Several tests series are executed by which only one parameter is changed between the test series. For the tests in the test series the wave height is increased (except for the test series where the number of waves is increased, here the wave height is kept constant) to receive a damage output from start of damage to failure. The variable parameters make sure that all the research questions are answered.

The first five test series comply with answering research questions 2, 3 and 7. In these tests the influences of different wave parameters on the stone stability are investigated. These parameters are the wave steepness, the breaker type and the wave height. The sixth test series complies with research question 4 and is used to investigate the influence of the number of waves on the development of the profile change to see the effect of multiple storms in succession. The seventh and eighth test series comply with research question 5. In these test series the influence of the layer thickness on the stability of the stones is investigated for different wave parameters. Research questions 1 and 6 can be answered by making use of the data of all the physical tests.

4.2 Test set-up

The test set-up is elaborated in this paragraph. The different elements of the test are explained and shown from different views. The dimensions in the test set-up are determined by the theory, previous research or set by the dimensions of the basin. The arguments for the determined parameters are given in Paragraph 4.2.1.

The physical tests are executed in the Pacific basin in the laboratory of Deltares in Delft, an independent institute for applied research in the field of water and subsurface. The dimensions of the Pacific basin are 28 m x 14 m x 1.25 m. The basin has two cradle-type wave boards moved by two wave

Figure 4.1: The Pacific basin at Deltares with inside the smaller flume used for the physical tests.

generators and a passive wave damping beach that reduces the reflection of the waves back into the basin. The basin with the wave generators and the used flume inside the basin is shown in Figure 4.1.

In the basin a small flume is build where the physical tests take place. The flume exists of two walls of limestone blocks with in between a slope made of steel plates and the bottommost part of concrete. For the tests a slope angle of tan α = 1:10 is chosen (the slope angle used for the tests is determined in Appendix C.2.1). The height of the slope is set to 1 m due to the depth of the basin. This gives a length of 10 m. The width is 1 m, because this gives enough stones over the width (minimum is $25d_{n50}$ for damage parameters that are averaged over the width (De Almeida Sousa, Damage Characterisation of Rock Armoured Slopes, 2017)) and the steel plates used have a width of 1 m. In the wall on the door side a window of 1 by 2 m is placed at the SWL of 0.75 m with around the window an enclosure for the camera. The water depth is determined in Appendix C.2.2. The window is placed where the most damage is expected according to the results of Kramer (2016) and where the waves break. Atop of the slope the stones are placed from the bottom to the top. The weight and diameters of the stones are obtained in C.2.3. Around the SWL stones are laid down in six strips of 0.5 m with six different colours. The strip widths are determined in Appendix C.2.4. Five strips are laid down below the SWL and one strip above the SWL. The used colours are red, blue, purple, yellow, green and orange. In Figure 4.3 the flume is showed in detail with all the distances in Appendix D. The basin and the flume are shown together in one schematic overview together with real-life pictures of the flume/basin before and during the testing.

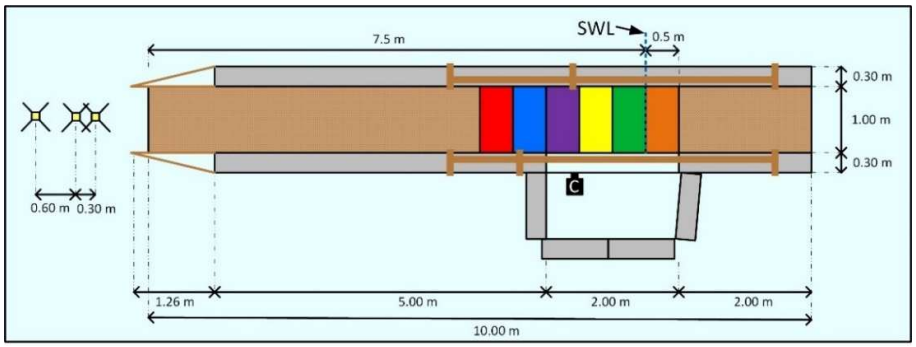

Figure 4.2: Side view of the test set-up zoomed in on the flume.

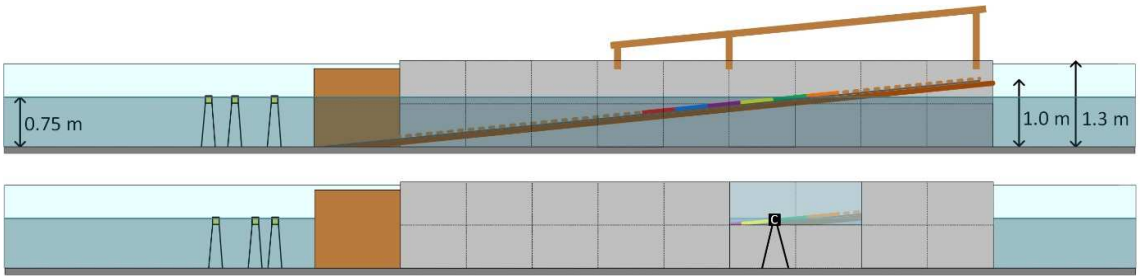

Figure 4.3: Top view of the test set-up zoomed in on the flume.

The ends of the limestone blocks are blunt and this could influence the incoming waves. Therefore, at the ends of the blocks wooden plates are placed in a triangle shape. These structures guide the waves inside the flume or to the side of the flume without reflecting the waves. In front of the slope three wave gauges are placed. Three wave gauges, with in-between distances of 0.6 and 0.3 m, are needed to distinguish the incoming waves from the wave signal that is a summation of the incoming and reflected waves. With less than three wave gauges or if distances in-between would be the same the incoming wave signal cannot be singled out from the total wave input signal. The incoming wave signal

is needed for the analyzation of the data. On top of the walls a wooden supportive construction is built that helps to take the photos that are needed for the profile difference measurements from the same height and place for each test, see for an impression Figure 4.2.

4.2.1 Input parameters

For the physical tests the parameters need to be determined. There are constant parameters that are equal for every test and variable parameters that have a different value per test. In the next paragraphs all the parameters are discussed briefly and the choices are elaborated. A severe elaboration of the determination of the parameters can be found in Appendix C.

4.2.1.1 Constant input parameters

The constant parameters are equal for every test done. An overview of the constant parameters is given in Table 4.1.

- The parameter that is determined first is the slope. The slope determines the values of the other parameters. The scope of the research requires a mild slope by which slopes are mild if tan α < 1:6. The chosen slope is tan α = 1:10. Further argumentation of the 1:10 slope can be found in Appendix C.2.1.
- The water depth, h, is determined to have the wave heights being developed in deep water. For the maximum significant wave height of the basin being 0.21 m, the water depth is set to 0.75 m. This is discussed in Appendix C.2.2.
- The stone nominal median diameter, d_{n50}, is determined by calculating the expected damage for the wave parameters within the wave height limitations of the basin and the natural limitations for the wave steepness. The chosen diameter has to be able give a damage in the range of start of damage to failure. This gives a nominal median diameter of 14.8 mm. The density of the stones, ρ_s, is determined to be 2944 kg/m^3. The water density, ρ_w, is 1000 kg/m^3. The relative density, Δ, is calculated with the stone and water density to be 1.94. The stone parameter choices are further elaborated in Appendix C.2.3.
- The strip width, W_{strip}, is set to have a compromise between a good workability and the error induced transport of the stones inside the strip. The strip width is decided to be 0.5 m. The determination of the strip width can be found in Appendix C.2.4.

Table 4.1: The constant parameters used for the physical tests.

Description	Parameter	Value	Unit
Slope	tan α	1:10	[-]
Water depth	h	0.75	[m]
Nominal median diameter	d_{n50}	14.8	[mm]
Density of stones	ρ_s	2944	[kg/m^3]
Density of water	ρ_w	1000	[kg/m^3]
Relative density	Δ	1.94	[-]
Strip width	W_{strip}	0.5	[m]

4.2.1.2 Variable input parameters

The variable parameters differ per test or test series. An overview of the variable parameters is given in Table 4.2. The variable parameters depend on the constant parameters and the other variable parameters.

- The layer thickness, T, used is a layer with a height of $2.5d_{n50}$ (that simulates a top layer of $2d_{n50}$ on a filter layer of $0.5d_{n50}$) and $5d_{n50}$. The higher layer thickness of $5d_{n50}$ is tested to determine the difference in stability for a higher permeability. This is elaborated further in Appendix C.3.1.

- The type of waves is determined in Appendix C.3.2 to be the JONSWAP spectrum.
- The wave steepness, s_{0p}, is set to the wave steepnesses that can occur in real life for irregular waves. The wave steepnesses that can occur are in the range from 0.01 to 0.05. Further argumentation for the used wave steepnesses is given in Appendix C.3.3
- The Iribarren number, ξ_p, follows from the wave steepness and the slope angle. The Iribarren numbers range from plunging waves to the transition to spilling waves and are in the range from 0.45 to 1.00. The Iribarren numbers used in the research are elaborated further in Appendix C.3.4.
- The number of waves, N, is determined to be able to develop failure of the slope and should be efficient in time. For all the tests except the 6th the number of waves is set to 1000, because this gives a test duration of about 30 minutes on average and the expected damage can vary between start of damage and failure. Test series 6 has an increasing number of waves till a cumulative total of 11,000 waves. Each test in test series 6 has a higher number of waves than the previous test to see the influence of a longer storm duration. The first test has 300 waves and the last one 4000. The choice of the number of waves used in the test is explained in more detail in Appendix C.3.5.
- The significant wave height, H_s, is determined by the Iribarren number, the diameter and the preferred damage output. This give a range of wave heights to be tested to cover the whole range of start of damage to failure of the slope. The range of wave heights used is from 0.06 to 0.23 m. The detailed determination of the used wave heights is given in Appendix C.3.6. The significant wave height is chosen to be equal to the average of the highest one-third of the waves, $H_{1/3}$.
- The wavelength, L_0, follows from the wave height and the wave steepness and is in between 14.0 and 2.0 m. This relation is shown in Appendix C.3.7.
- The wave period, T_p, follows from the wavelength by the linear wave theory and is in between 3.0 and 1.1 s. This relation is shown in Appendix C.3.8.
- The last column of Table 4.2 shows the damage level, S, that is expected from the tests with the variable parameters. This is no input parameter but shows why the variable parameters are set to their chosen values.

Table 4.2: The variable parameters used in the physical tests.

s_{0p} [-]	ξ_p [-]	N [-]	H_s [m]	L_0 [m]	T_p [s]	S [-]
0.01	1.00	1000	0.07-0.13	7.0-13.0	2.1-2.9	2.3-51.6
0.02	0.71	1000	0.08-0.18	4.0-9.0	1.6-2.4	1.9-110.5
0.03	0.58	1000	0.09-0.23	3.0-7.7	1.4-2.2	2.1-226.7
0.04	0.50	1000	0.10-0.20	2.5-5.0	1.3-1.8	2.5-78.7
0.05	0.45	1000	0.10-0.22	2.0-4.0	1.1-1.6	1.9-59.5

4.2.2 Overview of all the variable test parameters

In Table 4.3 is given an overview of all the constant input parameters per test series and in Table 4.4 of all the variable input parameters per test series. A complete overview of the input parameters per test is given in Appendix B.

Table 4.3: An overview of all the constant input parameters per test series.

Test series	tan α [-]	h [m]	d_{n50} [mm]	T [-]	ρ_s [kg/m^3]	ρ_w [kg/m^3]	Δ [-]
TL1	0.1	0.75	14.8	$2.5d_{n50}$	2944	1000	1.94
TL11	0.1	0.75	14.8	$2.5d_{n50}$	2944	1000	1.94
TL2	0.1	0.75	14.8	$2.5d_{n50}$	2944	1000	1.94
TL3	0.1	0.75	14.8	$2.5d_{n50}$	2944	1000	1.94
TL4	0.1	0.75	14.8	$2.5d_{n50}$	2944	1000	1.94
TL5	0.1	0.75	14.8	$2.5d_{n50}$	2944	1000	1.94
TL6	0.1	0.75	14.8	$2.5d_{n50}$	2944	1000	1.94
TL7	0.1	0.75	14.8	$5d_{n50}$	2944	1000	1.94
TL8	0.1	0.75	14.8	$5d_{n50}$	2944	1000	1.94

Table 4.4: An overview of all the variable input parameters per test series.

Test series	s_{0p} [-]	ξ_p [-]	N [-]	H_s [m]	L_0 [m]	T_p [s]
TL1	0.01	1.00	1000	0.07-0.11	7.0-11.0	2.1-2.7
TL11	0.01	1.00	1000	0.07-0.13	7.0-13.0	2.1-2.9
TL2	0.03	0.58	1000	0.09-0.23	3.0-7.7	1.4-2.2
TL3	0.05	0.45	1000	0.10-0.22	2.0-4.4	1.1-1.7
TL4	0.02	0.71	1000	0.08-0.18	4.0-9.0	1.6-2.4
TL5	0.04	0.50	1000	0.10-0.22	2.5-5.5	1.3-1.9
TL6	0.03	0.58	300-4000	0.15	5.0	1.8
TL7	0.01	1.00	1000	0.11-0.15	11.0-15.0	2.7-3.1
TL8	0.03	0.58	1000	0.17-0.21	5.7-7.0	1.9-2.1

4.3 Measuring techniques

The measuring techniques do apply to different outputs of the tests. The output is divided into three types. First, the profile output. This includes the profile changes of the slope in between the tests and the transport paths of the individual stones. Secondly, the process output that includes how the waves break and how this influences the transportation of the stones. At last, wave conditions need to be measured, which includes the exact incoming wave height. For the output there are different measuring techniques. In the paragraphs below the measuring techniques are elaborated per type of output needed and is concluded which technique is used. In Appendix E an extended version is given of the elaborations of the measuring techniques.

4.3.1 Profile measuring

The profile output includes the slope profile changes in between the tests and the transportation paths of the individual stones. These outputs are measured by different measuring techniques.

4.3.1.1 Profile measuring by creating 3D-images

Several measuring techniques were considered to obtain the slope profile changes from 3D-images. The considered techniques are stereo-photogrammetry, photogrammetry and 3D laser scanning. In Table 4.5 the trade-off matrix is given in which the measuring techniques are compared to each other by costs, the measuring and processing time, the accuracy and the construction needed for taking the measurements. Photogrammetry was concluded to be the best option. The photogrammetry gives a 3D model of the slope from which the profile changes can be elaborated. More information on photogrammetry can be found in Appendix E.

Table 4.5: A trade-off of the (dis)advantages of the different methods to measure the profile of the slope expressed in plusses and minuses for four requirements. The total score is a summation of the plusses and minuses.

Method	Costs	Time	Accuracy	Construction	Total
Stereo photogrammetry	+	+	+	-	++
Photogrammetry	++	-	+	+	+++
3D laser scan	-	+	++	--	0

4.3.1.2 Profile measuring by the movements of the stones

The transport of the individual stones is mapped by counting displaced coloured stones between two overlapping pictures taken before and after a test from a megapixel camera on a height of about 15 m. From this height, the total area of interest can be set on one photo. The counting of the coloured stones gives the original locations of the displaced stones together with the displacement lengths and directions.

4.3.2 Process measuring[1]

The process measuring concerning the breaking of the waves coupled to the transport of the stones have two measuring techniques that are available. With particle image velocimetry (PIV) the velocity and acceleration of the flow near the bed can be obtained. However, this method is very complicated in terms of construction, processing and safety for a flume in the Pacific basin. Due to this a different and easier method is chosen. The breaking of the waves and transport of the stones are recorded with a camera from the side of the flume through a window. With this method it can amongst others be checked at which moment of the wave breaking the stones start to move and if the succession of different types of wave breaking (that differs due to the irregular waves) influences the transport of the stones. This qualitatively way of following the transportation of the stones gives enough information on the location of breaking and the movement of the stones to use this to describe the stability of the stones on a mild slope under wave attack.

4.3.3 Wave conditions

The incoming wave conditions being the deep-water wave height and period need to be measured to relate these to the profile changes and the transport of the stones. The conditions are measured with three wave gauges that are placed in front of the slope in the deep-water region. There are three wave gauges needed to separate the incoming and reflected waves from the wave signal. The distances in between the wave gauges are 0.6 and 0.3 m, see Appendix E.3 for more explanation and the locations of the wave gauges.

4.4 Test procedure

The test procedure is written down in steps. This test procedure can be followed for each type of test. The slope is not rebuilt after every set of waves, only after the complete individual test series has experienced slope failure. To rebuild the slope after every test would consume too much time and the effect on the cumulative damage of not rebuilding after every test is small if the wave height is increased per test (Van Gent, personal communication, January 21, 2019). Measurements take place after every test. The flume has to be emptied before the measurements and filled afterwards to continue testing.

1. (Re)build the slope back to the original layer thickness. Place the coloured stones in the right strips also with the original layer thickness with the help of small strips. Remove these strips

[1] The results of the process measuring are not further elaborated in this research due to the limited time available for this research.

after the coloured stones are placed and smoothen the slope to reduce the possibility of small holes in the slope due to the removing of these strips.

2. Take a photo of the slope from a height of about 15 m with a high megapixel camera.
3. Photograph the slope with a regular camera (an iPhone was used in these tests) for the area of interest of 5 m from 66 locations, see Figure 4.4.
4. Fill the flume to the water depth of 0.75 m.
5. Put the input values for the wave generator into the computer that steers the wave generators.
6. Perform the test with the lowest wave height for 1000* waves.
7. Record (a part of) the test from the side of the flume with the camera to visualize the breaking of the waves and the transport of the stones.**
8. Empty the flume to a water depth of 0.35 m.
9. Photograph the slope for the area of interest of 5 m and photograph the area of coloured stones in detail.
10. Take a photo of the slope from the ceiling with a high megapixel camera.
11. Fill the flume to the water depth of 0.75 m.
12. Repeat step 5 – 11 until failure of the slope is reached.

Repeat this procedure for every individual test.

* The number of waves differs from 1000 for the test where the number of waves is increased.

** The recording of the wave breaking and the transport of the stones can be skipped for test 6 (the test with the increasing number of waves). The wave breaking is chosen the same as one of the first five tests and therefore the recording does not give new information.

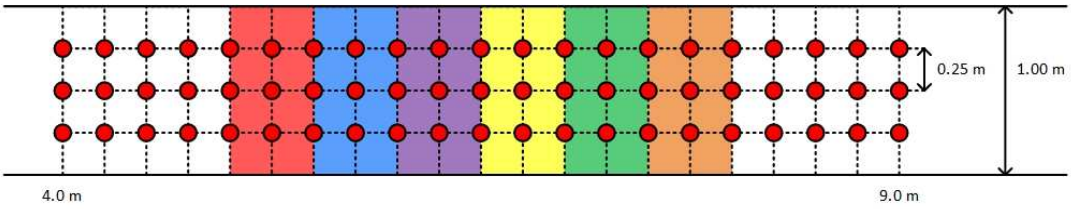

Figure 4.4: The locations from where the photos are taken, indicated by the red dots.

4.5 Physical test output

The tests have to give a few necessary output parameters. Firstly, the wave parameters (wave height, wave period and the number of waves) and secondly the damage parameters. The first need to be determined to check if the input wave parameters are correctly modelled by the basin and the output wave parameters are used to process the data. The output wave height is given by the $H_{1/3}$ as the significant wave height .The damage parameters have to be gathered indirectly from the photogrammetry measurements. The damage parameters that are measured are the damage level, S, to compare these results with the Van der Meer (1988) formula, the erosion depth, d_e, to check the maximal depth of the erosion hole and the damage depth, E_3. In Paragraph 3.4.3 two types of the damage depth were considered: E_{2D} and $E_{3D,m}$. According to De Almeida Sousa et al. (2019) is the damage depth with the maximum erosion depth determined at any location of the slope averaged over a circular area with the diameter equal to m times the d_{n50} more accurate than the damage depth averaged over the width of the flume. In the remaining part of the report is $E_{3D,m}$ used to describe the damage depth and is noted as E_m. It is decided to use E_3, because this gives a good average over the erosion hole but does not deviate too much from the actual erosion depth as was proposed by Hofland et al. (2011).

5 Results

In this chapter the data is processed and the results are analysed. The processing of the data is elaborated in Paragraph 5.1. This is done separately for the profile change measurements and the transportation of the stones. In Paragraph 5.2 are the results given that follow from the processing of the data. Paragraph 5.3 the results are further processed to the damage zones that indicate the locations where damage is most likely to occur.

5.1 Processing of the data

The processing of the results is divided into two parts: the profile change and the stone transport. The profile change is measured with photogrammetry and processed in Paragraph 5.1.1. The stone transport is measured by the overlay camera and processed in Paragraph 5.1.2.

5.1.1 Processing of the profile change

This paragraph follows the path from the photos taken of the slope via the 3D-profiles to the damage parameters and explains the processing of all these data. The slope was photographed 66 times per test, each photo from a different location, see Figure 4.4. These photos were processed to a 3D-profile with Agisoft Metashape. This program processes digital images to 3D spatial data by photogrammetry. The 3D-profile exists of a point cloud with around 30 million points that each contain an xyz-coordinate. This number of points is too large to be processed and the point cloud is therefore subsampled spatially to one point per 0.002 m. This results in a point cloud with around 2 million points. This subsampled point cloud still gives around the 43 points per stone instead of 680 points (these numbers differ a little per test). An impression of the subsampled point cloud of the profile of the slope is given in Figure 5.1.

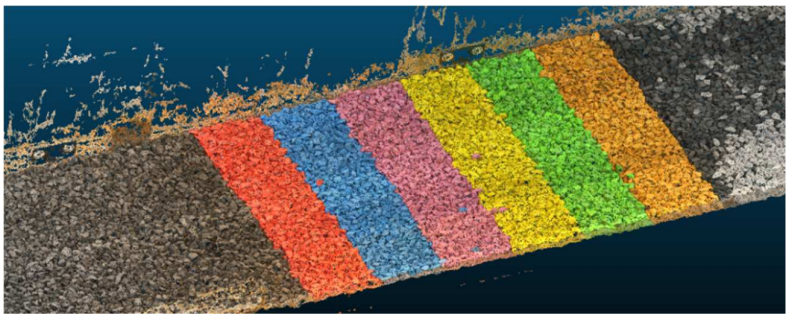

Figure 5.1: A 3D-profile existing of points as a result of the photos processed by Agisoft Metashape.

The xyz-coordinates of the profiles are further processed in Matlab. To gather all the damage parameters the pre (reference) and post profiles are laid over each other to measure the differences between the profiles. From these differences the damage parameters can be determined. Before each test series the profile is measured to get the pre profile. All the post profiles are compared to this pre profile. This gives a cumulative damage, because the slopes are not repaired in between the tests in the test series. For a real storm this is also the case, because it is expected that a slope has experienced some minor storms before the normative storm that causes failure of the slope.

To determine the damage parameters not all the points of the point cloud are taken into account, because this would give a too long process time. The point clouds are further processed with the help of a grid field. For each grid the median of the z-coordinates is taken of the points that lie within the x,y-coordinates of the grid. The median value gives a more accurate z-value than the average value, because outliers have less influence on the median than on the average.

Two grid sizes are developed, because the damage depth and the erosion depth each require a different grid size. The erosion depth, being the maximal depth of the erosion hole, has to be

determined with a small grid to be able to determine the erosion for each moved stone. The median nominal diameter is 0.0148 m and this is approached with a grid size of Δx = Δy = 0.02 m. This grid size gives a more regular distribution of the grid over the length and width over the flume. and about 200 points per grid. The damage depth uses the averaged erosion depth over a circle of three times the nominal median diameter. This averaged erosion depth is determined by taking a larger grid size than 0.02 m. The circle of three times the nominal diameter with an area of 0.044 m^2 is approached by a grid size of Δx = Δy = 0.04 m. These areas are almost equal. This grid size gives about 800 points per grid.

For each test the pre profile (the profile measured before the test series started) and the post profile are processed to the two grid fields by which every grid has the median value of all the z-coordinates of the points in the grid. The grid fields from the pre and post profile are laid over each other to determine a grid field by which every grid gives the difference in z-coordinate.

The photos are taken from 3.5 to 9.5 m in the length direction of the flume and from 0 to 1.0 m in the width direction. The ends in length direction were not all very well processed, because the overlap of the pictures became less towards the ends. The first 0.1 m on the sides of the flume in width direction experienced more damage than the middle of the slope due to irregularities in the flume. To prevent influence of this on the damage parameters the grid field is reduced to 4.5 to 9.0 m in length direction and 0.1 to 0.9 m in width direction.

To show the processing of the damage parameters the results of test 2c are used. How this is done is explained in Paragraph 5.1.1.1.

5.1.1.1 Determining the erosion depth

The erosion depth is determined with the grid field with a grid size of Δx = Δy = 0.02 m. The erosion depth is determined by taking the maximum negative value of the grid field. In Figure 5.2 the difference plot is shown for test 2c together with the SWL (red line).

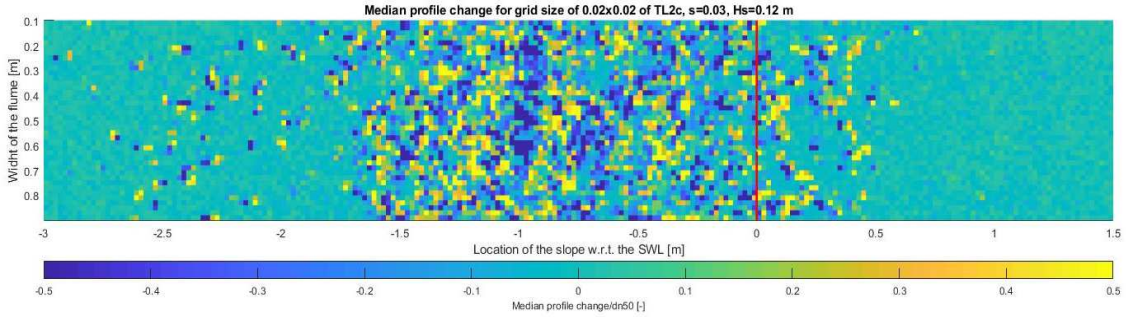

Figure 5.2: A plot with the profile changes between the pre and post profile with a grid size of 0.02 m. The red line indicates the SWL.

5.1.1.2 Determining the damage depth

The damage depth requires the average erosion depth over a circular area with a diameter of $3d_{n50}$. This is determined by taking the maximum negative value after a test of the grid field with a grid size $\Delta x = \Delta y = 0.04$ m. In Figure 5.3 is the difference plot shown for test 2c together with the SWL (red line). The damage depth is then calculated by Equation 3.12 with the nominal median diameter.

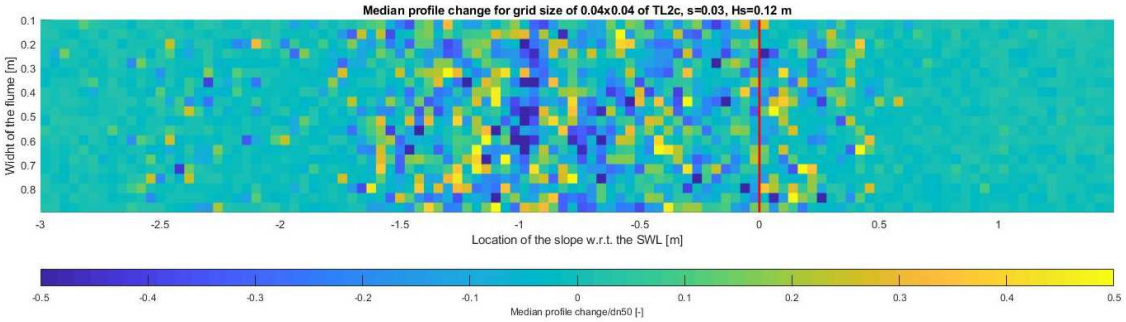

Figure 5.3: A plot with the profile changes between the pre and post profile with a grid size of 0.04 m. The red line indicates the SWL.

5.1.1.3 Determining the damage level

The grid field with grid size of 0.02 m is used to determine the damage level, because this gives a more accurate result for the erosion area. The grid field is averaged over the length, see Figure 5.4, and over the width, see Figure 5.5. These two profiles show the averaged profile change. The profile is averaged, because this was the method used by Van der Meer (1988). To be able to compare the results with Van der Meer (1988) the same method should be used. The profile change over the width should be almost zero, because in this direction the transport is negligible. The profile change of the length should show transport for the damage zone and zero transport for the profile outside the damage zone. From the damage zone is the erosion area determined by taking the maximum negative area. For mild slopes there develop multiple erosion holes and the hole with the largest area is used to determine the damage level. The consequences of this choice are discussed in Paragraph 0. With this area the damage level can be calculated by Equation 3.11. The directions in which the profiles are averaged are showed in Figure 5.6. The profile change plots of all the tests are given in Appendix F.

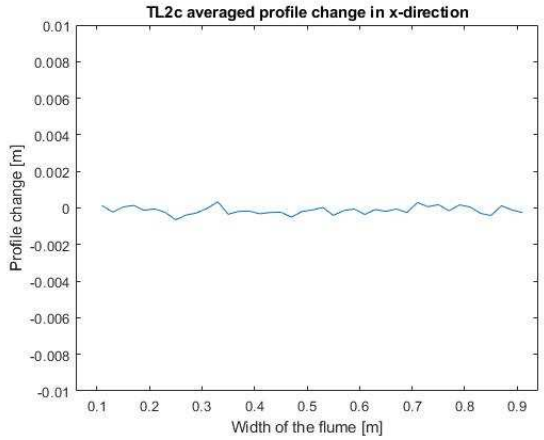

Figure 5.4: The profile change in x-direction averaged over the length.

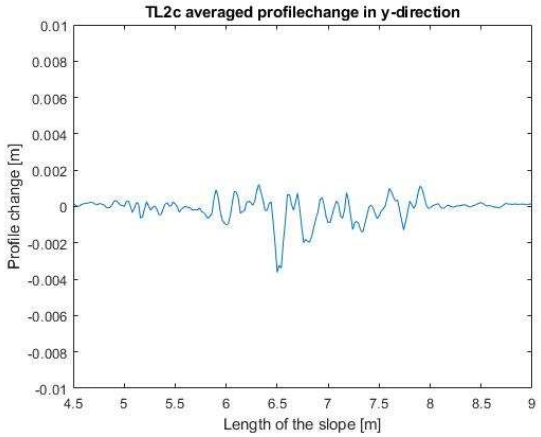

Figure 5.5: The profile change in y-direction averaged over the width.

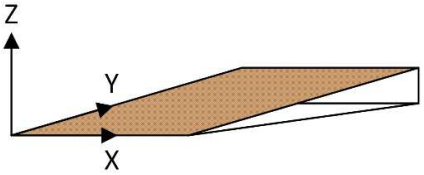

Figure 5.6: The directions of the coordinate system as used in the tests.

5.1.2 Processing of the stone transport

The stone transport is processed by comparing two overlay photos of the slope. The pre photo is taken before the test series and the post photo after each test. In Figure 5.7 are the overlay photos shown for test series 4 with the post photo of test 4d. The displacements of the stones are measured with a stone-counting script in Matlab made by Ivo van der Werf (2014). In this tool each transported stone has to be clicked and these are added up to the number of stones displaced. This method of counting the displaced stones is labour-intensive but can be 100 percent accurate is every stone is clicked. The stone transport is measured in three ways:

- The number of stones removed from one strip. This is determined by counting all the stones with colour A removed from the strip with colour A. This is done for each strip.
- The transportation lengths of the removed stones (with steps of 0.5 m, due to the strip width). This is determined by counting the stones with colour A transported to the strip with colour B. This is done for every combination of coloured strips and for the up- and downslope direction. The distance from one strip to the other is the transportation length.
- Next to this, for a few strips the inside transport is counted by counting the stones that are removed in one strip between the pre and post picture minus the stones that moved outside of the strip. The difference is the amount of stones picked up in a strip and laid down in the same strip.

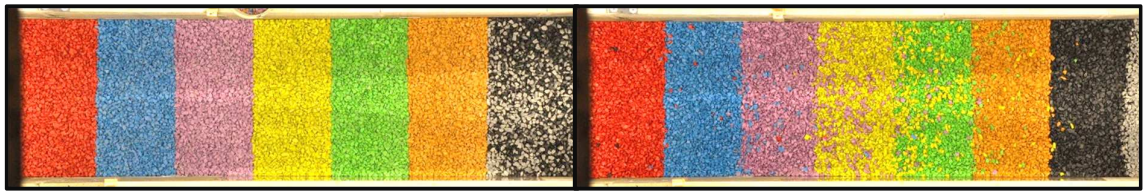

Figure 5.7: The overlay photos with on the left the pre photo before test series 4 and on the right the post photo after test 4d.

5.2 Results of the tests

The results of the tests are shown in this paragraph. From the profile change measurements follow the damage parameters described in Paragraph 3.4. These are compared for their applicability for the stability of stones on mild slopes under wave attack in Paragraph 5.2.1 and it is concluded which parameter is used further. In Paragraph 5.2.2 the chosen parameter is used to determine the influences of the varied parameters in the tests: the breaker type, the wave height, the number of waves and the layer thickness. Also, a new stability curve is made for start of damage, intermediate damage and failure. The methods used to determine the results are discussed in Paragraph 5.2.3.

The results of the transportation of the stones by counting the coloured stones are shown in Paragraph 5.2.4. With these results are the effects investigated of the same parameters as mentioned above on the stone stability. The results of the stone counting are discussed in Paragraph 5.2.5.

5.2.1 Results of the profile change

The results of the profile change follow from the processing of the data in Paragraph 5.1.1. In Table 5.1 are the results shown per test. The damage level, erosion depth and damage depth are given per test together with the wave steepness and the wave height. Further on in this paragraph these results are analysed to be able to answer the research questions given in Chapter 1. The damage parameters are analysed for their applicability for mild slopes. After these analyses a conclusion is given which damage parameter is best suited to describe the stability of mild slopes under wave attack.

After that the best suited parameter is further analysed for the effects of the hydraulic and structural parameters. With these analyses a relationship is formulated between the damage parameter and the hydraulic and structural parameters.

Table 5.1: The results of the processing of the profile change with all the damage parameters.

Test	s_{0p} [-]	$H_{1/3}$ [m]	$H_s/\Delta d$ [-]	S [-]	d_e [m]	E_3 [m]	Test	s_{0p} [-]	$H_{1/3}$ [m]	$H_s/\Delta d$ [-]	S [-]	d_e [m]	E_3 [m]
TL1a	0.009	0.062	2.16	3.9	0.013	0.53	TL4a	0.018	0.076	2.65	1.7	0.013	0.53
TL1b	0.010	0.087	3.03	3.1	0.019	0.80	TL4b	0.019	0.094	3.27	3.2	0.017	0.64
TL1c	0.009	0.109	3.80	40.7	0.030	1.93	TL4c	0.017	0.114	3.97	4.2	0.021	0.76
TL11a	0.009	0.066	2.30	2.2	0.015	0.66	TL4d	0.019	0.134	4.67	6.9	0.022	1.20
TL11b	0.010	0.086	3.00	5.4	0.025	1.18	TL4e	0.019	0.157	5.47	8.9	0.030	1.70
TL11c	0.009	0.110	3.83	13.3	0.029	1.80	TL4f	0.020	0.174	6.06	19.0	0.044	2.69
TL11d	0.010	0.126	4.39	51.5	0.040	2.44	TL5a	0.038	0.101	3.52	4.9	0.015	0.44
TL2a	0.030	0.089	3.10	2.1	0.014	0.47	TL5b	0.039	0.118	4.11	2.2	0.017	0.55
TL2b	0.031	0.106	3.69	2.2	0.014	0.47	TL5c	0.039	0.132	4.60	3.6	0.015	0.66
TL2c	0.027	0.121	4.21	5.0	0.020	0.88	TL5d	0.036	0.150	5.22	4.6	0.017	0.70
TL2d	0.029	0.141	4.91	5.8	0.020	1.05	TL5e	0.037	0.169	5.89	5.0	0.017	0.73
TL2e	0.028	0.159	5.54	13.5	0.023	1.31	TL5f	0.038	0.189	6.58	11.1	0.019	0.76
TL2f	0.028	0.179	6.23	20.5	0.022	1.18	TL5g	0.036	0.207	7.21	16.4	0.019	1.05
TL2g	0.030	0.205	7.14	27.4	0.027	1.37	TL6a	0.029	0.145	5.05	4.6	0.017	0.79
TL2h	0.031	0.225	7.84	33.5	0.031	2.05	TL6b	0.029	0.143	4.98	5.4	0.022	0.99
TL3a	0.052	0.099	3.45	2.2	0.010	0.30	TL6c	0.028	0.141	4.91	5.4	0.022	0.97
TL3b	0.052	0.116	4.04	1.7	0.013	0.54	TL6d	0.029	0.142	4.95	13.0	0.023	1.11
TL3c	0.051	0.134	4.67	4.9	0.015	0.64	TL6e	0.029	0.143	4.98	6.5	0.023	1.24
TL3d	0.050	0.148	5.15	7.5	0.018	0.73	TL6f	0.029	0.142	4.95	11.0	0.029	1.55
TL3e	0.048	0.165	5.75	5.2	0.015	0.59	TL7a	0.009	0.109	3.80	17.0	0.029	1.64
TL3f	0.044	0.183	6.37	11.3	0.019	0.90	TL7b	0.010	0.126	4.39	46.1	0.042	2.36
TL3g	0.045	0.203	7.07	7.1	0.020	0.85	TL7c	0.010	0.137	4.77	50.6	0.039	2.09
							TL8a	0.028	0.161	5.61	7.1	0.019	0.91
							TL8b	0.028	0.184	6.41	15.4	0.032	1.81
							TL8c	0.029	0.203	7.07	19.2	0.030	1.84

5.2.1.1 Damage level

The damage level complies with the Van der Meer (1988) formula. Therefore, the results of the tests are compared to the damage level according to the Van der Meer (1988) formula for plunging waves. To compare the formula with the results of the tests, the test results are processed to get the stability number ($H_s/\Delta d_{n50}$) per Iribarren number for start of damage (S=2), intermediate damage (S=8) and failure (S=17) (Schiereck & Fontijn, 1996). In Appendix G is shown how the stability numbers are determined by the method of Van der Meer (1988) from the results of the tests.

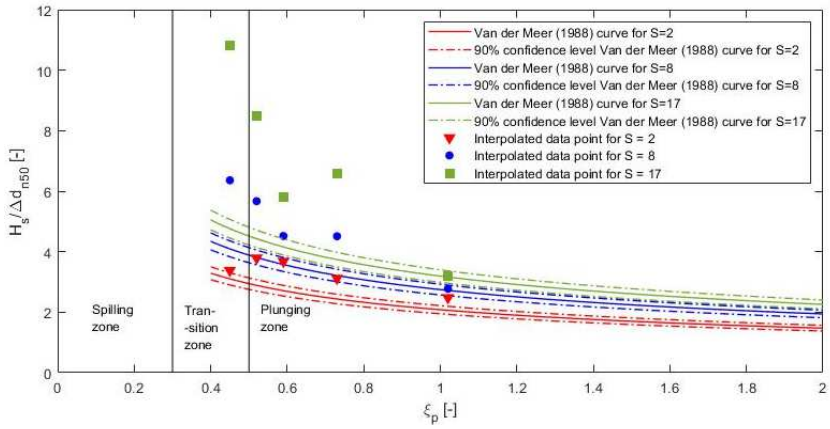

Figure 5.8: The results of the tests compared with the design formula of Van der Meer (1988).

The comparison is made in Figure 5.8 for the damage levels of 2, 8 and 17. In Figure 5.8 becomes clear that the damage level predicted by Van der Meer (1988) underestimates the stability of mild slopes. The data points that are the results of the tests of this research lie above the extrapolated formula of Van der Meer (1988) and its confidence bounds. These confidence bounds are determined by Van der Meer (1988) itself with a standard deviation of 0.4 for the coefficient 6.2 in Equation 2.6. This confirms the test results of Schiereck and Fontijn (1996) and Kramer (2016). This was expected due to the previous tests and according to the theory. The energy of the waves is more spread for mild slopes. This decreases the forces on the stones and increases the stability. For the start of damage of S=2 the mild slope is a bit more stable than Van der Meer (1988) predicts. For intermediate damage and failure is the stability much more stable than Van der Meer (1988) predicts. The extrapolated data points tend to deviate more from the Van der Meer (1988) formula if the damage level increases.

The Van der Meer (1988) formula is conservative, because the formula is extrapolated towards more spilling waves. These waves have a completely different spread in the energy density spectrum by which the energy is spread wider over the slope and causes a decrease in the forces exerted on the stones. This decrease of the forces causes the stones to be more stable for the same wave height. The Van der Meer (1988) damage level is also conservative in the damage level itself. This damage parameter is defined as a damage area and made dimensionless by the d_{n50} squared. The damage level for start of damage is defined as S = 2. Van der Meer (1988) used the definition for start of damage described by Hudson (1959). Hudson determined “no damage” as the removal of 1% of the total number of stones from the top layer. The difference in definition for “no damage” between mild and steep slopes is shown in Figure 5.9. For steep slopes the area around the SWL for the same damage zone contains less stones than for mild slopes. The removal of 1% of the stones is reached therefore sooner for steep slopes than for mild slopes. Also, a damage area determined over the same height gives a deeper damage depth for steep slopes than for mild slopes, because for mild slopes the damage area is spread more widely over the length of the slope. Next to this, the damage profile of a mild slope exists of multiple erosion holes (see Figure 5.5) and for steep slopes mostly one erosion hole develops. It is unclear from the theory of Van der Meer (1988) how the erosion area should be defined for mild slopes. This could be by the area of the total of all the erosion holes or by the area of the largest erosion hole. These are the reasons that the damage level is not a good damage parameter for mild slopes.

By the damage definition of Hudson (1959) it is not strange that the stability parameter for a ξ_p of 0.45 lies on the formula of Van der Meer (1988), because the milder a slope becomes the less the damage level can say anything about the start of damage and failure of the slope. This also follows from Figure 5.10 where the damage level is set out against the significant wave height per wave steepness. For the lower damage levels there is only a small difference in between the different wave steepnesses. For the small damages there is no clear distinction between the different steepnesses and for some tests an increase in wave height did not mean a direct increase in the damage level. The latter also happened for the physical tests done by Kramer (2016) for the 1:15 slope, where an increase of 0.05 m in wave height gave a decrease of 0.35 in damage level. This can be caused by the spread of the damage over the slope due to the higher wave height and a different breaking depth.

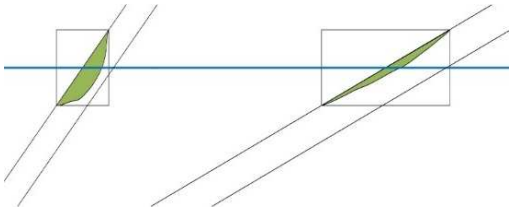

Figure 5.9: The damage level compared between the steep and mild slope.

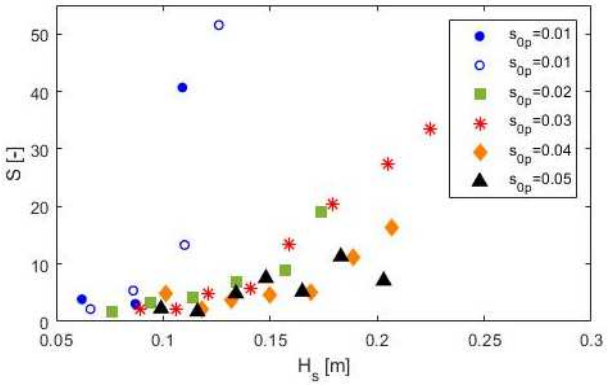

Figure 5.10: The damage level set out against the significant wave height per wave steepness.

5.2.1.2 Damage depth

The damage depth, E_3, defined as the averaged erosion depth over a circle with a diameter of three times the d_{n50} divided by the d_{n50} is plotted in Figure 5.11 against the significant wave height per wave steepness. The damage depth shows a clear increase per wave height for each wave steepness. The difference in damage depth per wave steepness is for the lower wave steepnesses very clear. For the higher steepnesses the damage depth does not differ much if the wave steepness is changed.

For the damage depth also the stability number is determined with the method explained in Appendix G. The result is shown in Figure 5.12 where the stability number is set out against the Iribarren number per set value of the damage depth. It can be concluded that the damage depth shows a good distinction between the Iribarren numbers for an increase of the stability parameter (and significant wave height) if the damage depth is higher. Again, it is visible that for the two higher wave steepnesses (the two lower Iribarren numbers) the difference in stability is small per equal damage depth.

The damage depth shows a good spread from start of damage towards failure. The start of damage is around the same value of 0.5 for all the wave steepnesses, because the first data point of each wave steepness lie almost on the same line. Due to the definition of the damage depth the parameter is only partly influenced if one stone removes. If all the other stones stay in the same location in the circle of three times the diameter the increase in the damage depth is 0.11.

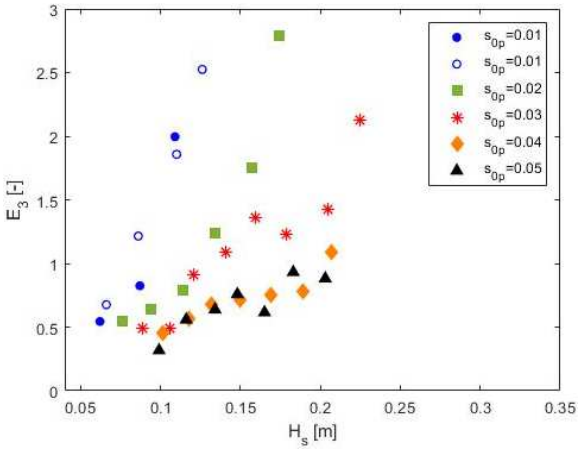

Figure 5.11: The damage depth set out against the significant wave height per wave steepness.

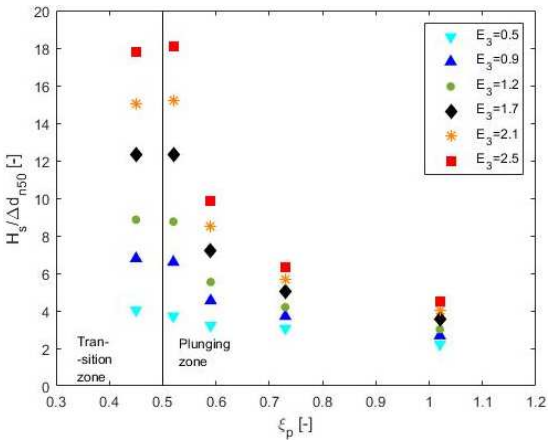

Figure 5.12: The stability number set out against the Iribarren number per set value of the damage depth.

5.2.1.3 Erosion depth

The erosion depth, d_e, is shown in Figure 5.13 against the significant wave height per wave steepness. As for the damage depth the erosion depth shows a clear distinction per wave steepness and increases per wave height. For the lower wave steepnesses the distinction is very clear between the wave steepnesses. For the higher wave steepness of 0.04 and 0.05 the erosion depths are almost equal per wave height. The stability number is also determined for the erosion depth and set out against the Iribarren number per set value of the erosion depth shown in Figure 5.14. The erosion depth shows a good distinction between the Iribarren numbers for an increase of the stability number (and significant wave height) if the erosion depth is higher. The data points for the Iribarren number of 0.52 seem to be outliers if compared to the other stability parameter data points. The increase in the stability number per increasing erosion depth is very quick. This is caused by the very slow development of the erosion depth per increasing wave height (visible in Figure 5.13). The development of the erosion depth for the wave steepness of 0.05 is less slow, because for the lower wave heights the increase in damage is larger per wave height than for the wave steepness of 0.04.

The erosion depth has per wave height a good spread of the damage between the start of damage and failure. The start of damage is around 0.015 m. This is close to the d_{n50}. The definition of the erosion depth being the maximal erosion depth of the bed not averaged over a width means that the removal of one stone directly gives an erosion depth equal to the d_{n50}. This means that the removal of one stone has a large influence on the erosion depth by increasing the erosion depth with the diameter of the removed stone. Not directly the d_{n50}, because the diameters of the stones vary between 0.01 and 0.02 m.

Due to the definition the erosion depth can be a good indicator of damage for steep slopes, because a removal of one stone can cause severe damage to these structures. However, for mild slopes the removal of a single stone is less determinate for the damage than for steep slopes. Therefore, the damage depth is not a good parameter to describe the damage (especially the start of damage) for mild slopes.

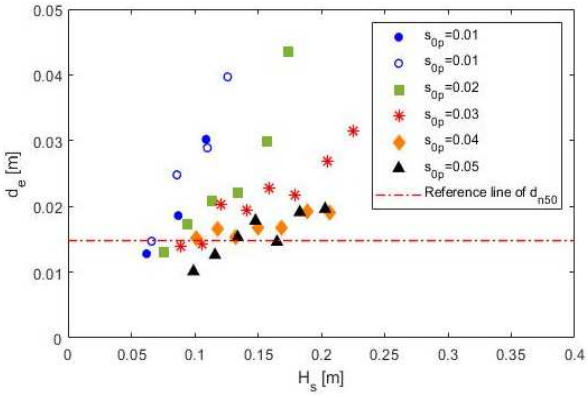

Figure 5.13: The erosion depth set out against the significant wave height per wave steepness.

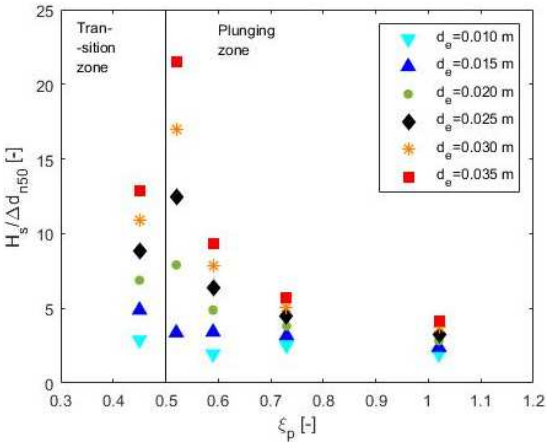

Figure 5.14: The stability number set out against the Iribarren number per set value of the damage depth.

5.2.1.4 Conclusion

In the above paragraphs the results are shown of the different damage parameters. In Paragraph 5.2.1.1 is already concluded that the damage level cannot be used to describe the damage for mild slopes. This was due to the definition of the damage level that included the damage area. For the same height over the SWL the same damage area means a smaller decrease in erosion depth for mild slopes than for steep slopes. Compared to the Van der Meer (1988) formula for plunging waves the results of the tests with a mild slope the formula is very conservative, because the data points all lie above the

lines of the formula. This confirms that the Van der Meer (1988) formula for plunging waves should not be used to design slopes milder than tan α > 1:10.

The damage depth can be concluded to be a good damage parameter for mild slopes. The damage depth shows a clear distinction if set out against the wave height per wave steepness. Also, the stability number gives results per Iribarren number that are all in line with each other. The influence of the removal of one stone gives an increase of the damage depth of 0.11. Start of damage and failure can both be distinguished.

The erosion depth shows a good distinction if set out against the wave height per wave steepness. However, the stability parameter does not give good results for the Iribarren number of 0.52. The definition of the erosion depth causes the parameter to be very influenceable by the removal of one stone and it is therefore concluded that the erosion depth is not a good parameter for the description of damage for mild slopes.

The above conclusions state that the damage depth is the best to be used for mild slopes. Therefore, the damage depth is further analysed with respect to the hydraulic and structural parameters to answer the research questions.

5.2.2 Analysation of the damage depth

In this paragraph, the damage depth is further analysed. It is elaborated what the influences are of the breaker type, the wave height, the number of waves and the layer thickness on the damage depth. From these analyses a new stability formula can be obtained and the consequences of changing a variable parameter are known.

5.2.2.1 Breaker type

To check the influence of the breaker type on the damage the damage depth is set out against the Iribarren number per increasing wave height, see Figure 5.15. A decrease of the Iribarren number causes the damage depth to decrease per equal wave height. If the wave height is kept in the same range the damage depth decreases when the Iribarren number goes from plunging to spilling.

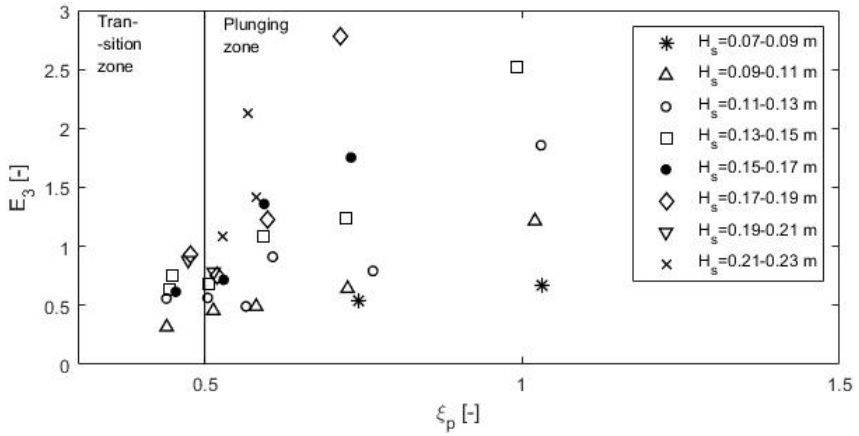

Figure 5.15: The damage depth set out against the Iribarren number per increasing wave height.

The influence of the wave height is also checked with the direction coefficients of the trendlines of the damage depth versus the wave height (plotted in Figure 5.18). The direction coefficients are plotted against the Iribarren number in Figure 5.16. The direction coefficient is the 'a' in: $E_3 = aH_s$. If the breaker type changes from plunging to spilling the direction coefficient decreases. A decrease in the direction coefficient means that the damage development is slower for an equal increase in the wave

height. For more spilling breakers the damage develops much slower compared to the plunging breakers for the same increase in wave height.

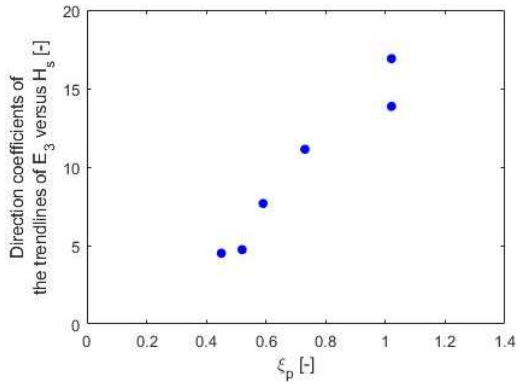

Figure 5.16: The direction coefficients of the trendlines of the damage depth versus the wave height plotted against the Iribarren number.

If the Iribarren number decreases the breaker type changes from a spectrum with only plunging breakers to a spectrum with both plunging and spilling breakers, because the lowest Iribarren number tested is in the range of the transition zone from plunging to spilling breakers. The spilling breakers cause less damage per wave impact. These waves are already steep if they approach the shoreline and if the water depth decreases the wave starts to break at the top of the wave. This is due to the lower part of the wave being slowed down gradually due to the friction of the bottom and the top of the wave is not. Then the top of the wave overtakes the lower part of the wave and starts to break. This breaking wave spills down over the lower part of the wave. This process of gradual breaking and slow dissipation of the energy continues until all the wave energy is dissipated. The plunging breaker has a lower wave steepness than the spilling breaker before the shoreline is reached. If the water depth decreases the wave starts to steepen very fast. The wave becomes almost vertical until it cannot steepen any further and starts to break. Because the wave is almost vertical the breaking wave drops down in front of the wave and not on the wave like the spilling wave does. The wave breaking then plunges directly into the water depth with a lot more impact than the spilling wave, because the breaker force is higher for the plunging wave and it plunges into a smaller water depth. This causes the plunge to reach the bottom with more force and cause more damage. This can reasonably be expected to cause the decrease of damage if more spilling breakers occur in the spectrum. The transition from plunging to spilling waves is a gradual transition. The breaking wave becomes less vertical if the wave steepness increases or the slope angle decreases and the wave breaks more on the wave itself.

The gradual transition is obtained from the wave spectrums used for the physical tests. During the testing videos have been made from the breaking waves to determine the percentage of plunging and spilling waves in a wave spectrum. In Figure 5.17 the transition from plunging to spilling waves is shown

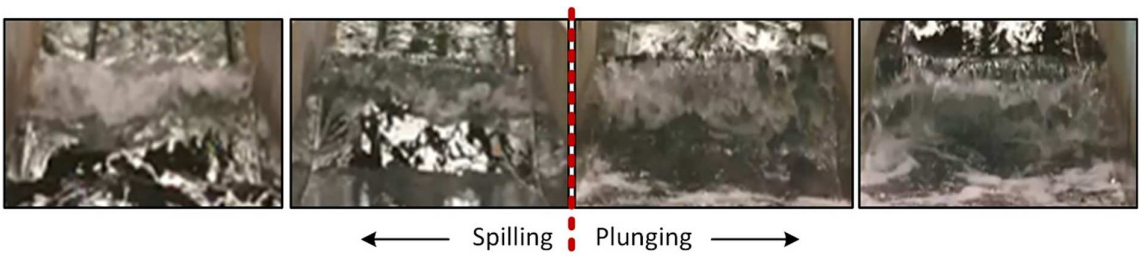

Figure 5.17: The gradual transition from plunging to spilling breaker as obtained during the testing. The images are taken from the videos made during the testing, hence the low quality.

by images taken from the videos. On the right the plunging wave is given that has no breaking on top of the wave but falls down in front of the wave. On the left the spilling wave is shown that breaks on the top and falls down on the wave itself. In the middle the transition is shown where the wave breaks more onto itself until it changes to the spilling wave.

Of each test a video with a length of about 100 waves was made. From these videos the distribution between the plunging and spilling breakers is determined. Each wave in the video was categorised into a plunging or spilling breaking wave. The results are given in Table 5.2. The lower the Iribarren number the more spilling waves. For the lowest Iribarren number during the tests (ξ_p = 0.45) the distribution is almost fifty-fifty and can be said to be the middle of the transition zone. It was also notable that for each spectrum the higher waves appeared more frequently to be the spilling breaking waves.

Table 5.2: The distribution of the plunging and spilling waves in a wave spectrum per Iribarren number.

ξ_p [-]	Percentage plunging [%]	Percentage spilling [%]
1.00	100	0
0.71	94	6
0.58	73	27
0.50	64	36
0.45	51	49

5.2.2.2 Wave height

In Figure 5.18 the wave height is shown versus the damage depth per wave steepness. For each wave steepness the wave height has to increase to cause an increase in the damage depth. For the lower wave steepnesses an increase of 0.02 m in wave height causes a larger increase in the damage depth than for the higher wave steepnesses. The dominance of the wave height over the damage depth is shown in Figure 5.18 by the trendlines given per wave steepness. The trendlines become more horizontal if the wave steepness increases. This means that the influence of the wave height is less dominant if the wave steepness increases. For the two highest wave steepnesses tested (0.04 and 0.05) the trendlines are almost equal.

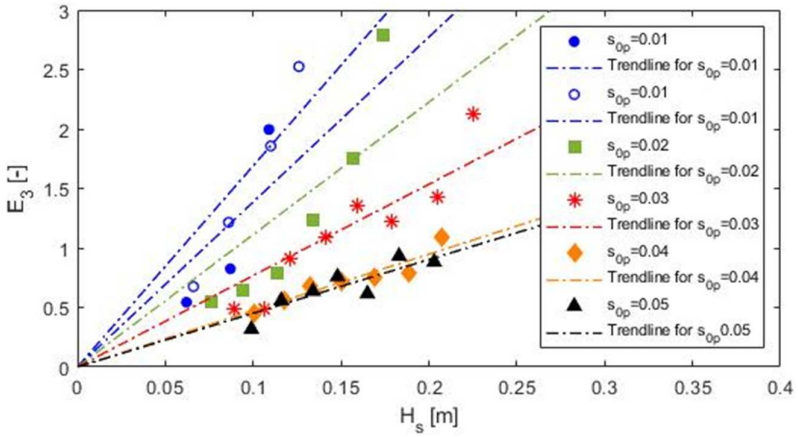

Figure 5.18: The wave height versus the damage depth per wave steepness with their trendlines.

A larger wave height causes more damage to the bed than a lower wave height. An increase in wave height gives an increase in wave energy by Equation 5.1. A small increase in wave height gives a rapid increase of the energy density, because of the quadratic relationship between the wave height and the energy. The higher wave steepnesses produce a more plunging wave and according to Paragraph 5.2.2.1 does this breaker type transfer a lot of wave energy towards the bottom. If the wave height increases, and by that the wave energy, then most of this energy is transferred to the bottom and the

damage depth increases rapidly. For the lower wave steepnesses that have more spilling waves less wave energy is transferred to the bottom due to the breaking of the wave. An increase in wave height and wave energy do not cause the same increase in damage depth as for the plunging waves. A higher wave gives a larger water depth for the wave to break into for spilling waves than for the lower wave heights. The wave energy also increases but if the wave breaks into a larger water depth compared to the lower waves the energy transferred to the bottom only increases a little compared to the lower wave steepnesses.

$$E_{wave} = \frac{1}{8}\rho g H_s^2 \qquad 5.1$$

In Figure 5.18 a few decreases in the damage depth are visible while the wave height increased. This could be explained by the different breaker depths per wave height. For mild slopes there develop several small erosion holes over the slope. If the wave height increases the breaker depth also increases and the wave breaks more downslope. This can give erosion holes at other locations than for the smaller wave height. The erosion holes made by the smaller wave height can be filled up with the stones transported from the holes made by the larger wave height. This can cause a decrease of the damage depth.

In Figure 5.19 the Iribarren number is plotted against the damage depth divided by the wave height and against the percentage of plunging waves in the wave spectrum. This is done to show the dependency of the damage depth versus the wave height. For the higher wave steepnesses the data points lie close to each other. This confirms that the wave height does not have a big influence on the damage depth for the lower Iribarren numbers. For the lower wave steepnesses the data points lie more spread over the graph. This confirms that for the more plunging waves the wave height has more influence on the development of the damage depth as was expected according to the theory in Paragraph 3.2.3. A decrease in the percentage of plunging waves in the wave spectrum gives a decrease in the damage development for an equal increase in wave height.

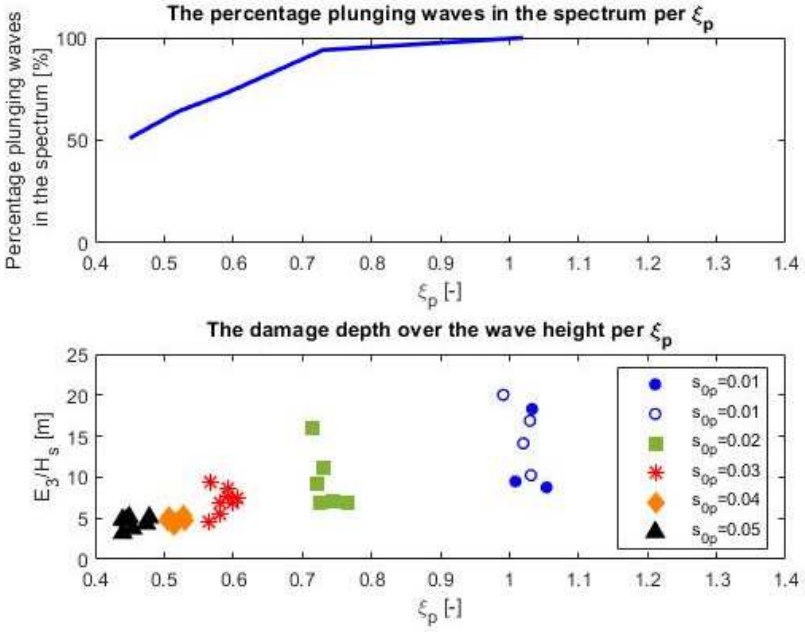

Figure 5.19: The Iribarren number plotted against the damage depth divided by the wave height per wave steepness and against the percentage of plunging waves in the wave spectrum.

5.2.2.3 Number of waves

The development of the damage depth for an increasing number of waves is shown in Figure 5.20. From the graph can be concluded that after a cumulative total of 11,456 waves the development of the damage is not yet stabilized. If the test would have been stopped after 2236 waves the conclusion would be that the damage was already stable, because the damage depth for this number of waves is almost equal to the damage depth after 1135 waves. However, the test is continued up to 11,456 waves and the damage depth increases still up to this number of waves. Due to the outlier at 1000 waves the data is declared not completely reliable. More physical tests have to be done to give a reliable conclusion about the influence of the number of waves on the stability.

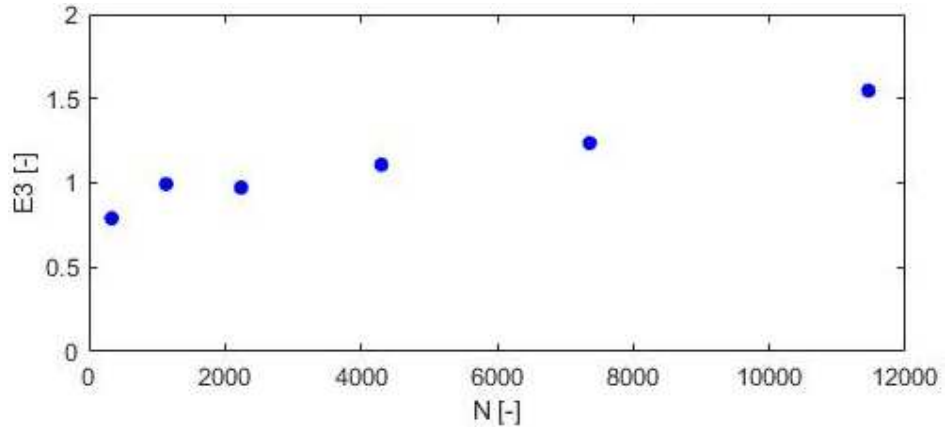

Figure 5.20: The number of waves plotted against the damage depth with the (linear) trendline.

The overall profile of the bed does not change much in slope if the damage depth develops. If this slope angle stays stable the breaking of the waves continues in the same way during all the waves and the development rate of the damage also does not change. For steep slopes with a lot of damage the wave breaking does change, because the slope angle starts to deviate from the original profile and the wave breaking starts to have less impact on the damage. The tests done by Thompson and Shuttler (1975) had slopes up to 1:6. This can be the reason for the difference between the graphs in Figure 3.5 and in Figure 5.20.

5.2.2.4 Layer thickness

The influence of the layer thickness is tested by comparing tests that have a layer thickness of $2.5d_{n50}$ and $5d_{n50}$. These two layer thicknesses have been tested for a wave steepness of 0.01 and 0.03. The results of these tests are displayed in Figure 5.21. The results of the damage depth, E_3, are investigated first (top left image in Figure 5.21). For the wave steepness of 0.01 the difference in damage depth per wave height is very small. For the highest wave height tested for the higher layer thickness no data point is known for the layer thickness of $2.5d_{n50}$. An estimation is made for this data point. For the wave steepness of 0.03 the damage depth is smaller for the lower layer thickness than for the higher layer thickness.

According to the theory, if a wave breaks onto the slope the water volume enters the top layer of the slope. This water travels through the slope and runs down between the bottom of the top layer and the impermeable core. For a higher layer thickness, it takes a longer time to reach the bottom, because there are more voids for the water to be stored into. This reduces the energy of the water before it reaches the bottom and the destabilizing forces are smaller. If the wave period is longer each wave carries more water into the layer. This water flows down over the impermeable core and decreases the stability. For a shorter wave period the water is stored mostly inside the top layer and does not reach the bottom of the top layer, which causes the stones to be more stable.

The wave steepness (and the wave period) shows a large impact on the damage depth. For the wave steepness of 0.03 the damage depth is much smaller than for the wave steepness of 0.01. This confirms the above explained theory. For the wave steepness of 0.01 it is visible that the difference in damage depth is very small between the both layer thicknesses. The water volume that is transferred by the long waves into the top layer reaches the bottom for both the layer thickness of $2.5d_{n50}$ and $5d_{n50}$ and both decrease the stability by almost the same amount. For the wave steepness of 0.03 the results seem to deviate from the theory. It is expected that the stability is larger for the higher layer thickness, but in Figure 5.21 the data points for the higher layer thickness are above the data points for the lower layer thickness for the two higher wave heights. For the wave steepness of 0.01 the results are in line with the expectations, because for the higher wave steepness (and shorter wave period) the bottom is reached and destabilized for the smaller layer thickness and for a higher layer thickness the bottom is not reached, which gives a higher stability.

To check the influence of the damage parameter on the damage influenced by the layer thickness also other damage parameters are checked if these do comply with the theory above. First, the damage depth area is increased to a circle with a diameter of $6d_{n50}$, which gives E_6. This damage depth is obtained by a moving average over the width and length of the grid size for E_3. In this way the damage depth is doubled in diameter size and the damage is averaged over a larger area. These results are shown in the top right image in Figure 5.21. These give the same unexpected results as for E_3. For the lower layer thickness the damage is lower than for the higher layer thickness. The same results follow from investigating the results of the erosion depth, d_e (given in bottom left image in Figure 5.21). The

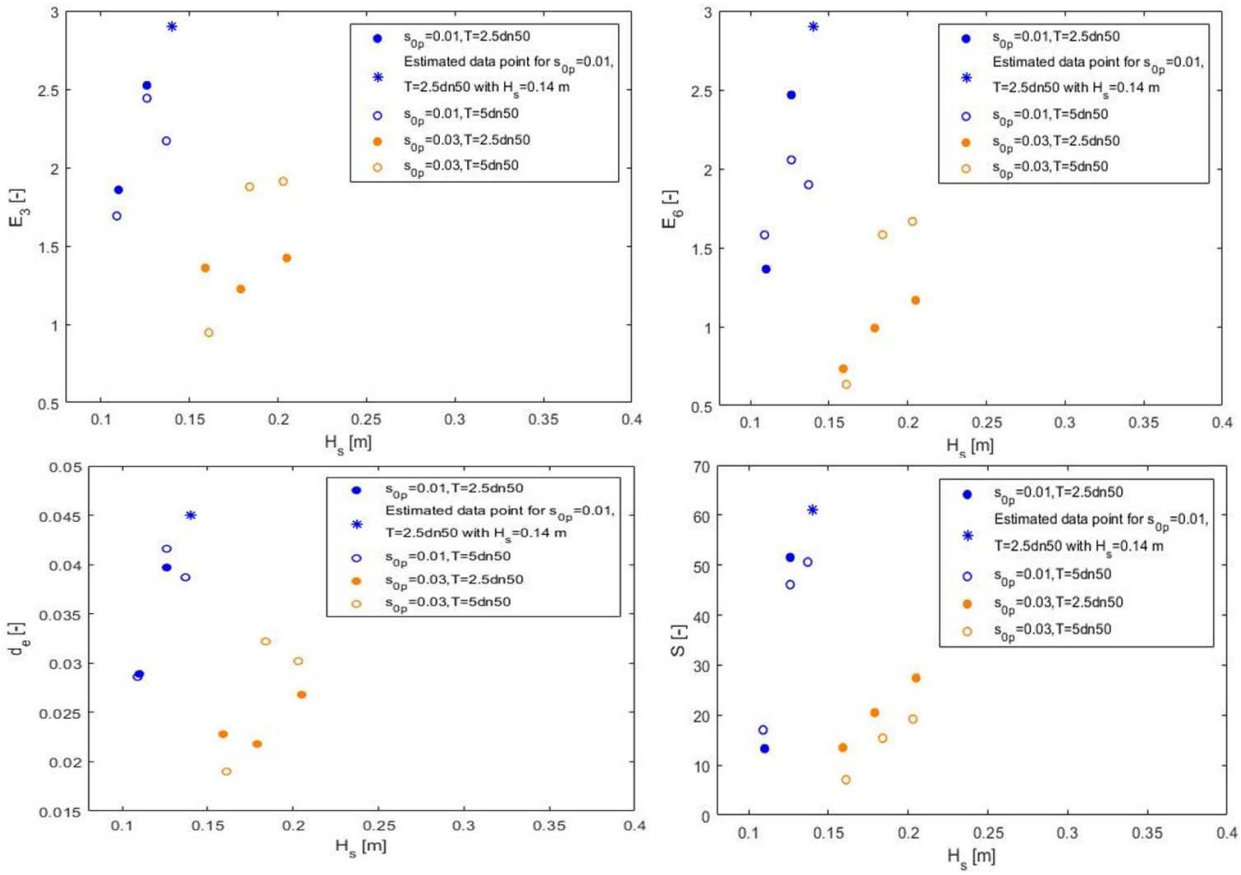

Figure 5.21: The wave height versus the damage parameters. The data points are for a wave steepness of 0.01 and 0.03 and a layer thickness of $2.5d_{n50}$ and $5d_{n50}$. The top left gives the results for the damage depth (E_3), the top right also for the damage depth (E_6), the bottom left for the erosion depth (d_e) and the bottom right for the damage level (S).

only damage parameter that complies with the theory is the damage level, S. For this parameter the damage is lower for the higher layer thickness.

To get more insight in the damage development between both layer thicknesses the profile changes are displayed in Figure 5.22. The damage for the higher layer thickness is more downslope of the SWL. The erosion is more spread over the width of the slope and is spread over a larger area in the length of the slope. This spreading of the damage over the slope can influence the development of the damage as was obtained during the tests. If the damage gets more spread the damage depth does not have to increase but the damage level does. This can explain the difference in the results obtained with the different damage parameters.

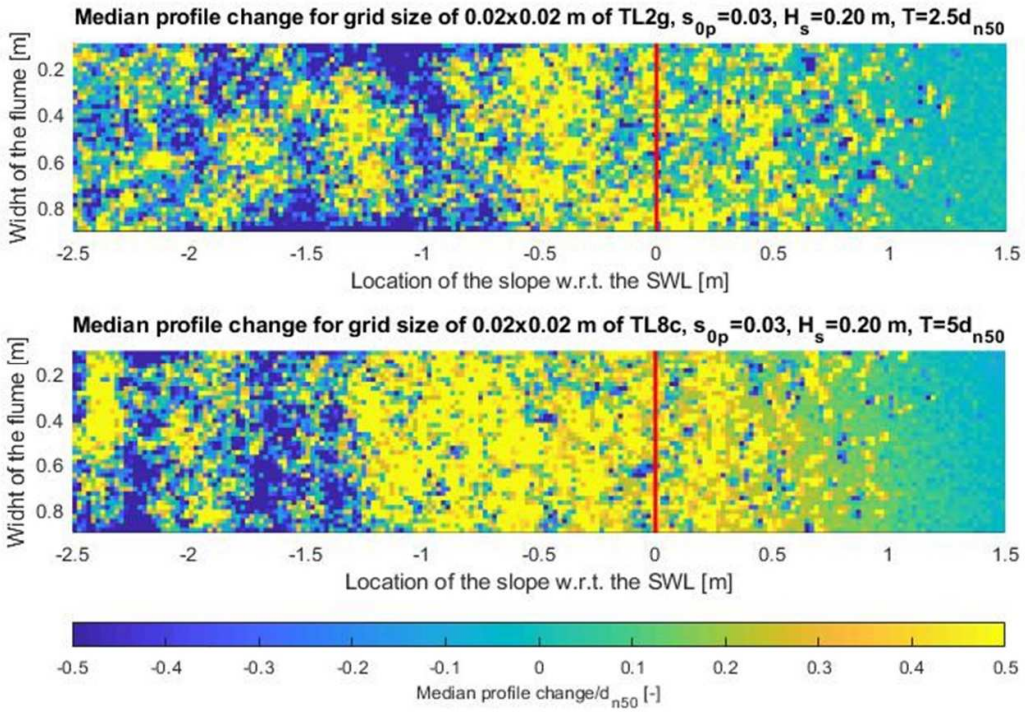

Figure 5.22: The profile change plots for tests with a different layer thickness and the same hydraulic parameters displayed for a grid size of 0.02 m.

5.2.2.5 Design stability relation with E_3

From the results in the above paragraphs the values of the damage depth for start of damage, intermediate damage and failure are determined. The start of damage is set to E_3 is 0.5. For each Iribarren number the start of damage was equal to this value. The profile change plots showed only very small damages and the overlay photos only showed a few displaced stones. The damage has started here, because the threshold for transport has been reached. Intermediate damage is set to E_3 = 1.2. For each test series after checking the profile change plots and the overlay photos this was the damage depth value that belonged to the hydraulic parameters. Failure is set to a damage depth of E_3 = 2.3. The value for failure is smaller than the layer thickness, because due to the averaging of the erosion depth for the damage depth, the filter layer could be laid bare for an average value of 2.3. Failure of the slope is only reached for the two lower Iribarren numbers. If the profile change plots and the overlay photos are checked for this damage depth, it can be said that the filter layer is laid bare and the slope has failed. The profile change plots and overlay photos are coupled to these damage parameters in Appendix H.

These values deviate from the values found by Hofland et al. (2011) for start of damage, intermediate damage and failure. For steep slopes the values are therefore different than for mild slopes.

In Figure 5.23 the stability curves are presented that belong to the damage level values given above. The stability curves are interpolated between the stability points given in Figure 5.12. These stability curves apply to the Iribarren number range of 0.45 to 1.0 for a layer thickness of $2.5d_{n50}$ and a storm duration of 1000 waves. The Van der Meer (1988) formula can be applied to a ξ_p of about 1.0. The stability of the stones has to be checked for the Iribarren numbers around 1.0, because the stability curves do not connect to each other. More physical tests have to be done with a steeper slope to test the stability of the stones in the Iribarren number range inside the grey box (in Figure 5.23).

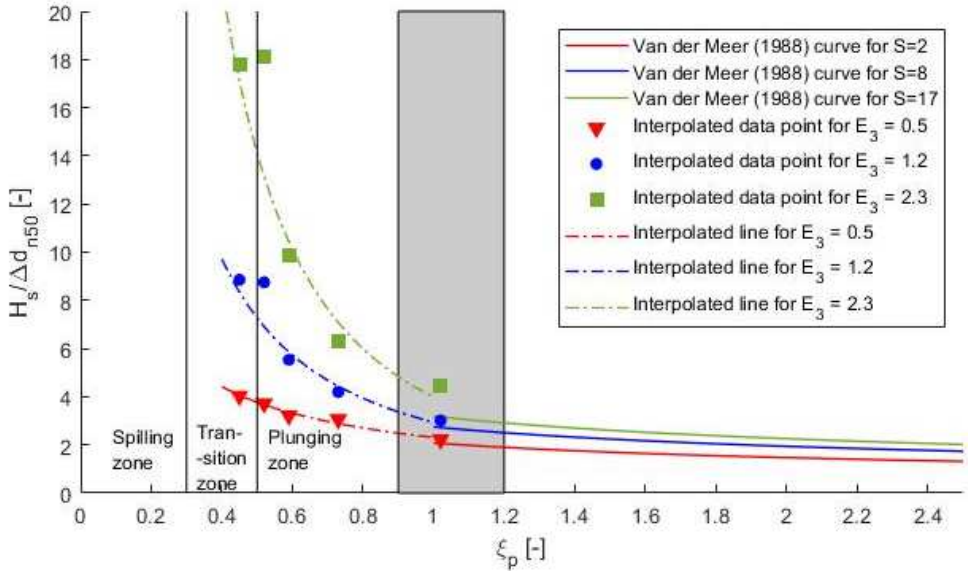

Figure 5.23: The stability curve for plunging waves of Van der Meer (1988) up to $\xi_p = 1$. From $\xi_p = 1$ the stability curve is plotted of the damage depth. The grey area is the connection area between the stability curve of Van der Meer (1988) and the stability curve for the damage depth. For this area more physical research is needed to connect the two stability curves.

It has to be clearly stated that the results of the damage depth values and the stability curves are only applicable for this slope angle, layer thickness and number of waves. The start of damage value stays the same for a higher layer thickness. The values for the intermediate damage and failure have to increase if the layer thickness increases. If the layer thickness increases the damage depth can be higher before the filter layer is laid bare and the slope has failed. For milder slopes the values are also expected to increase, because the damage is spread more over the slope.

With all the results of the tests a new stability curve is obtained. It has to be specifically stated that this stability curve can only be used for a permeability of 0.1 ($T = 2.5d_{n50}$). It can be debated if the stability curve can be used for slopes milder than tan α < 1:10. These slopes are expected to have the same type of damage spread over the slope due to the decrease in gravity force parallel to the slope. The stability curve is fitted through the data points of the tests for three parameters: E_3, ξ_p and N. These parameters showed a relation with the stability that could be expressed in a stability curve. The influence of the permeability (that changes with the layer thickness) is taken out of the stability curve, because the influence was rather unclear for the higher layer thickness. It is therefore chosen to insert the permeability as a constant and not as a parameter. The permeability constant is included in the factor of 6.1 This gives the stability formula given by Equation 5.2.

$$\frac{H_s}{\Delta d_{n50}} = 6.1 * E_3^{0.6} * \xi_p^{-1.31} * N^{-0.12} \qquad 5.2$$

The right coefficients of the parameters are obtained by fitting the curve through the data points. The root mean square error is determined from the data points by Equation 5.3. By varying the coefficients, the minimum error is obtained. The minimum error is 0.62. The coefficients that comply to the minimum error are used in the stability formula. The root mean square error of 0.62 is assumed to be adequate. The data points with a small stability number are close to the relation .The points with a higher stability number are more spread around the formula. The latter cause the root mean square error to increase. For a data point with a stability number of 6 this error of 0.62 means a relative error of 10 percent.

$$RMSE = \sqrt{\frac{\sum\left(x_{measured} - x_{formula}\right)^2}{N}} \qquad 5.3$$

The stability curve is plotted in Figure 5.24 against the data points from the physical tests. The data points of the tests are further compared to the stability curve in Appendix I. Next to the data points and the new stability curve, the 90 percent confidence bounds are also plotted in Figure 5.24. These confidence bounds show the line in between which 90 percent of all the data points are present. They indicate where the stability curve lies with a 90 percent confidence.

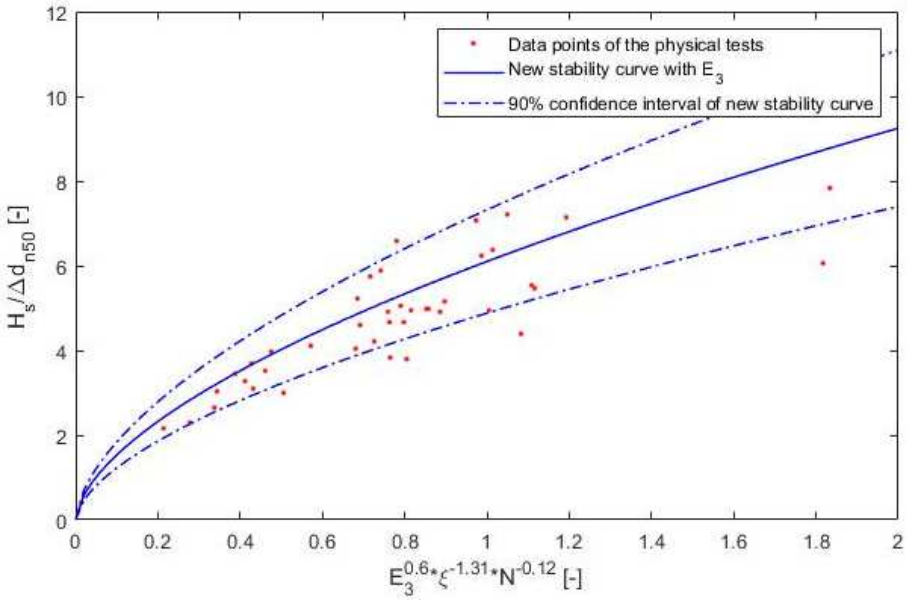

Figure 5.24: The stability curve plotted against the data points from the physical tests. The 90% confidence bounds are added to the profile. These indicate the lines in between which 90% of the data points are.

A quality of fit for the new stability formula is done with a Monte Carlo simulation. For each of the parameters in the formula a standard deviation is determined/assumed. With these values the standard deviation of the new stability formula can be determined by performing the Monte Carlo simulation. In this simulation for each parameter a random number is picked from the normal distribution for a given mean and standard deviation. This is done for every parameter and then the stability formula is calculated with these parameters. After doing this simulation 100,000 times (for statistical purposes) the standard deviation of the stability formula is obtained.

The standard deviation of the number of waves is assumed to be 1, because the wave gauges are expected not to miscount more than one wave on the time scale of these waves (1-2 seconds). The standard deviation of the slope angle is assumed to be very small, 0.001 degrees, because the construction was built with the help of a laser. The wave height and period standard deviations are assumed also to be rather small, 0.005 m and 0.01 s respectively, because the wave gauges are

calibrated and can measure the waves within millimetres and -seconds. The standard deviation of the damage depth averaged over a circle of three stone diameters is determined by checking the standard deviation of a part of the slope that should be unchanging in between the tests. This was done for the most upslope part of the slope and was on average equal to 1E-4 m. The nominal median diameter is assumed to have a standard deviation of 5E-4 m. This could be caused due to an uncertainty in the stone density and the stone diameter. From the Monte Carlo simulation then followed that for the new stability formula the standard deviation of the stability number is 0.22 for a mean value of 5.3. A summary of the standard deviations is given in Table 5.3.

Table 5.3: The standard deviations determined/assumed per parameter and a mean value needed to perform the Monte Carlo simulation.

Parameter	μ (only needed for Monte Carlo simulation)	σ	Unit
N	1000	1	-
tan α	0.1	0.001	-
H_s	0.1	0.005	m
T	1.5	0.01	s
$\langle d_e \rangle_{3d_{n50}}$	0.015	0.0001	m
d_{n50}	0.0148	0.0005	m

The standard deviation of the stability formula that is a combination of the standard deviations of all the different parameters is used to give the error bars of the data points. This indicates that every data point can deviate with 0.22 in the stability number value. The error bars are shown in the plot in Figure 5.25. Compared to the values of the stability number that belong to the data points, the error bars are rather small. The quality of the data seems therefore to be rather good, because the standard deviation is small with respect to the values of the stability number.

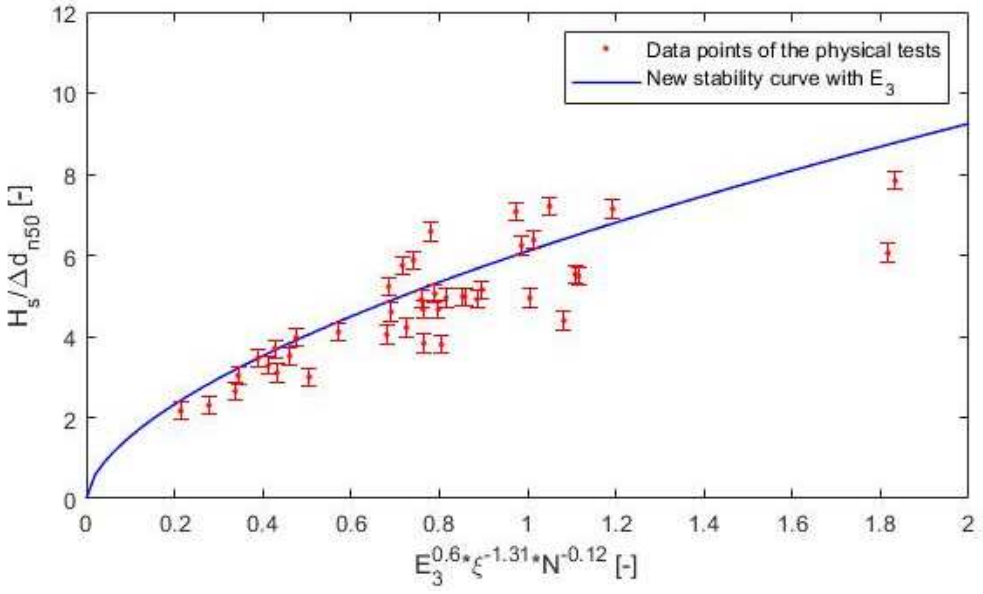

Figure 5.25: The new stability curve plotted together with the data points of the physical tests. The error bars are given per data point obtained from the standard deviation.

5.2.3 Discussion of the profile change processing and results

In this paragraph the results and the processing of the profile change data is discussed. The consequences of the choices made are elaborated and how these choices could influence the results.

The erosion profiles of mild slopes are different than for steep slopes. For steep slopes mostly one erosion hole develops. For mild slopes different smaller erosion holes develop over the length of the profile. Van der Meer (1988) determined the erosion area for the one erosion hole that develops for the steep slopes. It is unclear if for the calculation of A_e for mild slopes the total of the all areas of the mild slopes have to be taken or the area of the largest erosion hole. It is decided to take the largest erosion hole. This is a more conservative choice than smoothing the entire profile (see later paragraph). By smoothing the erosion areas, the damage level would decrease and the stability would be higher. By showing that the Van der Meer (1988) formula is already conservative by taking one erosion area it is sure that for the other choice of A_e the conclusion would be the same.

The values of the damage depth can be influenced by the way they are determined. The minimum value of the grid with $\Delta x = \Delta y = 0.04$ m is taken to be equal to the damage depth. This grid size has the same area as the circular area used for E_3 with a diameter of $3d_{n50}$. The depth of the erosion hole found by this method could be different if the grid does not overlap the erosion hole in total. If the grid only halve covers the erosion hole the damage depth is measured to be lower than the actual depth. For the damage depth that goes towards the intermediate damage the erosion holes are significantly larger than $3d_{n50}$. It is expected that for these erosion holes the erosion depths do not vary much if the grid would be shifted, because there are multiple grids that cover one erosion hole. For the damage depth of start of damage, the removal of a few stones is leading for the damage. In this case for an erosion hole with a diameter of $2\text{-}3d_{n50}$, the damage depth could be underestimated if the grid does not completely cover this erosion hole. However, from the results follows that the start of damage value is for every test almost equal and it is expected that the influence of the grid is small. It could be checked in further research what the exact influence is by taking a much smaller grid and get the maximum damage depth by a moving average over the smaller grids in the shape of a circle.

Another discussion point with respect to the damage depth is if the value taken for the minimum depth should be the average or the median value. For the grid size of 0.04 m there are about 500 points per grid. For this amount of points, it is expected that there is no difference in output if the average or the median would be taken. For a small data set the average is more influenced by the outliers than the median value. However, for this large amount of data points per grid the outliers would have been smoothed out by taking the average. Therefore, it does not matter for this data set if the median or average value is taken per grid.

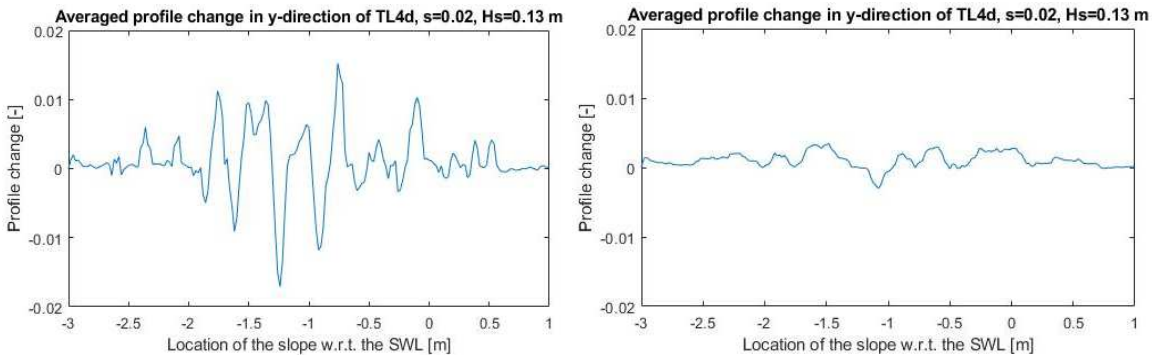

Figure 5.26: Left: The erosion profile that is only slightly smoothed with the individual erosion holes clearly visible. Right: The very smoothed erosion profile where the individual erosion holes are smoothed into one erosion hole.

To obtain the damage level of the erosion profiles the erosion profiles are a bit smoothed. The unsmoothed erosion profiles showed some noise along the profile. These small noise effects were taken out by a little smoothing. The individual erosion holes are still present, because these are typical for mild slopes. If the profiles would be smoothed a lot more these individual holes would become one shallow erosion hole. However, to detect if the filter layer is laid bare it is preferred to use the individual erosion holes. It is checked with an individual test what would happen if the erosion profile was smoothed to one large erosion hole. The difference in erosion profile is given in Figure 5.26. The damage level for the unsmoothed profile for an individual erosion hole is 6.9 and for the smoothed profile 1.8. If the smoothed profile with one erosion hole would have been used the damage level would have been underestimated with a factor 4. This confirms that the choice of taking one only slightly smoothed erosion hole was correct and not to smooth the entire profile until one erosion hole is present over the slope.

The sides of the flume experienced significantly more damage than the middle of the flume. This was caused by side effects of the flume. After measuring the flume appeared not to be exactly 1.00 m over the width. This narrowing (of a few mm) of the flume caused the waves to break earlier on the sides of the flume than in the middle of the flume. This was observed visually. Friction is not the cause of this, because friction would slow the wave down at the sides of the flume and not speed them up. To prevent this to have impact on the results, the outer 0.10 m of both sides of the flume were taken out of the data.

The standard deviation of surface elevations for an undisturbed part of the profile is determined for eight tests to see how accurate the post profiles are with respect to the pre profile. The standard deviation was taken for the upper part of the slope that was left undisturbed by the waves and the difference should be zero or very small. The standard deviation averaged over all the grids in this area varied between the 9E-5 m and 1E-4 m. This confirms that the accuracy of the measurements and processing is good enough to measure damages in O(1E-3).

5.2.4 Results of the stone transport

In this paragraph the results of the stone counting are shown to investigate the transport of the stones for different hydraulic and structural parameters. The nett transport is defined as the number of stones transported after a test from the original strip to another strip. This is equal to the erosion. The deposition is the number of stones that are added to a certain strip. The nett total transport is the deposition minus the erosion.

Table 5.4: The results of the stone counting are split up in the erosion, deposition and nett total transport per strip expressed in number of stones. Under the table the location of each strip is given with respect to the SWL.

Eroded stones per strip							
Test	Bl	R	B	P	Y	G	O
1.2a	0	0	0	6	31	9	0
1.2b	0	2	7	214	207	32	5
1.2c	6	23	213	870	420	44	14
2a	0	1	3	3	0	3	0
2b	3	2	11	13	1	7	0
2c	22	60	48	27	22	12	1
2d	54	107	100	43	28	18	3
2e	162	224	167	67	48	25	13
2f	339	379	216	93	63	37	22
3a	0	0	0	0	1	1	0
3b	0	0	0	0	2	6	0
3c	0	0	0	1	9	10	0
3d	0	0	2	4	24	22	0
3e	0	0	2	14	51	36	7
4a	0	0	0	3	25	5	0
4b	0	1	0	15	45	17	0
4c	1	5	17	87	151	38	3
4d	6	19	55	412	313	50	13
5a	0	0	0	0	3	1	0
5b	0	0	0	0	22	3	0
5c	0	0	1	0	40	19	0
5d	0	0	7	18	89	38	3
6a	0	11	8	55	50	17	9
6b	0	11	22	104	92	46	7
6c	0	13	31	174	134	85	8
6d	0	15	57	271	229	109	13
6e	0	31	86	399	333	131	12
7a	6	92	456	244	137	30	0
8a	5	37	123	141	50	34	0
8b	19	102	328	265	112	52	0

Deposited stones per strip								
Test	Bl	R	B	P	Y	G	O	Bl
1.2a	0	0	0	2	6	29	9	0
1.2b	0	0	3	34	215	180	29	6
1.2c	0	8	70	229	645	494	127	17
2a	0	0	1	3	3	0	3	0
2b	0	3	2	11	13	1	7	0
2c	0	34	56	38	23	25	14	2
2d	11	64	79	87	44	36	27	5
2e	70	148	138	149	75	63	40	23
2f	131	254	243	186	119	92	67	57
3a	0	0	0	0	0	1	1	0
3b	0	0	0	0	1	2	5	0
3c	0	0	1	1	1	7	10	0
3d	0	0	2	5	4	19	22	0
3e	0	0	5	6	9	45	38	7
4a	0	0	0	0	3	25	5	0
4b	0	0	1	0	17	45	15	0
4c	0	3	8	27	87	136	37	4
4d	0	8	38	93	263	376	72	18
5a	0	0	0	0	0	3	1	0
5b	0	0	0	0	1	22	2	0
5c	0	0	0	5	6	35	14	0
5d	0	4	2	14	20	73	39	3
6a	0	0	13	18	53	39	18	9
6b	0	3	34	35	78	75	50	7
6c	0	3	35	37	142	116	104	8
6d	0	3	42	65	228	196	144	16
6e	0	15	62	89	296	304	207	19
7a	0	8	79	390	270	179	39	0
8a	0	14	41	108	127	64	36	0
8b	0	52	96	266	227	152	83	2

Total transported stones per strip								
Test	Bl	R	B	P	Y	G	O	Bl
1.2a	0	0	0	-4	-25	20	9	0
1.2b	0	-2	-4	-180	8	148	24	6
1.2c	-6	-15	-143	-641	225	450	113	17
2a	0	-1	-2	0	3	-3	3	0
2b	-3	1	-9	-2	12	-6	7	0
2c	-22	-26	8	11	1	13	13	2
2d	-43	-43	-21	44	16	18	24	5
2e	-92	-76	-29	82	27	38	27	23
2f	-208	-125	27	93	56	55	45	57
3a	0	0	0	0	-1	0	1	0
3b	0	0	0	0	-1	-4	5	0
3c	0	0	1	0	-8	-3	10	0
3d	0	0	0	1	-20	-3	22	0
3e	0	0	3	-8	-42	9	31	7
4a	0	0	0	-3	-22	20	5	0
4b	0	-1	1	-15	-28	28	15	0
4c	-1	-2	-9	-60	-64	98	34	4
4d	-6	-11	-17	-319	-50	326	59	18
5a	0	0	0	0	-3	2	1	0
5b	0	0	0	0	-21	19	2	0
5c	0	0	0	-1	5	-34	16	14	0
5d	0	4	-5	-4	-69	35	36	3
6a	0	-11	5	-37	3	22	9	9
6b	0	-8	12	-69	-14	29	43	7
6c	0	-10	4	-137	8	31	96	8
6d	0	-12	-15	-206	-1	87	131	16
6e	0	-16	-24	-310	-37	173	195	19
7a	0	-6	-84	-377	146	133	149	39
8a	0	-5	-23	-82	-33	77	30	36
8b	0	-19	-50	-232	1	115	100	83

Bl: < -2.5 m	B: -1.5 - -2.0 m	Y: -0.5 - -1.0 m	O: 0 - 0.5 m
R: -2.0 - -2.5 m	P: -1.0 - -1.5 m	G: 0 - -0.5 m	Bl: > 0.5 m

The results of the counting are displayed in Table 5.4. The transport is split up in the erosion and deposition per strip expressed in number of stones. By subtracting the erosion from the deposition, the nett total transport of the stones per strip is determined. A negative nett total transport for a strip determines erosion for that strip. A positive value means that the strip accreted in number of stones. In Appendix J the total table is given with which stones of a certain strip moved where.

The nett total transport of the stones is displayed in Figure 5.27. These test results all have intermediate damage. It stands out that all the stones are transported upwards. The stones are eroded mostly from 1.0 m to 1.5 m below SWL, because in this strip the nett total transport of the stones is at its minimum. They are mostly transported upslope to the strip 0 to 0.5 m below the SWL. These locations of maximal erosion and deposition are for intermediate damage and failure almost equal for each hydraulic and structural parameter. Naturally, there is some spread around these locations by which the gradual almost sine-like transport graphs are formed. For the start of damage, the erosion shifts more towards 0.5 m to 1.0 m below SWL, because the waves break also closer towards the SWL due to the lower wave heights.

The nett total transport graphs should give the same erosion profiles as the erosion profiles determined with the photogrammetry (given in Appendix F). Both erosion profiles are qualitatively compared to each other per test. The erosion profiles do agree very well with each other in general. The locations of maximum damage and accretion comply between both erosion profiles. There are some differences that are caused by the inside transport in the strips. The erosion profiles determined with the photogrammetry do show these transportations and the erosion profiles by the stone counting do not due to the large strip width.

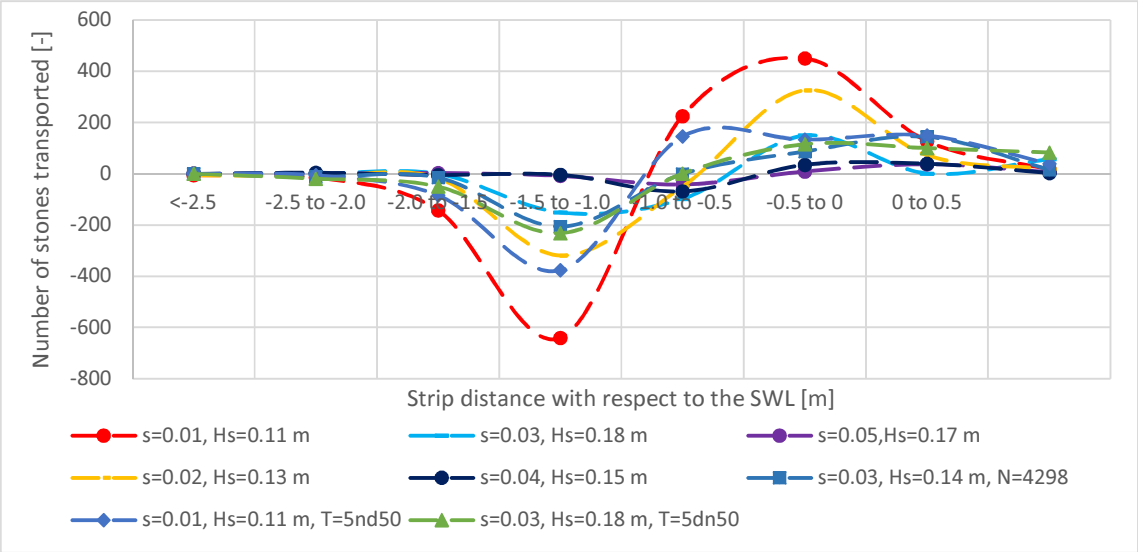

Figure 5.27: The nett total transport of the stones is plotted here. For each test series one test result for intermediate damage is given. A negative number of stones transported means erosion in that strip and a positive number means deposition.

5.2.4.1 Comparison of both erosion profile measurements

From both erosion profiles the damage parameters can be obtained. From the erosion profiles of the stone counting a damage parameter can be determined that gives the damage averaged over the strip, because only one number of transported stones is known per strip. The damage, given as the change of the height of the bed in time, can be determined by Equation 5.4. The change of the bed height is given by the nett total number of stones, the volume of the stone and the area of the strip.

$$e = \frac{\partial z_b}{\partial t} = \frac{(E - D)d_{n50}^3}{A_{strip}} \qquad 5.4$$

To compare both type of erosion profiles the same damage parameter has to be determined for the erosion profiles determined by photogrammetry. This is done by taking the average damage over the width of the strip and the slope. In Table 5.5 both results are shown for a few tests (and for the maximum eroded strip) for which the damage parameters are obtained. Both damager parameters differ very much for each test. This can be explained by the difference in the erosion profiles due to the inside transport in the strips. It follows from these damage parameters that for the strip width of 0.5 m the erosion profiles can only be compared qualitatively and not quantitatively. In order to do the last, the strip width should be much smaller than 0.5 m.

Table 5.5: The damage parameter for the stone counting and photogrammetry that is the average damage per strip area.

Test	e (stone counting) [mm]	e (photogrammetry) [mm]
TL11a	0.16	0.81
TL11b	1.17	0.06
TL4d	2.07	0.05

5.2.4.2 Spread of the eroded stones over the slope

From the stone counting follow the erosion and deposition per strip. Next to this, also the transportation lengths are determined by following the stones from their original strip to the strip they ended up after the test. These transportation lengths are only given in steps of 0.5 m. The erosion and deposition of the stones per strip of one test are displayed in Figure 5.28. A negative column means erosion and a positive column deposition. The same conclusion as in the previous paragraph can be made. The erosion is maximum in the strip 1.0 m to 1.5 m below SWL and the deposition 0 m to 0.5 m below SWL. The transportation lengths can be obtained by following the eroded stones from a strip to where they are transported and end up. Take for example the stones eroded from the purple strip. The purple stones move only for a small part downslope, about 10 percent of the total eroded stones, and for the most part upslope, by 90 percent. The maximum transportation length for the purple stones in this test is 1.5 m and for the most part the stones are transported over a length of around 0.5 m. In Appendix J the other column graphs are given of a few tests. From each graph the same conclusion can be made about the downslope and upslope transport. From Table 5.4 can be concluded that the transportation lengths differ if the wave height and steepness change. If the wave height increases the transportation length also increases due to an increase in the wave energy. If the wave steepness increases the transportation lengths decrease, because the wave energy decreases for spilling waves. For the most tests an increase in the wave height of 0.02-0.04 cm caused in increase in the transportation length of 0.5 m along the slope.

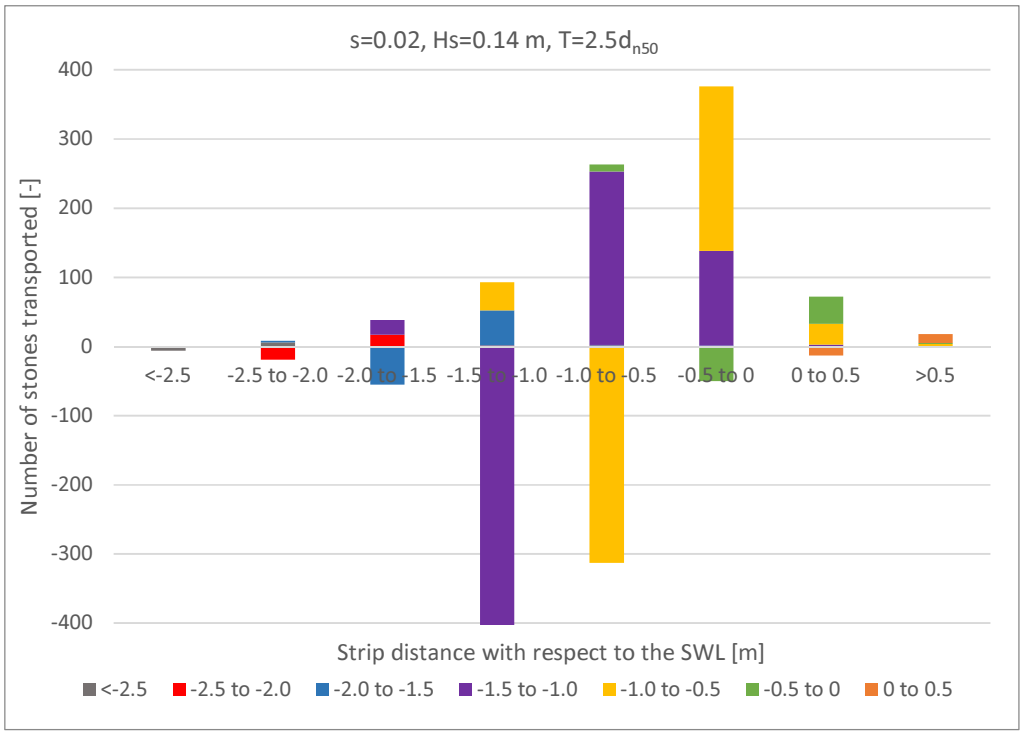

Figure 5.28: The column graph that gives the erosion and deposition per strip given in number of stones. A negative column means erosion and a positive column deposition.

5.2.4.3 Breaker type

The effect of the breaker type is shown in Figure 5.29. Per wave steepness tested the results of the transported stones are shown for the same wave height. The graphs show that the transport of the stones increases rapidly if the wave steepness decreases. This confirms the results of Paragraph 5.2.2.1 where the damage depth increases for a decreasing wave steepness, because plunging waves exert larger forces on the bottom and induce more transport.

The location of the damage for the same wave height also differs between the wave steepnesses. For the lower wave steepnesses the picking-up and lying down of the stones is shifted downslope with respect to the higher wave steepnesses. This means that plunging waves cause damage more downslope than the spilling waves. The more spilling waves occur in the spectrum the more upslope the damage occurs.

A plunging wave causes more local damage due to the plunge of the wave exerting more local forces on the stones. This plunge causes the wave to lose a lot of wave energy to turbulence and only a small amount of energy is transported upslope by the run-up. A spilling wave breaks more gradually and has more wave energy after the breaking. This gives a higher run-up of the wave and the stones that are pick up after breaking are transported further upslope than for plunging waves.

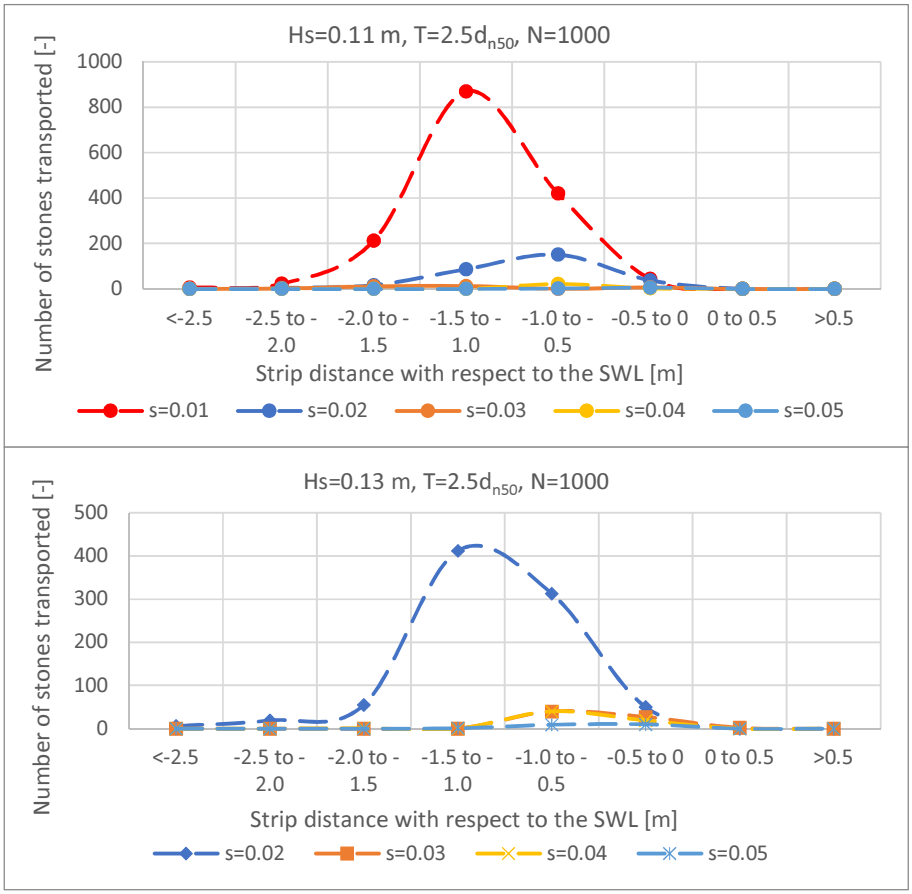

Figure 5.29: Above: the eroded stones per strip for Hs = 0.11 m for different wave steepnesses. Under: the eroded stones per strip for Hs = 0.13 m for different wave steepnesses.

5.2.4.4 Wave height

The influence of the wave height on the transportation of the strips is shown in Figure 5.30. If the wave height increases with equal steps the transport of the stones increases exponentially. All the tests gave the same results, see Appendix J for the other test results with respect to the wave height. The increase in wave height gave no difference in location of the most damage. The location where most stones were eroded for the lower wave heights was in the strip located 0.5 m to 1.0 m below SWL and for an increasing wave height shifts towards the strip located 1.0 m to 1.5 m below SWL. It was expected that the location with the most erosion goes downslope if the wave height increases. The breaker depth increases and the waves break more downslope. An increasing wave height therefore shift the location of the damage gradually more downslope and increases the number of eroded stones.

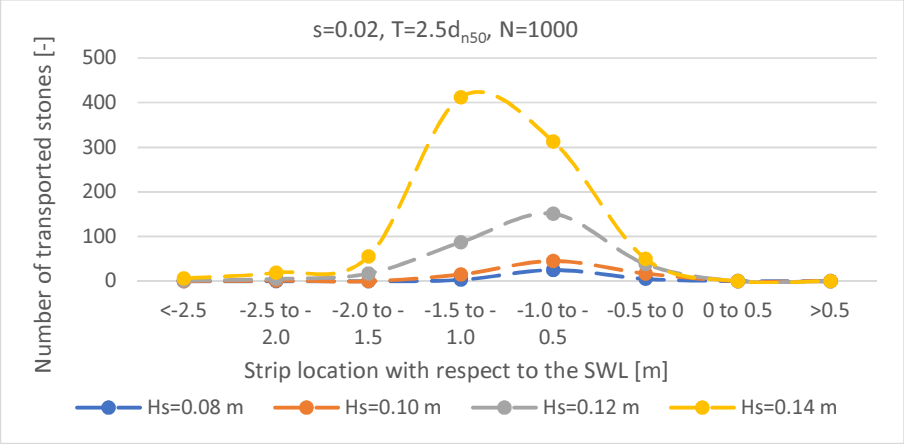

Figure 5.30: The eroded stones per strip for s=0.02 and different wave heights.

5.2.4.5 Number of waves

The stones are also counted for the test series with an increasing number of waves, see Figure 5.31 for the results. The graphs show that for each test the maximum erosion location is equal. The only difference is the amount of stones transported. This increases per increasing number of waves. These results also show a linear relationship between the amount of stones transported and the number of waves. According to Van der Meer (1988) the linear relationship ends after 500-1000 waves (see Figure 3.5) for steep slopes and an exponential relationship develops. For mild slopes this changes to a total

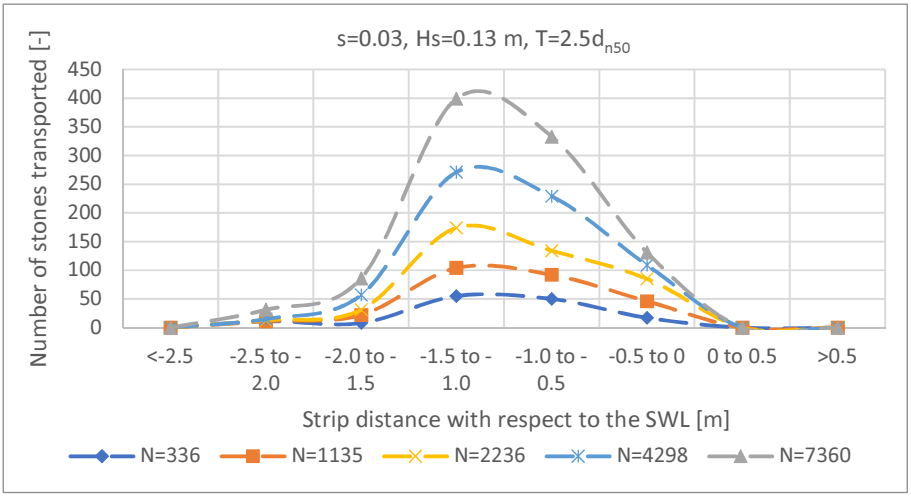

Figure 5.31: The eroded stones per strip for s=0.03 and Hs=0.13m for an increasing number of waves.

linear relationship up to 11456 waves (if the results of the profile change are also taken into account). For mild slopes there are more stones in the profile to be transported. This can cause the longer linear relationship, because for a steep slope it is less easy to transport the stones. After these stones are removed the transportation rate goes down. For mild slopes there are more stones in a given area to transport and it takes longer for the transportation rate to go down after a certain number of waves.

5.2.4.6 Layer thickness

The effect of the layer thickness is compared for the wave steepnesses of 0.01 in Figure 5.32. The tests with the different layer thicknesses of $2.5d_{n50}$ and $5d_{n50}$ are compared for the same wave height. The locations of maximum erosion are equal for both layer thicknesses. The number of stones eroded from a strip is smaller for the higher layer thickness almost by a factor of two. The wave energy is reduced more rapidly for a higher layer thickness, because the energy can be dissipated in a larger volume inside the layer.

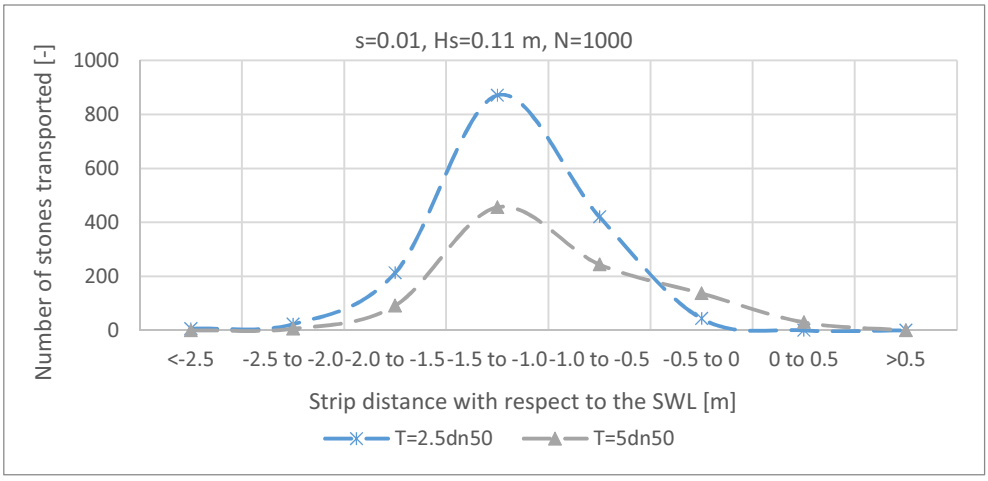

Figure 5.32: The eroded stones per strip for s=0.01 and Hs=0.11 m for a different layer thickness.

5.2.5 Discussion stone counting results

The results of the stone counting depend on the width of the strips. A smaller strip width gives a smaller underestimation of the actual transport. The transport inside the strips is counted for two tests with the same hydraulic and structural parameters. One test has a strip width of 0.25 m and the other test a width of 0.5 m. Per strip is counted how much stones are removed from their location inside the strip and how much stones are transported outside the strip. The results are given in Table 5.6. The difference between these two numbers is the stones that are transported inside the strip. For the 0.25 m strips the inside transport is less than for the 0.5 m strips. This is logical, because for the same parameters the transportation lengths are the same and the stones are transported more outside of the strip. If the inside transport of the stones is compared with the outside transport of the stones it can be concluded that a strip width of 0.25 m gives a ratio of 1:2 to 1:8 (1 to the outside transported stone means 2-8 transported stones inside the strip). A strip width of 0.5 m gives a ratio of 1:3 to 1:12. The underestimation increases for the more upslope strips, because the forces exerted on the stones get less. The waves have already dissipated their energy when the upper strips are reached and the stones are only transported for small lengths. Stones transported for these small lengths end up more likely inside the same strip.

This underestimation can be accounted for if the actual erosion or nett total transport has to be determined. If the ratio is known, this ratio can be used. The ratio has to be determined for all the tests to get a more certain parameter that can be used to predict the actual erosion or nett total transport.

To compare the results of the different tests with the same strip width the results can be used to determine the difference in stone transport if a parameter is changed. To determine the stone transport with the transportation length per stone and in steps smaller than 0.5 m the strips have to be smaller. However, for mild slopes the transport is present over a very long part of the slope and this becomes very hard to count.

Table 5.6: The transport inside the strips. For every test the inside and outside transport is counted for two or four strips (depending on the strip width). For the test with strip widths of 0.25 m two strips are added up (test 2d_sum) to compare the inside and outside transport between the two tests. Next to this, the ratios are given between the inside and outside transport per test.

Total number of stones transported inside the strip				
Strip location [m]	-0.5 to -0.25	-0.25 to 0	0 to 0.25	0.25 to 0.5
Test 2d	86	73	30	24
Test 2d_sum	131		38	
Test 6b	158		81	
Total number of stones transported outside the strip				
Strip location [m]	-0.5 to -0.25	-0.25 to 0	0 to 0.25	0.25 to 0.5
Test 2d	43	28	18	3
Test 2d_sum	43		5	
Test 6b	46		7	
Ratio of stones transported inside and outside the strip				
Strip location [m]	-0.5 to -0.25	-0.25 to 0	0 to 0.25	0.25 to 0.5
Test 2d	1:2.0	1:2.6	1:1.7	1:8.0
Test 2d_sum	1:3.0		1:7.6	
Test 6b	1:3.4		1:11.6	

5.3 Damage zones

In this paragraph the damage zones are obtained. The damage zones indicate in which areas of the slope the most damage occurs. With this knowledge, the designs of future slopes can be improved for a better protection at these areas. This can lead to more efficient designs.

The damage zones are obtained by giving the total area in which damage occurs, the area of the maximum damage and the location of the maximum erosion for every test. The damage depths are also given. The results are given in Table 5.7 for test series 1 and the results of the other test series are presented in Appendix K. The results are given by the boundaries in between which the total or maximum damages are present or by the location where the maximum damage occurred. In Figure 5.33 is shown how the boundaries and locations are determined. The total damage area is set to the total area where damage occurred. The boundaries are set to the most down- or upslope location where the erosion profile goes from erosion back to the zero line. The maximum damage area is determined in the same way for the erosion hole with the maximum erosion. The location of the maximum damage is set to the location of the maximum erosion.

The downslope boundary is defined as the boundary that is downslope with respect to the total damage area. The upslope boundary is defined as the upslope boundary with respect to the total damage area. It indicates the direction in which the boundary is laid down.

Table 5.7: In this table, the total damage area and maximum damage area are determined by giving the down- and upslope boundaries. The maximum location of the damage is also given. This are the results for test series 1. The results of the other test series are presented in Appendix K.

	Total damage area		Maximum damage area		Maximum damage	
Test	Downslope boundary [m]	Upslope boundary [m]	Downslope boundary [m]	Upslope boundary [m]	Location [m]	E_3 [-]
TL1a	-2.0	-0.2	-	-	-0.7	0.54
TL1b	-1.6	-0.3	-0.8	-0.75	-0.77	0.82
TL1c	-2.4	0.3	-1.2	-0.9	-1.0	2.00

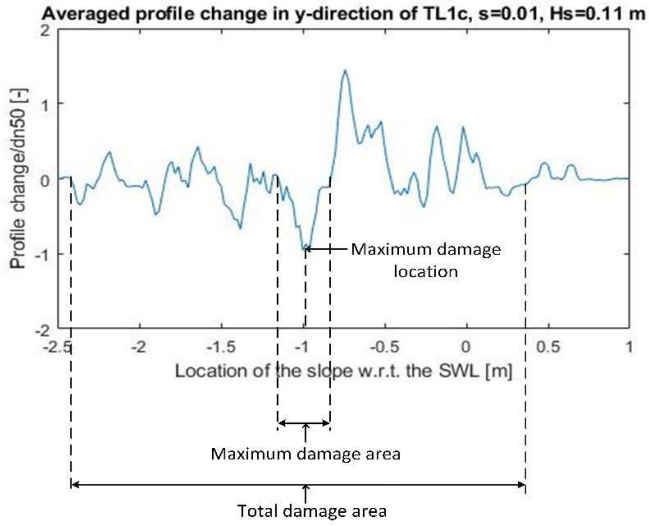

Figure 5.33: Example in which is shown how the damage areas/locations are determined.

The results of all the damage boundaries/locations are processed in boxplot graphs for the tests with a layer thickness of $2.5d_{n50}$, see Figure 5.34. From these boxplots follows that the most damage occurs in between the SWL and $-1.8H_s$. The maximum damage occurs for the most part in between $0.5H_s$ and $1.0H_s$ under the SWL.

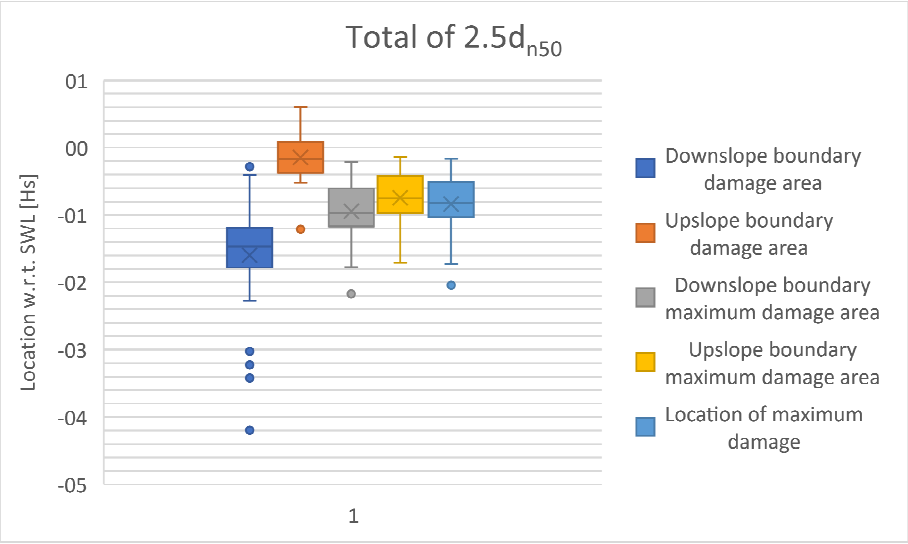

Figure 5.34: Boxplot graphs of the damage boundaries/locations for the tests with $T=2.5d_{n50}$

In Appendix K boxplot graphs for the damage areas for a layer thickness of $5d_{n50}$ are present and for the damage areas per sorted level of the damage depth. The damage depths are sorted from start of damage to intermediate damage and failure. By this sorting it can be investigated where the damage areas occur per level of damage depth.

In Figure 5.35 the results are displayed that follow from all the boxplots for the tests with a layer thickness of $2.5d_{n50}$. The dark areas give the areas in which the maximum damage is most likely to occur. These are determined with the first and third quartiles of the boxplot of the location of the maximum damage. The lighter areas give the areas in which damage occurs. These are determined with the first quartile of the upslope boundary and the third quartile of the downslope boundary. In Figure 5.35 can be seen that if the level of the damage depth is below failure the damage occurs mostly between the SWL and $-1.9H_s$. The location of maximum damage does not shift very much in between all the levels of the damage depth. If the slope has failed, the damage is more spread over the slope and shifted more downslope. This can be explained by the higher waves breaking more downslope and causing damage over a wider area of the slope.

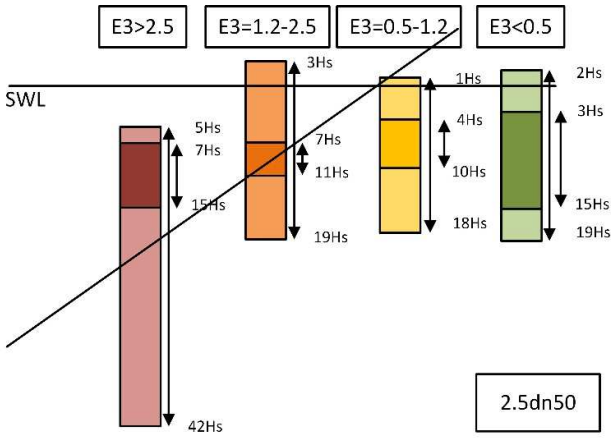

Figure 5.35: The damage zones per level of the damage depth for the layer thickness of $2.5d_{n50}$. The damage zones are expressed in Hs with respect to the SWL. The dark areas give the areas in which the maximum damage is most likely to occur. These are determined with the first and third quartiles of the boxplot of the location of the maximum damage. The lighter areas give the areas in which damage occurs. These are determined with the first quartile of the upslope boundary and the third quartile of the downslope boundary.

In Figure 5.36 are the results shown of the damage zones for all the tests, divided between the layer thickness of $2.5d_{n50}$ and $5d_{n50}$. This shows that the area in which damage occurs is almost the same in between both the layer thicknesses. The most damage occurs in between the SWL and $-2.0H_s$. The location of maximum damage differs slightly between the different layer thicknesses. For the higher

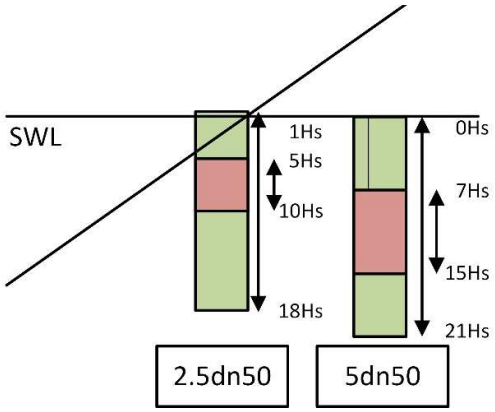

Figure 5.36: The damage zones per layer thickness. In green the areas in which the damage occurs mostly and in red the areas in which the maximum damage occurs mostly.

layer thickness the location of maximum damage shift downslope by 0.2-0.5H_s. An explanation could be that the lower waves that break more upslope do not induce a lot of damage, because their energy can still be dissipated into the higher layer thickness. For the higher waves that break more downslope, this energy cannot be dissipated enough by the layer to prevent damage and damage occurs. For the lower layer thickness, the energy can be dissipated less into the layer. The lower waves, that break more upslope, already cause damage with their amount of energy. The higher waves do also cause damage but these occur less often. Therefore, the maximum damage for the lower layer thickness is more upslope than for the higher layer thickness.

6 Conclusions and recommendations

The conclusions and recommendations following from the results are elaborated in this chapter. The conclusions are given in Paragraph 6.1. The recommendations are written down in Paragraph 6.2.

6.1 Conclusions

The research subquestions are answered in Paragraph 6.1.1 and help to answer the main research question. The conclusion of the main research question is given in Paragraph 6.1.2.

6.1.1 Research questions

The subquestions are answered separately in this paragraph with the help of the results in Chapter 5. The subquestions themselves help to answer the main research question.

1. **Which damage output parameter fits the static stability description of mild slopes the most?**

Three damage parameters were compared and obtained from the erosion profiles.

- **Damage level, S:** the damage level should not be used for mild slopes. The parameter is defined by the erosion area. For mild slopes this cannot give a good indication of the depth of the erosion hole. A mild slope has a much larger area of wave attack if compared to steep slopes. This means that the erosion area is also large. However, while this gives a high damage level the erosion depth can still be small. From the test results follows that the damage level does not give a clear distinction between the different types of breaking for the smaller damage levels also due to the definition. Both these arguments give the conclusion that the damage level is not representative for the damage of mild slopes.
- **Erosion depth, d_e:** the erosion depth is very sensitive to the removal of a single stone. Thus, a high value of the erosion depth does not have to be representative for high damage of the slope. The erosion depth can only be used if the d_{n50} and the layer thickness are known before anything can be concluded about the amount of damage. The stability curve showed a large outlier due to the very slow development of the erosion depth for a wave steepness of 0.04. These results conclude that the erosion depth should not be used to describe the damage of mild slopes.
- **Damage depth, $E_{(3D,)3}$:** the damage depth uses an averaged erosion depth and is therefore less sensitive to the removal of a single stone. The stability curve shows good results with no outliers. From the results start of damage and failure can be distinguished. Thus, the damage depth is the damage parameter that fits the static stability description of mild slopes the most. The most important advantage of the damage depth is the averaging of the erosion depth. Therefore, the above conclusion would be the same for damage depths averaged over a larger area.

2. **What is the difference in stability for the different types of breaking of the waves?**

- The conclusion is that for mild slopes with only plunging and spilling breakers the stability increases if the percentage of spilling breakers in the wave spectrum increases. The wave spectrums with plunging waves cause more damage to the profile than the wave spectrums that include a larger percentage of spilling waves. The stability is therefore lower for plunging waves. For Iribarren numbers lower than 0.5 the damage development does not change for an even lower Iribarren number. In other words: the plunging breaker induces a low stability of the stones. Thus, if more spilling breakers are present in the wave spectrum the stability of the stones increases.
- For the start of movement, the type of breaker is of less influence. This point was for the different breaker types around the same value. For failure the breaker type is of much more influence. For plunging waves, a slight increase of wave height is enough to go from start of movement to failure. For spectra with more spilling waves the wave height has to increase by more than 300 percent to cause failure.

- There is also a difference in the stability for the same Iribarren number but a different slope. The same type of plunging breaking in Iribarren number gives a higher stability on milder slopes.

3. **What is the relation between the significant wave height and the stability?**

- It can be concluded that the influence of the significant wave height over the damage depends on the Iribarren number but in general an increase in wave height means an increase in damage. By the trendlines given in Figure 6.1 can be concluded that a decrease in Iribarren number decreases the influence of the wave height over the damage. For the plunging waves the influence of the wave height is very high. A small increase in wave height means a high increase in damage. If more spilling breakers are present the influence of the wave height over the damage decreases. A large increase in wave height means only a small increase in damage.
- The significant wave height influences the transportation length of the eroded stones. If the wave height is increased the transportation lengths also increases. The amount of increase depends on the wave steepness and on the original location of the stone along the slope. The more downslope eroded stones are transported further than the more upslope eroded stones due to the decrease in wave energy during the wave breaking.

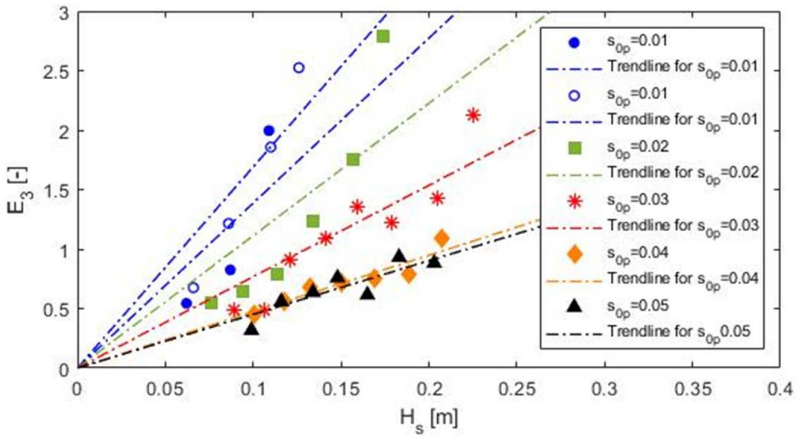

Figure 6.1: The wave height versus the damage depth per wave steepness with their trendlines.

4. **How does the stability of the stones on the slope develop with an increasing number of waves?**

- A conclusion about the development of the stability for an increasing number of waves cannot be given with certainty. The test results show a trendline that up to 11,000 waves the relationship between the damage depth and the number of waves is still linear. This is due to only small changes in the slope angle and the amount of stones available for transport when compared to steep slopes. However, the results showed some unexpected results in the data points. Thus, more physical tests have to be performed to investigate the development of the stability of stones on mild slopes with an increasing number of waves.
- The number of stones eroded increases linearly with respect to an increase of the number of waves.

5. **How is the stability of the stones influenced by a different layer thickness of the structure?**

- The stability of the stones is influenced by a layer thickness of $2.5d_{n50}$ and $5d_{n50}$. For an Iribarren number of 1, the difference in stability between these two layer thicknesses is very small, slightly more stable for the layer thickness of $5d_{n50}$. For the lower Iribarren number the results of the influence of the layer thickness on the stability were also quite unexpected, because the stability was higher for the layer thickness of $2.5d_{n50}$. The same conclusion was made for all the damage parameters obtained during the testing, except the damage level. Thus, more

physical tests have to be performed to investigate the development of the stability of stones on mild slopes with an increasing layer thickness.
- It can be concluded that a higher layer thickness of $2.5d_{n50}$ gives a small decrease in the total number of stones eroded for both the wave steepness of 0.01 and 0.03.

6. **What is the difference in movement of the stones for the different types of breaking of the waves?**

- The movement of the stones is followed by the counting of the transported stones from coloured strips. The conclusion is that the higher Iribarren numbers result in a lot more erosion than the lower Iribarren numbers. For the same wave height, the difference in the number of transported stones is a factor of 10-100 per decrease in wave steepness of 0.01.
- It can also be concluded that for every wave height, Iribarren number and storm duration, the main direction of the transport is upslope by 90 percent of the eroded stones. The plunging breaking waves have a transportation path that is more downslope than for the spilling breakers.
- The transportation length is different between the types of breaking. For an equal wave height, the stones are transported less far if the percentage of spilling breakers increases in the wave spectrum. For the most tests an increase in the wave height of 0.02-0.04 cm caused in increase in the transportation length of 0.5 m along the slope.

7. **How does the stability curve of the physical tests of this research compares to the stability curves of Van der Meer (1988)?**

The results of the physical tests for mild slopes are compared with the Van der Meer (1988) formula of plunging. It can be concluded that the Van der Meer (1988) formula for plunging waves is conservative for the design of mild slopes for an Iribarren number below 1. All the data points show a higher stability per Iribarren number than the formula states. It is therefore advised not to use the Van der Meer (1988) formulae for mild slopes. For mild slopes the stability of the stones can better be predicted by using the stability formula that includes the damage depth, given in Equation 5.2. This formula gives for the Iribarren range tested with spilling and plunging waves, a higher stability for the stones on mild slopes compared to Van der Meer (1988).

6.1.2 Main research question

How to describe the static stability of stones on mild slopes under wave attack?

- From the physical tests it is concluded that the stability of stones on mild slopes under wave attack could be described by the local damage depth, $E_{3D,3}$. With this damage depth the stability curves are determined for start of damage, $E_3 = 0.5$, intermediate damage, $E_3 = 1.2$ and failure, $E_3 = 2.3$, see Appendix H. These values are applicable for a layer thickness of $2.5d_{n50}$.
- A new stability formula that includes the damage depth is empirically determined from the results of the physical tests. The formula is given in Equation 6.1 and plotted against the data points in Figure 6.2. The formula is applicable in the Iribarren number range of 0.45 to 1.0 for a layer thickness of $2.5d_{n50}$ and a storm duration of 1000 waves. The slope angle used for the tests was tan α = 1:10. The stability formula can be used for slopes milder than 1:10, because the erosion profile stays equal. More physical tests need to be executed to determine the application range of the stability formula for slopes milder than tan α = 1:10. The stability formula of Van der Meer (1988) should be used for situations with an Iribarren number higher than 1.0.

$$\frac{H_s}{\Delta d_{n50}} = 6.1 * E_3^{0.6} * \xi_p^{-1.31} * N^{-0.12} \qquad 6.1$$

- The stability of the stones is directly influenced by the breaker type and the significant wave height. It can be concluded that the breaker type has the most influence on the damage. For the plunging waves the significant wave height is also very dominant in the amount of damage. However, if more spilling breakers occur in the wave spectrum the significant wave height becomes less dominant. Slopes milder than tan α = 1:10 induce more spilling breakers in the spectrum and are expected to become even less affected by the wave height.

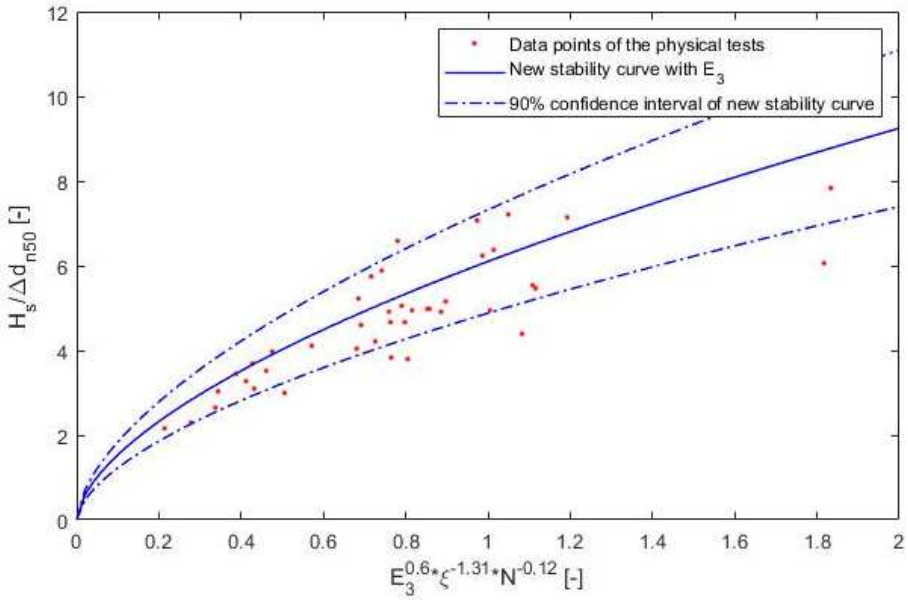

Figure 6.2: The stability curve plotted against the data points from the physical tests. The 90% confidence bounds are added to the profile. These indicate the lines in between which 90% of the data points are.

6.2 Recommendations

From the research done follow some recommendations for further research. These recommendations are stated below.

- More physical tests have to be done to investigate the stability of the stones around the Iribarren number of 1.0. Then the stability curve of Van der Meer (1988) and the stability curves based on the damage depth can be connected to each other. This should be tested with a slope angle in between 1:6 and 1:10 to fill up the gap between the tested slopes of 1:6 (Van der Meer (1988)) and 1:10 (this research). The slope angle should give a different profile than the steep and mild slopes develop.
  Also, a slope milder than the 1:10 is recommended to test to investigate the stability for milder slopes. The slope should be able to give Iribarren numbers that give only spilling waves. Then a stability relationship can be developed for the whole range of the Iribarren number.
  For tests with a lower Iribarren number are higher waves needed for the same parameters used in these tests to receive failure of the slope. It should be checked if the possibilities of the wave flume comply with this.
- The influence of the layer thickness should be investigated further. The results of the two test series with a higher layer thickness are not enough to give a clear relation between the increase of the layer thickness. Mild gravel beaches are built with layer thicknesses up to 10-20d_{n50}. It is therefore recommended to do future tests with layer thickness varying from 5 to 20d_{n50} for different hydraulic parameters.
- In a new research can together with future test results a better applicable stability formula be developed to design gravel beaches. This formula has to take into account all the elements

tested. From the test results of this research is gathered a lot of information for a design formula. However, there have to be done tests for other slope angles to be able to fully describe spectrum of the Iribarren numbers possible for gravel beaches. If this data is known a design formula can be developed that is applicable to all gravel beaches.

- To couple the empirical relations derived in this research with more physical relations more research has to be done in which the velocities and accelerations are derived at the bottom. This can be done with the BIV/PIV measurements as used by Kramer (2016). These physical relations can be implemented in a numerical model like XBeach-G.
- The data received with the physical tests is not all processed to gather the results. It is recommended to check the data, because a lot of information can be taken out of this. There are made videos of the breaking of the waves together with the transport of the stones from under water. This can couple the location of the wave breaking to the location of the transport of the stones. It also shows when the stones are transported if a breaking wave passes and the difference in stone transport between the up- and downward forces of the waves.

Acknowledgements

The financial contribution by the TKI project "Dynamica van waterbouwkundige constructies, fase 2", for facilitating the physical model tests at Deltares and the supervision by participants, is acknowledged.

List of symbols

Symbol	Description	Unit	Symbol	Description	Unit
a	Acceleration	m/s^2	$H_{1/3}$	Highest one third of the wave heights	m
A_B	Exposed stone surface area	m^2	H_{max}	Maximum wave height	m
A_e	Cross-sectional erosion area	m^2	H_s	Significant wave height	m
C_B	Bulk coefficient	-	K_D	Empirical coefficient	-
C_F	Friction coefficient	-	l_e	Erosion length	m
C_M	Acceleration coefficient	-	L	Wavelength	m
d	Stone diameter	m	L_0	Deep-water wavelength	m
d_*	Dimensionless stone diameter	-	M, m	Mass of the stone	kg
d_{15}	Stone diameter with 15% passing	m	M_{50}	Median mass	kg
d_{50}	Median stone diameter	m	n	Number of displaced stones	-
d_{85}	Stone diameter with 85% passing	m	N	Number of waves	-
d_e	Erosion depth	m	P	Notional permeability	-
d_{n50}	Nominal median stone diameter	m	Re_*	Particle Reynolds number	-
E	Dimensionless damage depth	-	S	Damage level	-
E_{wave}	Wave energy	J/m^2	s_{0p}	Fictious wave steepness based on the peak period	-
E_{2D}	Dimensionless damage depth averaged over the width of the slope	-	t	Time	s
E_3	Dimensionless damage depth averaged over a circle of three stone diameters	-	T	Layer thickness	m
$E_{3D,m}$	Dimensionless damage depth taken at location of maximum damage averaged over a circle of m stone diameters	-	T	Wave period	s
f_{peak}	Peak frequency	1/s	T_m	Mean wave period	s
F_{acc}	Accelerating force	N	$T_{m-1,0}$	Spectral wave period	s
F_B	Bulk force	N	T_p	Peak wave period	s
F_D	Drag force	N	u	Flow velocity	m/s
F_F	Friction force	N	u_{*c}	Critical bed shear velocity	m/s
F_G	Gravitational force	N	u_b	Near-bed flow velocity	m/s
F_L	Lift force	N	u_c	Critical flow velocity	m/s
F_S	Shear force	N	V	Volume	m^3
g	Gravitational acceleration	m/s^2	W	Weight force	N
h	Depth	m	W_{strip}	Strip width	m
h_b	Breaker depth	m	X_{nm}	Distance between n^{th} and m^{th} probe	m
H	Wave height	m	z	Eroded profile height w.r.t. the reference level	m
H_0	Deep-water wave height	m	z_0	Initial profile height w.r.t. the reference level	m
$H_{1\%}$	Highest 1% of the wave heights	m			

Symbol	Description	Unit	Symbol	Description	Unit
α	Slope angle	°	ρ_s	Density of stone	kg/m^3
β	Angle of resultant force	°	ρ_w	Density of water	kg/m^3
γ_b	Breaker index	-	ϕ	Internal friction angle	°
Δ	Relative density	-	ν	Kinematic viscosity	m^2/s
ψ_{cr}	Critical Shields parameter	-	ξ_m	Breaker parameter with mean period	-
τ_{cr}	Critical bottom shear stress	N/m^2	$\xi_{(0)p}$	Breaker parameter with peak period	-
ρ	Density	kg/m^3			

Abbreviations

SWL Still Water Level
NLSWE Non-Linear Shallow Water Equations

List of figures

List of tables

References

AquaPublications. (2015). *Modelling Package Update 2015: Engineering tools and databases on Sediment Transport and Morphology.* Retrieved January 29, 2019, from https://www.aquapublications.nl/page2.html

Bagnold, R. A. (1966). An approach to the sediment transport problem from general physics. *Geological Survey Professional Paper 422-1*.

Battjes, J. (1974). *Computation of set-up, longshore currents, run-up and overtopping due to wind-generated waves.* PhD Thesis, Delft: Delft University of Technology.

Bertin, S., Friedrich, H., Delmas, P., Chan, E., & Gimel'farb, G. (2014). Digital stereo photogrammetry for grain-scale monitoring of fluvial surfaces: Error evaluation and workflow optimisation. *ISPRS Journal of Photogrammetry and Remote Sensing*, 193-208.

Bezuyen, K. G., Stive, M. J., Vaes, G. J., Vrijling, J. K., & Zitman, T. J. (2007). *Inleiding waterbouwkunde.* Delft: VSSD.

Broderick L, & Ahrens , J. P. (1982). *Rip-rap stability scale effects.* Fort Belvoir, Virginia: U.S. Army Coastal Engineering Research Center.

CIRIA, CUR, & CETMEF. (2007). *The Rock Manual. The use of rock in hydraulic engineering (2nd edition).* London: CIRIA C683.

Dai, Y. B., & Kamel, A. M. (1969). *Scale effects tests for rubble-mound breakwaters.* Washington D.C.: U.S. Army Engineer Waterways Experiment Station.

De Almeida Sousa, E. (2017). *Damage Characterisation of Rock Armoured Slopes.* MSc Thesis, Delft: Delft University of Technology.

De Almeida Sousa, E., Van Gent, M. R., & Hofland, B. (2019). Damage characterization of rock slopes. *Journal of Marine Science and Engineering, volume 7, issue 1*.

Frostick, L. E., McLelland, S. J., & Mercer, T. G. (2011). *Users Guide to Physical Modelling and Experimentation.* Boca Raton: CRC Press.

GIS Resources. (2019). *Basics of Photogrammatry*. Retrieved May 8, 2019, from http://www.gisresources.com/basic-of-photogrammetry_2/

Grote, W. (1994). *Protection of outfall structures.* MSc Thesis, Delft: Delft University of Technology.

Hardisty, J., Collier, J., & Hamilton, D. (1984). A calibration of the Bagnold beach equation. *Marine Geology 61*, 95-101.

Higuera, P., Lara, J. L., & Losada, I. J. (2013). Realistic wave generation and active wave absorption for Navier-Stokes models Application to OpenFOAM®. *Coastal Engineering, volume 71*, 102-118.

Hoan, N. T., Stive, M. J., Booij, R., Hofland, B., & Verhagen, H. J. (2011). Stone Stability in Non-uniform Flow. *Journal of Hydraulic Engineering, volume 137, issue 9*.

Hofland, B. (2005). *Rock & Roll: Turbulence-induced damage to granular bed protections.* PhD Thesis, Delft: Delft University of Technology.

Hofland, B., Raaijmakers, T., Van Gent, M. R., & Liefhebber, F. (2013). Damage evaluation using the damage depth. *Proceedings of the 6th International Conference: Coastal Structures 2011*, 812-823.

Holthuijsen, L. (2007). *Waves in Oceanic and Coastal Water.* Cambridge: Cambridge University Press.

HR Wallingford. (2016). *Modelling shingle beaches in bimodal seas.* Retrieved January 30, 2019, from http://www.channelcoast.org/shingleb/Final_Report_CAS1227-RT002-R01-00.pdf

Hudson, R. Y. (1959). Laboratory investigations of rubble-mound breakwaters. *Journal of the Waterways and Harbors Division (ASCE), proc. paper 2171*, 93-121.

Iglesias, G., Rabuñal, J., Losada, M. A., Pachón, H., Castro, A., & Carballo, R. (2006). A virtual laboratory for stability tests of rubble-mound breakwaters. *Ocean Engineering, Volume 35, Issues 11-12*, 1113-1120.

IH2VOF. (2019). *IH2VOF: Physics*. Retrieved January 29, 2019, from IHCantabria: http://ih2vof.ihcantabria.com

Iribarren, R. (1938). *Una fórmula para el calculo de los diques de escollera [A formula for the calculation of rock-filled dikes].* Madrid: Revista de Obras Públicas. Translated by D. Heinrich, Berkeley: Fluid Mechanical Laboratory, University of California.

ISEC. (n.d.). *ISEC Model Repository Contributed Models*. Retrieved January 28, 2019, from http://isec.nacse.org/models/

Izbash, S. (1935). *Construction of Dams by Dumping Stones into Flowing Water.* Eastport, Maine: US Engineering Office, War Department/Scientific Research Institute of Hydrotechnics.

Jennings, R., & Shulmeister, J. (2001). A field based classification scheme for gravel beaches. *Marine Geology, Volume 186, Issues 3-4*, 211-228.

Johnson, B. D., Kobayashi, N., & Gravens, M. B. (2012). *Cross-Shore Numerical Model CSHORE for Waves, Currents, Sediment Transport and Beach Profile Evolution.* Washington D.C.: US Army Corps of Engineers.

Jumelet, H. D. (2010). *The influence of core permeability on armour layer stability.* MSc Thesis, Delft: Delft University of Technology.

Kobayashi, N. (2016). Coastal Sediment Transport Modeling for Engineering Applications. *Journal of Waterway, Port, Coastal, and Ocean Engineering, volume 142, issue 6*.

Koster, M. J. (1990). Static stability of loose materials under wave attack: New design formulae and probabilistic approach. *Proc. "Current problems of coastal hydrotechnics on the Bulgarian Black Sea Coast".* Varna.

Kramer, R. (2016). *Stability of rock on mild slopes under wave attack.* MSc Thesis, Delft: Delft University of Technology.

Lara, J. L., Losada, I. J., & Liu, P. L.-F. (2006). *Breaking waves over a mild gravel slope: Experimental and numerical analysis.* Journal of Geophysical research, 111, C11019.

Leica Geosystems AG. (2017). *Leica ScanStation P30/40.* Retrieved January 30, 2019, from https://w3.leica-geosystems.com/downloads123/hds/hds/general/brochures-datasheet/Leica_ScanStation_P30-P40_Plant_DS_en.pdf

Li, L., Pattiaratchi, C. B., & Masselink, G. (2001). BeachWin: modelling groundwater effects on swash sediment transport and beach profile changes. *Environmental Modelling & Software, Volume 17, Issue 3*, 313-320.

Mansard, E. P., & Funke, E. R. (1980). The Measurement of Incident and Reflected Spectra Using a Least squares Method. *Coastal Engineering Proceedings, 1(17)*, 8.

McCall, R. T. (2015). *Process-based modelling of storm impacts on gravel coasts.* PhD Thesis, Plymouth: Plymouth University.

Melby, J., & Kobayashi, N. (1998). Progression and variability of damage on rubble mound breakwaters. *Journal of Waterway, Port, Coastal and Ocean Engineering, 124(6)*, 286-294.

Mendonça, A., Juana Fortes, C., Capitão, R., da Graça Neves, M., Moura, T., & Simão Antunes do Carmo, J. (2012). Wave hydrodynamics around a multi-funtional artificial reef at Leirosa. *Journal of Coastal Conservation, 16(4)*, 543-553.

Miche, M. (1944). *Mouvements ondulatoires de la mer en profondeur constante ou décroissante.* Paris: École nationale des ponts et chaussées.

Nielsen, P. (2002). Shear stress and sediment transport calculations for swash zone modelling. *Coastal Engineering Proceedings, 45(1)*, 53-60.

Postma, M. G. (2016). *XBeach-G as a Design Tool for Rock on mild slopes under wave loading.* MSc Thesis, Delft: Delft University of Technology.

Rance, P. J., & Warren , N. F. (1968). The threshold of movement of coarse material in oscillatory flow. *Proceedings of the 11th Conference on Coastal Engineering*, 487–491.

Riegl. (2017). *Long Range, High Speed 3D Terrestrial Laser Scanner with Online Waveform Processing.* Retrieved January 29, 2019, from https://www.3dlasermapping.com/wp-content/uploads/2017/10/DataSheet_VZ-2000_2017-06-07.pdf

Schiereck, G. J., & Verhagen, H. J. (2016). *Introduction to bed, bank and shore protection (2nd edition).* Delft: Delft Academic Press/VSSD.

Schiereck, G. J., Fontijn, H. L., Grote, W. V., & Sistermans, P. G. (1994). Stability of rock on beaches. *Coastal Engineering Proceedings, 1(24)*.

Schiereck, G., & Fontijn, H. (1996). Pipeline protection in the surfzone. *Coastal Engineering Proceedings, 1(25)*, 4228-4241.

Shen, Y., Lindenbergh, R. C., Hofland, B., & Kramer, R. (2017). Change analysis of laser scans of laboratory rock slopes subject to wave attack testing. *ISPRS Annals of the Photogrammetry, Remote Sensing and Spatial Information Sciences, volume IV-2/W4*, 139-147.

Shields, A. (1936). *Application of similarity principles and turbulence research to bed-load movement.* PhD Thesis, Pasadena, California: Soil Conservation Service, Cooperative Laboratory, California Institute of Technology.

Sistermans, P. (1993). *Stability of rock on beaches.* MSc Thesis, Delft: Delft University of Technology.

Sleath, J. F. (1978). Measurements of bed load in oscillatory flow. *Journal of the Waterway, Port, Coastal and Ocean Division, 104(3)*, 291–307.

Terrile, E. (2004). *The threshold of motion of coarse sediment particles by regular non-breaking waves.* MSc Thesis, Delft: Delft University of Technology.

Thompson, D. M., & Shuttler, R. M. (1975). *Riprap design for wind-wave attack, a laboratory study in random waves.* Wallingford: HR Wallingford.

Tromp, M. (2004). *Influences of fluid accelerations on the threshold of motion.* MSc Thesis, Delft: Delft University of Technology.

USACE. (2015). *Coastal Engineering Manual - Part II.* Retrieved January 7, 2019, from Plainwater: http://www.plainwater.com/pubs/EM-1110-2-1100P2.pdf

Van den Berg, I. (2018). *Effect of irregularities in the under layer on the stability of XblocPlus concrete armour unit.* MSc Thesis, Delft: Delft University of Technology.

Van den Bos, J. P. (2006). *Design of granular near-bed structures in waves and currents.* MSc Thesis, Delft: Delft University of Technology.

Van der Meer, J. W. (1988). *Rock Slopes and Gravel Beaches under Wave Attack.* PhD Thesis, Delft: Delft University of Technology.

Van der Plas, T., Van der Meer, J., Ripoll Dominguez, E., & Bijl, E. (2017). Stability of very wide graded material, designed as breakwater core, under wave attack. *Proc. ICE Coasts, Marine Structures and Breakwaters.* Liverpool.

Van Eeden, F. (2017). *SWASH: A robust numerical model for shallow water coastal engineering applications.* MSc Thesis, Stellenbosch: University of Stellenbosch.

Van Hijum, E. (1974). Equilibrium profiles of coarse material under wave attack. *Coastal Engineering Proceedings, Volume 1(14)*, 939-957.

Van Rijn, L. C. (2007). Unified view of sediment transport by currents and waves. I: Initiation of motion, bed roughness, and bed load transport. *Journal of Hydraulic Engineering, 133(6)*, 649-667.

Van Rijn, L. C. (2010). *Modelling erosion of gravel/shingle beaches and barriers.* Retrieved January 28, 2019, from http://www.conscience-eu.net/documents/deliverable13b-modelling.pdf

Van Rijn, L. C., & Sutherland, J. (2011). Erosion of gravel barriers and beaches. *Proceedings of the Coastal Sediments 2011*, 2019-2032.

Vellinga, P. (1982). Beach and dune erosion during storm surges. *Coastal Engineering, volume 6, issue 4*, 361-387.

Wendt, E. (2017). *Stability of stones on mild slopes.* MSc Thesis, Delft: Delft University of Technology.

Wenneker, I., & Hofland, B. (2014). *Optimal wave gauge spacings for separation of incoming and reflected waves.* Delft: Deltares.

Wit, M. (2015). *Stability of Gravel on Mild Slopes in Breaking Waves.* MSc Thesis, Delft: Delft University of Technology.

Wolters, G., Van Gent, M. R., Allsop, W., Hamm, L., & Muhlestein, D. (2009). HYDRALAB III: Guidelines for physical model testing of rubble mound breakwaters. *Coasts, Marine Structures and Breakwaters.* Edinburgh: Institution of Civil Engineers - ICE.

Ye, L. (1996). *Stability of rock on beaches.* MSc Thesis, Delft: Delft University of Technology.

Appendix A: Numerical modelling

To make a choice between physical and numerical modelling the possibilities of numerical modelling need to be investigated. In this chapter, the existing models are referenced with an elaboration why the model can or cannot be used for the modelling of the forces on the bed of mild slopes under wave attack. At first, the specifications for the models to comply with are written down. Then each model is checked if it complies with the specifications.

A.1 Specifications for "ideal" numerical model

In this paragraph the specifications are set out which the models have to comply with. The specifications are set with respect to the waves, the flow and the sediment transport.

A.1.1 Waves

The waves need to be modelled for storm events, because storm events are the normative situations for failure of the structure. Wave breaking has to be implemented in the model to model the local velocity and acceleration on the bed. The flow velocity and acceleration exert forces on the bed which destabilize the stones on the bed. These forces consist of the drag, lift and shear force. There are two types of breaking that need to be modelled which are the plunging and spilling type. These two types need to be modelled, because these are the breaking types that occur on mild slopes.

A.1.2 Flow

The flow needs to be representative with the local velocity and acceleration near the bed. The velocity and acceleration need to be calculated for multiple layers over the depth. For a depth-averaged flow is the local flow near the bed overestimated and will the stability of the bed be underestimated. Therefore, the depth needs to be divided in multiple layers, because than the local velocity and acceleration near the bed can be modelled. The velocity and acceleration following from the wave breaking at the surface need to be translated through these layers to the local velocity and acceleration near the bed.

A.1.3 Sediment transport

The inclusion of sediment transport in the model is needed to check the stability of the bed for wave breaking. The bed has to consist of stones, which can be transported if they are destabilized by the local velocity and acceleration. The transportation of the stones leads to a new bed profile and determines if the structures fails or not.

A.2 Models

There are various types of models to numerically model waves approaching a shoreline. There are conceptual, empirical, parametric and process-based models. Conceptual models only qualitatively describe the process and the situation. Empirical and parametric models are calibrated with existing data. They have no or limited physical basis in the formulas. Process-based models are based on the underlying physics. This is the type of model that has the preference for this research.

Process-based models can be distinguished in wave resolving and wave-averaged models. Wave resolving models model each wave and the response of the model for each wave. They are developed for situations with man-made structures which may not deform. Wave-averaged models average a certain number of waves and then calculate the response of the model. They are based on already existing formulae for sandy beaches (Postma, 2016).

The different summaries of the models are presented in the following paragraphs. At the end a conclusion of the applicability of the models is given. In Table A.1 each of the models is summarized

for their hydro- and morphodynamics, if they are able to model breaking waves and a flow for multiple layer and their (dis)advantages.

A.2.1 SWASH (Simulating WAves till SHore)

SWASH is a wave resolving and process-based model. The waves are simulated with the non-linear shallow water equations (NLSWE) with non-hydrostatic pressure. In the NLSWE are the mass and momentum balance included that follow from the Reynolds-averaged Navier-Stokes (RANS) equations. A turbulence model is also included to approximate the dissipation and (turbulent) mixing in the water due to the wave breaking.

The NLSWE are capable of simulating the overall characteristics of a quasi-steady breaking bore in the surf zone. A jump-discontinuity develops in which energy is lost by turbulence and the wave height decreases. This does not require additional measures to account for wave-breaking processes or to keep track of energy dissipation. A high resolution of about 20 layers in horizontal and vertical direction is needed. Naturally, the wave front becomes turbulent and overturns or spills along the front face. The bore front is stabilized to a quasi-steady bore by downward transport of momentum due to turbulent stresses. This downward transport is not accounted for in the model. Instead the wave steepness increases till a jump-discontinuity develops. For this reason, SWASH cannot simulate the breaking of the waves for the plunging and spilling breaker, because they cannot be simulated correctly in the free surface of the water. Therefore, the forces on the slope are assumed not to be entirely correct to describe the stability of stones on mild slopes. The model can simulate turbulence over the vertical by vertical mixing and at the wave breaking process (Van Eeden, 2017).

The water area is divided in several layers for which each layer is described with these equations. Therefore, the model can accurately describe the processes over the depth.

M. Zijlema (personal communication, January 10, 2019) explained that SWASH only describes the waves, the flow and their interaction with the slope. The slope can only be modelled as a static impermeable slope and is constant through the test. Morphological updating of the bed is not included in the model, because there is no sediment transport.

Concluding, the model is able to describe the forces in the flow for multiple layers. However, the breaking process is not correctly modelled for plunging breakers. For mild slopes, the flow forces are not correct and there is no sediment (transport) included in the model.

A.2.2 OpenFOAM (Open Field Operation And Manipulation)

OpenFOAM is a wave resolving and process-based model. The model describes the flow and the waves with the 3D Reynolds averaged Navier-Stokes equations. The flow velocities and the pressure are linked. The model includes bed and suspended transport in the flow, but there is no response of the immobile bed.

Wave breaking can be modelled correctly by OpenFOAM, because it is possible to model the free surface in detail. The wave breaking is correct for smooth and refined bathymetry. Modelling of spilling and plunging breakers is possible.

OpenFOAM is still under development. The model is not able to model porous structures. It can only model impervious structures. The model in his current state of development is already able to describe the free surface very accurately. The physical background is the largest of all the other present models. However, the disadvantage of the RANS approach for the detailed free surface is that the calculation time is very high and therefore it is very costly to do tests with this model for the scope of this research (Higuera, Lara, & Losada, 2013).

A.2.3 XBeach-G

XBeach-G(ravel) is a 1D process-based and wave resolving model specialized for gravel slopes. The model solves the waves and depth-averaged currents. These currents do interact with the sediment on the slopes and with the groundwater. Exchange between the surface and groundwater is due to pressure differences. The input in the model is the significant wave height, the peak period, the water depth, the storm duration, the spectrum type, the stone diameter, the stone density, the slope, the pre-profile, the hydraulic conductivity and the thickness/composition of the base and underlayers. The output is the post-profile from which the damage can be concluded (Postma, 2016).

The surface water is solved with the non-linear shallow water equations including non-hydrostatic pressure and groundwater exchange. Spilling and plunging breakers can be simulated in XBeach-G. The groundwater is modelled with conservation of mass, equations of motion and parameterisation of non-hydrostatic groundwater pressure. The exchange between the surface and groundwater is by submarine exchange which is modelled by in- and exfiltration according to the Darcy-Forchheimer model (McCall, 2015).

According to Postma (2016), XBeach-G is not accurate for mild slopes, because with the Van Rijn (2007) method the shear stress is ten times higher than compared to physical data and modelling with the sediment transport formula of Nielsen (2006) is incorrect due to a lack of feedback to the hydrodynamics. The Shields values found from the tests were very high. There is also an incorrect slope correction factor for coarse material, because the translation from morphodynamics to hydrodynamics is incorrect as well. The local hydrodynamics at the surface and near the bed are not available, because the model is a one-layer model. This means that the output for waves and flow are depth-averaged. The forces on the bottom are therefore too high and there is more transport than in reality. Lastly, the surface- groundwater exchange is not correctly implemented in the model.

A.2.4 IH-2VOF model (IH-Cantabria)

IH-2VOF is a wave resolving and process-based model. The model solves the flow in 2D for hybrid domains with the Navier-Stokes equations outside (Reynolds averaged) and inside the porous medium (volume averaged). It gives insight in relevant physical parameters like friction coefficients. The free surface is modelled by applying the Volume of Fluid technique and turbulence by applying a non-linear k-ε turbulence model. IH-2VOF can model porous models but does not include sediment transport. Wave breaking is possible to model but requires a high vertical solution which makes the model computationally expensive. The model has multiple layers in horizontal and vertical direction (IH2VOF, 2019).

A.2.5 COBRAS (Cornell breaking waves and structures)

COBRAS is a wave resolving and process-based model. The waves and flow are solved with the volume-averaged and Reynold-averaged Navier-Stokes equations. The model is able to solve wave breaking for plunging and spilling breakers. The flow velocity on the bottom is modelled incorrectly, because the local bottom induced flows disrupt the flow near the bed. The in physical tests observed high frequency velocity oscillations cannot be modelled in the numerical experiments. The undertow velocities are underestimated inside the surfzone, especially for the plunging waves. Sediment transport is not included in the model (Lara, Losada, & Liu, 2006).

A.2.6 Coulwave

Coulwave is a wave resolving and process-based model (Postma, 2016). The NLSWE are included with some weakly dispersive Boussinesq wave type equations (ISEC, n.d.). Sediment transport is implemented by the Meyer-Peter and Mueller equations. Groundwater processes are not included.

Coulwave can model nearshore, wave-driven hydrodynamic processes for a depth-averaged flow. The spatial details are in the order of 1 m and therefore this model is too rough for the scope of this research. The energy dissipation due to wave breaking is modelled by an eddy viscosity term into the momentum equations on the front face of the breaking waves. Due to the Boussinesq equations overturning of the crest cannot be modelled (Mendonça, et al., 2012).

A.2.7 Beachwin

BeachWin is a wave resolving and process-based model (Postma, 2016). The waves and flow are solved by the NLSWE over a depth-averaged flow and the groundwater flow by the Darcy law. Sediment transport is modelled by the model of Bagnold (1966) and Hardisty (1984). Wave breaking is not included (Li, Pattiaratchi, & Masselink, 2001).

A.2.8 CSHORE

CSHORE is a wave averaged and probabilistic model (Postma, 2016). It predicts temporal changes of the armour layer profile and the hydraulic response such as wave overtopping and transmission. Permeable layers are possible. Not very accurate, but robust and versatile. The model can be used for the prediction of wave run-up, reflection, overtopping, transmission and armour layer damage on entire rubble mound structures of arbitrary geometry located on a beach with(out) a bar (Kobayashi, 2015). In CSHORE the time-averaged cross-shore continuity and momentum equations are derived from the NLSWE. CSHORE is able to model the bed load sediment transport with the quasi-steady application of the formula of Meyer-Peter and Mueller (Johnson, Kobayashi, & Gravens, 2012). The wave energy dissipation due to wave breaking is modelled with roller energy equations. The model is depth-averaged. The model does not include swash-zone processes or groundwater interactions (McCall, 2015).

A.2.9 Shingle-B

Shingle-B is a wave averaged parametric model in which the sediment transport is modelled with a regression model. A study has been done with a mobile bed flume with different bimodal wave spectra by which the model is calibrated. The model predicts the changes to gravel beaches based on the input conditions. The slope is modelled with different empirical formulas that are fitted to the real slope. In the empirical formulas are the wave input parameters taken into account that change the slope. This method is apparently not very accurate when validated with the reality, because the results of the model do not agree with reality for situations different than to which the model was calibrated (HR Wallingford, 2016).

A.2.10 CROSMOR2008

CROSMOR2008 is a process-based model with a wave by wave approach (Postma, 2016). Model for computation of cross-shore and longshore sand transport rates and morphological changes along coastal profiles during storms. Groundwater processes are not included. The model is depth-averaged (AquaPublications, 2015). The wave energy equations are solved for each individual wave. There are no detailed swash processes, but this is schematized by introducing an onshore directed time-averaged effective swash velocity (Van Rijn, Modelling erosion of gravel/shingle beaches and barriers, 2010). Sediment transport is based on the TRANSPOR2004 formulations of Van Rijn. Wave breaking is modelled by the wave energy dissipation. The output of the model is a slope change in 2D in the cross-shore view (Van Rijn & Sutherland, Erosion of gravel barriers and beaches, 2011).

A.3 Conclusion

Currently, there is no model which can correctly model the velocities and accelerations (the forces) on the bottom at the breaking point. The models which are depth-averaged cannot be used, because they

overestimate the forces on the bed. The models that cannot simulate the plunging breaking waves correctly cannot be used, because they cannot give the local forces on the bed that correspond to the local forces in reality. OpenFOAM and IH-2VOF are the only models that have multiple layers and can model plunging breaking waves. However, at this moment these models are very time consuming for modelling the plunging wave, because the free surface is very difficult to model for each grid. Next to this, both models do not include sediment transport and morphological updating of the bed.

Therefore, it can be concluded that none of the model are applicable to model the forces on the slope at breaking point correctly or within the short time of the research.

Table A.1: Overview of the models with the hydrodynamics, morphodynamics, the breaking of the waves, the availability of multiple layers and the (dis)advantages.

Model	Hydrodynamics	Morphodynamics	Breaking waves	Multiple layers	(Dis)advantages	Reference
SWASH	Wave resolving and process-based model. The non-linear shallow water equations (NLSWE) with the mass and momentum balance from the Reynolds-averaged Navier-Stokes (RANS) equations with non-hydrostatic pressure.	The slope is impermeable and constant. No sediment is included in the model, so no exchange between the slope and the flow.	Plunging waves are simulated by a jump-discontinuity. Breaking of the waves is simulated by shock capturing. A turbulence model is included to approximate dissipation and (turbulent) mixing due to wave breaking.	Multiple layers in horizontal and vertical direction.	+ Forces on the bottom. + Efficient calculation time. - No correct breaking simulation of the waves. - No sediment transport.	Van Eeden, 2017.
OpenFOAM	Wave resolving and process-based model. 3D Reynolds-averaged Navier-Stokes equations with continuity and mass conservation. Link between pressure and velocity.	Bed and suspended load. No response of the bed (immobile bed).	Correct modelling of wave breaking for smooth and refined bathymetry. Modelling of overturning waves possible. Requires high vertical resolution which makes them computationally expensive.	Multiple layers in horizontal and vertical direction.	+ Correct modelling of free surface and breaking. - Very time consuming due to long calculation time of the free surface. - Immobile bed, so no slope changes.	Higuera, et al., 2013.
XBeach-G	Wave resolving and process-based model. Surface water: NLSWE. Mass and momentum balance with non-hydrostatic pressure term and groundwater exchange.	Nielsen transport formula and Van Rijn transport formula. Bed shear stress by drag and inertia terms. Shields for the critical shear stress.	Simulates spilling and plunging waves.	Depth averaged. Only vertical grids.	+ Mobile bed, so damage output. - Depth averaged. Too large forces on the bed.	Postma, 2016, McCall, 2015.

Model	Hydrodynamics	Morphodynamics	Breaking waves	Multiple layers	(Dis)advantages	Reference
IH-2VOF	Wave resolving and process-based model. 2D Reynolds-averaged Navier-Stokes equations in the fluid domain and Volume-averaged RANS in the porous domain. Free surface by applying the Volume of Fluid technique.	Can have porous structures implemented in the model. No sediment transport included in the model.	Modelling of overturning waves possible. Requires high vertical resolution which makes them computationally expensive.	Multiple layers in horizontal and vertical direction.	+ Gives insight in relevant physical parameters like friction coefficients. - For plunging waves very time consuming. - No sediment transport and no slope changes.	IH2VOF, 2019.
COBRAS	Wave resolving and process-based model. Volume-averaged and Reynolds-averaged Navier-Stokes (VARANS) equation.	No sediment transport included in the model.	Plunging and spilling breakers. Velocity incorrect near the bottom, correct near SWL. No high frequency velocity oscillations in the model. Undertow velocities are underestimated.	Depth averaged.	- Depth averaged. - No sediment transport. - Velocities near bottom and undertow not correctly modelled.	Lara, Losada, & Liu, 2005.
Coulwave	Wave resolving model. NLSWE and some Boussinesq wave type equations. No groundwater processes.	Meyer-Peter and Müller transport equation.	Energy dissipation due to wave breaking by an eddy viscosity term into the momentum equations on front face of the breaking waves. Overturning of the crest during breaking cannot occur in a Boussinesq-model.	Depth-averaged.	+ Friction factor for uprush and backwash. - Depth-averaged. - No plunging breaking.	Postma, 2016, ISEC, n.d., Mendonça, et al., 2010.
BeachWin	Wave resolving and process-based model. NLSWE and groundwater flow in 2D with Darcy law.	Model of Bagnold (1966) and Hardisty (1984).	No wave breaking.	Depth-averaged.	- Depth-averaged. - No wave breaking.	Postma, 2016, Li, Pattiaratchi, & Masselink, 2001.
CSHORE	Wave averaged and probabilistic model. Time-averaged cross-shore continuity and momentum equations derived from the NLSW wave equations.	Bed load sediment transport. Quasi-steady application of the formula of Meyer-Peter and Mueller.	Wave energy dissipation due to wave breaking. Roller energy equations.	Depth-averaged.	+ Permeable layer possible. - No swash-zone processes or groundwater interactions. - Depth averaged.	Postma, 2016, McCall, 2015, Johnson, Kobayashi & Gravens, 2012.

Model	Hydrodynamics	Morphodynamics	Breaking waves	Multiple layers	(Dis)advantages	Reference
Shingle-B	Wave averaged parametric model.	Regression model.	No breaking waves.	Depth-averaged.	- Only for calibrated situations. - No wave breaking.	HR Wallingford, 2016.
CROSMOR-2008	Wave-by-wave solving and process-based model. Solving wave energy equation for each individual wave.	Sediment transport based on TRANSPOR2004 formulations of Van Rijn (2006, 2007). Bed load and suspended load sediment.	No swash processes but represented as an effective onshore-directed swash velocity. Wave energy dissipation due to wave breaking.	Depth-averaged.	+ For computation of cross-shore and longshore sand transport rates and morphological changes along coastal profiles during storms. - No groundwater processes. - Depth averaged.	Van Rijn & Sutherland, 2011, Van Rijn, 2010, Aqua-Publications, 2015.

Appendix B: Overview of all the tests

In the tables below is an overview given of every test series and individual test with the corresponding parameters. The constant parameters are given in a table separate from the variable parameters, see Table B.1. The tables with the variable parameters include the input and output values. There are three types of tests executed in this research. First, the response of the slope is tested to wave height and steepness, see Table B.2. Secondly, the damage development is tested for an increasing number of waves, see Table B.3. At last, the response of the slope is tested for a higher layer thickness of the stones, see Table B.4. All the tests are done with irregular waves.

Table B.1: An overview of the constant parameters of test series 1 to 5.

Test series	tan α [-]	h [m]	d_{n50} [mm]	D [-]	ρ_s [kg/m^3]	ρ_w [kg/m^3]	Δ [-]
TL1	0.1	0.75	14.8	$2.5d_{n50}$	2944	1000	1.94
TL11	0.1	0.75	14.8	$2.5d_{n50}$	2944	1000	1.94
TL2	0.1	0.75	14.8	$2.5d_{n50}$	2944	1000	1.94
TL3	0.1	0.75	14.8	$2.5d_{n50}$	2944	1000	1.94
TL4	0.1	0.75	14.8	$2.5d_{n50}$	2944	1000	1.94
TL5	0.1	0.75	14.8	$2.5d_{n50}$	2944	1000	1.94
TL6	0.1	0.75	14.8	$2.5d_{n50}$	2944	1000	1.94
TL7	0.1	0.75	14.8	$5d_{n50}$	2944	1000	1.94
TL8	0.1	0.75	14.8	$5d_{n50}$	2944	1000	1.94

Table B.2: An overview of the in- and output of the variable parameters used for test series 1 to 5.

Input parameters						
Test	s_{0p} [-]	ξ_p [-]	N [-]	H_s [m]	L_0 [m]	T_p [s]
TL1a	0.01	1.0	1000	0.07	7.00	2.1
TL1b	0.01	1.0	1000	0.09	9.00	2.4
TL1c	0.01	1.0	1000	0.11	11.00	2.7
TL11a	0.01	1.0	1000	0.07	7.00	2.1
TL11b	0.01	1.0	1000	0.09	9.00	2.4
TL11c	0.01	1.0	1000	0.11	11.00	2.7
TL11d	0.01	1.0	1000	0.13	13.00	2.9
TL2a	0.03	0.58	1000	0.09	3.00	1.4
TL2b	0.03	0.58	1000	0.11	3.67	1.5
TL2c	0.03	0.58	1000	0.13	4.33	1.7
TL2d	0.03	0.58	1000	0.15	5.00	1.8
TL2e	0.03	0.58	1000	0.17	5.67	1.9
TL2f	0.03	0.58	1000	0.19	6.33	2.0
TL2g	0.03	0.58	1000	0.21	7.00	2.1
TL2h	0.03	0.58	1000	0.23	7.67	2.2
TL3a	0.05	0.45	1000	0.10	2.00	1.1
TL3b	0.05	0.45	1000	0.12	2.40	1.2
TL3c	0.05	0.45	1000	0.14	2.80	1.3
TL3d	0.05	0.45	1000	0.16	3.20	1.4
TL3e	0.05	0.45	1000	0.18	3.60	1.5
TL3f	0.05	0.45	1000	0.20	4.00	1.6
TL3g	0.05	0.45	1000	0.22	4.40	1.7

Input parameters						
Test	s_{0p} [-]	ξ_p [-]	N [-]	H_s [m]	L_0 [m]	T_p [s]
TL4a	0.02	0.71	1000	0.08	4.00	1.6
TL4b	0.02	0.71	1000	0.10	5.00	1.8
TL4c	0.02	0.71	1000	0.12	6.00	2.0
TL4d	0.02	0.71	1000	0.14	7.00	2.1
TL4e	0.02	0.71	1000	0.16	8.00	2.3
TL4f	0.02	0.71	1000	0.18	9.00	2.4
TL5a	0.04	0.50	1000	0.10	2.50	1.3
TL5b	0.04	0.50	1000	0.12	3.00	1.4
TL5c	0.04	0.50	1000	0.14	3.50	1.5
TL5d	0.04	0.50	1000	0.16	4.00	1.6
TL5e	0.04	0.50	1000	0.18	4.50	1.7
TL5f	0.04	0.50	1000	0.20	5.00	1.8
TL5g	0.04	0.50	1000	0.22	5.50	1.9

Output parameters									
Test	s_{0p} [-]	ξ_p [-]	N [-]	$H_{1/3}$ [m]	H_{m0} [m]	H_{max} [m]	L_0 [m]	T_p [s]	$T_{m-1,0}$ [s]
TL1a	0.009	1.05	1390	0.062	0.065	0.138	6.89	2.10	1.875
TL1b	0.010	0.99	1332	0.090	0.090	0.164	8.85	2.38	2.131
TL1c	0.010	1.01	1381	0.113	0.113	0.216	11.63	2.73	2.317
TL11a	0.010	1.01	1196	0.066	0.069	0.136	7.02	2.12	1.872
TL11b	0.010	1.00	1216	0.086	0.089	0.160	8.95	2.39	2.132
TL11c	0.010	1.02	1200	0.11	0.112	0.188	11.66	2.73	2.363
TL11d	0.010	0.99	1273	0.126	0.127	0.236	12.37	2.82	2.465
TL2a	0.031	0.57	837	0.089	0.094	0.159	3.00	1.39	1.272
TL2b	0.033	0.55	1241	0.106	0.112	0.210	3.38	1.47	1.347
TL2c	0.028	0.59	1211	0.121	0.127	0.220	4.46	1.69	1.512
TL2d	0.030	0.58	1277	0.141	0.146	0.259	4.94	1.78	1.616
TL2e	0.030	0.58	1253	0.159	0.166	0.275	5.60	1.89	1.714
TL2f	0.029	0.59	1254	0.179	0.185	0.328	6.43	2.03	1.805
TL2g	0.030	0.57	1246	0.205	0.210	0.344	6.91	2.10	1.897
TL2h	0.032	0.56	1252	0.225	0.230	0.362	7.24	2.15	1.979
TL3a	0.054	0.43	964	0.099	0.104	0.151	1.92	1.11	1.058
TL3b	0.054	0.43	1005	0.116	0.120	0.197	2.24	1.20	1.138
TL3c	0.052	0.44	1037	0.134	0.138	0.220	2.65	1.30	1.224
TL3d	0.053	0.43	1024	0.148	0.159	0.236	2.99	1.38	1.305
TL3e	0.050	0.45	1043	0.165	0.172	0.272	3.41	1.48	1.392
TL3f	0.045	0.47	1066	0.183	0.189	0.291	4.19	1.64	1.486
TL3g	0.046	0.46	1044	0.203	0.211	0.320	4.56	1.71	1.583
TL4a	0.019	0.73	1152	0.076	0.079	0.148	4.20	1.64	1.418
TL4b	0.020	0.71	1164	0.094	0.099	0.180	4.94	1.78	1.596
TL4c	0.018	0.75	1140	0.114	0.120	0.209	6.67	2.07	1.792
TL4d	0.020	0.70	1168	0.134	0.141	0.244	6.99	2.12	1.888
TL4e	0.019	0.72	1139	0.157	0.162	0.279	8.37	2.32	2.059
TL4f	0.020	0.70	1188	0.174	0.181	0.326	8.86	2.38	2.135

Output parameters									
Test	s_{0p} [-]	ξ_p [-]	N [-]	$H_{1/3}$ [m]	H_{m0} [m]	H_{max} [m]	L_0 [m]	T_p [s]	$T_{m-1,0}$ [s]
TL5a	0.039	0.50	928	0.101	0.105	0.174	2.66	1.31	1.203
TL5b	0.041	0.49	1103	0.118	0.123	0.201	3.00	1.39	1.274
TL5c	0.041	0.49	1063	0.132	0.140	0.230	3.38	1.47	1.359
TL5d	0.037	0.52	1093	0.15	0.155	0.253	4.21	1.64	1.451
TL5e	0.038	0.51	1076	0.169	0.175	0.279	4.55	1.71	1.551
TL5f	0.039	0.50	1053	0.189	0.196	0.323	5.00	1.79	1.650
TL5g	0.038	0.52	1048	0.207	0.217	0.320	5.77	1.92	1.739

Table B.3: An overview of the in- and output of the variable parameters used for test series 6.

Input parameters						
Test	s_{0p} [-]	ξ_p [-]	N [-]	H_s [m]	L_0 [m]	T_p [s]
TL6a	0.03	0.58	300	0.15	5.00	1.8
TL6b	0.03	0.58	700	0.15	5.00	1.8
TL6c	0.03	0.58	1000	0.15	5.00	1.8
TL6d	0.03	0.58	2000	0.15	5.00	1.8
TL6e	0.03	0.58	3000	0.15	5.00	1.8
TL6f	0.03	0.58	4000	0.15	5.00	1.8

Output parameters									
Test	s_{0p} [-]	ξ_p [-]	N [-]	$H_{1/3}$ [m]	H_{m0} [m]	H_{max} [m]	L_0 [m]	T_p [s]	$T_{m-1,0}$ [s]
TL6a	0.031	0.57	336	0.145	0.153	0.213	5.00	1.79	1.62
TL6b	0.030	0.58	799	0.143	0.149	0.268	4.96	1.78	1.61
TL6c	0.030	0.58	1101	0.141	0.149	0.254	5.04	1.80	1.62
TL6d	0.030	0.57	2062	0.142	0.150	0.316	4.94	1.78	1.62
TL6e	0.030	0.58	3062	0.143	0.149	0.302	4.95	1.78	1.61
TL6f	0.030	0.58	4096	0.142	0.148	0.249	4.96	1.78	1.61

Table B.4: An overview of the in- and output of the variable parameters used for test series 7 and 8.

Input parameters						
Test	s_{0p} [-]	ξ_p [-]	N [-]	H_s [m]	L_0 [m]	T_p [s]
TL7a	0.01	1.00	1000	0.11	11.00	2.7
TL7b	0.01	1.00	1000	0.13	13.00	2.9
TL7c	0.01	1.00	1000	0.15	15.00	3.1
TL8a	0.03	0.58	1000	0.17	5.67	1.9
TL8b	0.03	0.58	1000	0.19	6.33	2.0
TL8c	0.03	0.58	1000	0.21	7.00	2.1

Output parameters									
Test	s_{0p} [-]	ξ_p [-]	N [-]	$H_{1/3}$ [m]	H_{m0} [m]	H_{max} [m]	L_0 [m]	T_p [s]	$T_{m-1,0}$ [s]
TL7a	0.010	1.02	1194	0.109	0.112	0.187	11.70	2.74	2.36
TL7b	0.010	0.99	1292	0.126	0.127	0.240	12.40	2.82	2.46
TL7c	0.010	0.99	1315	0.137	0.141	0.259	13.75	2.97	2.55
TL8a	0.029	0.59	1076	0.161	0.168	0.267	5.75	1.92	1.71
TL8b	0.029	0.58	1136	0.184	0.191	0.310	6.49	2.04	1.82
TL8c	0.030	0.58	1137	0.203	0.210	0.334	7.01	2.12	1.90

Appendix C: Test input parameters

For the physical tests the parameters to use in the test need to be considered. There are constant parameters that are equal for every test and variable parameters that have a different value for the different tests. In the next paragraphs all the parameters are discussed and the choices are elaborated. Several assumptions and limitations are made to be able to determine the input parameters of the tests.

C.1 Assumptions and limitations

The assumptions and limitations are elaborated in this paragraph. The assumptions have to be made to determine all the parameters for the testing. The assumptions for some parameters can be validated during the testing. The limitations depend on the wave generator of the flume and the scaling laws.

C.1.1 Assumptions

The assumptions are presented below and are split in two lists. The first list includes assumptions that can be validated during testing and the second list included assumptions that cannot be validated.

Assumptions that can be validated:

- The density of the water is 1000 kg/m^3.
- The irregular waves form a complete JONSWAP spectrum within 1000 waves.

Assumptions that cannot be validated:

- The gravitational acceleration is 9.81 m/s^2.
- The water is incompressible.
- Normal incident waves only.
- The waves can develop in deep water conditions.

C.1.2 Limitations

Physical tests are subject to certain limitations due to scale effects and the possibilities of the wave generator of the wave basin (the Pacific basin at Deltares). The tests are executed on scale and scale effects have to be taken into account.

- The wave generator is limited in wave height. For irregular waves the highest significant wave height that can be produced is 0.21 m with a peak period of 1.9 s.
- The scale law of Weber includes the ratio of inertia over the surface tension. If the waves are higher than 0.05 m there are no scaling problems as is stated in Hydralab III, because the effect of the surface tension on the waves is negligible (Wolters, Van Gent, Allsop, Hamm, & Muhlestein, 2009).
- The scale law of Reynolds includes the ratio of inertia over the viscosity. The flow has to be turbulent to prevent viscous scale effects. The Reynolds number should be higher than 4000 (Bezuyen et al., 2007).

C.2 Constant parameters

The constant parameters do not change during the tests. An overview of the constant parameters is given in Table C.4 in Paragraph C.2.5.

C.2.1 Slope angle

The purpose of the research is to define the stability of stones on mild slopes. This means that the slope angle for the physical tests needs to be in the mild section. According to Van der Meer (1988), slopes are mild if tan α > 1:6. Kramer (2016) executed tests for slopes of 1:5, 1:10 and 1:15. For this research there are different criteria that the slope angle has to meet.

- The slope has to be in the mild section, that is tan α > 1:6 or milder.
- The slope has to give a damage profile that complies to that of mild slopes.
- The wave breaking on the slope must be able to be in the range of plunging and if possible spilling breakers.

The influence of the slope on the stability is investigated by Wit (2015) and Kramer (2016). They both concluded that a milder slope gives a higher stability and a lower damage depth. They also concluded from their research that a different slope angle gives different transport directions of the stones over the slope. From the tests done in XBeach-G by Wit (2015) followed that a steep slope has mostly downslope transport of the stones and a mild slope mostly upslope. The slopes in between are a transition from steep to mild slope and here the stones can move both up- and downslope, see Figure C.1.

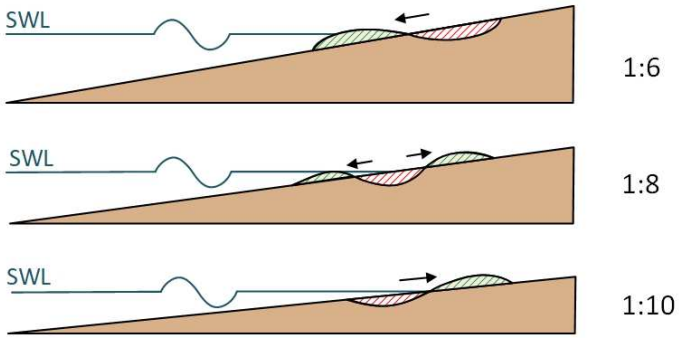

Figure C.1: The damage profile on the slopes for different slope angles with the overall movement direction of the stones by the wave forces.

The profile that develops for the 1:6 slope is a bar profile by which the bar mostly develops below SWL. The stones are transported in downslope direction. These stones form the bar. Upslope of the bar an erosion hole develops from which the stones are removed. The profile that develops for the 1:10 slope is the crest profile. The stones are transported upslope and form a crest. Downslope of the crest the erosion hole is formed. The crest mostly develops around the SWL (Van Hijum, 1974).

The difference in movement direction of the stones is explained by the difference in how the gravity force acts in the direction parallel to the slope. For a steep slope this force is larger than for a milder slope. The stones that are destabilized for steep slopes are pulled to the downside of the slope by the gravity force and for milder slopes the stones are pushed upslope by the wave forces. These wave forces exceed the gravity forces.

For the chosen slope it is preferred that both plunging and if possible spilling breakers can be developed. Both these breaker types are preferred to be researched, because both can occur in reality. Therefore, it needs to be investigated what the effects are of both types of wave breaking on the stability and the direction of the transport of the stones.

The types of wave breaking are determined by a combination of the slope angle and the wave steepness for irregular waves. For a slope of 1:6 only plunging breakers can be realised. For a slope of 1:8 still only plunging breakers can be realised. For a slope of 1:10 the transition area can be reached from plunging to spilling breakers. Spilling breakers can only occur for very mild slopes and it is therefore not possible to develop a wave spectrum with only spilling breakers for irregular waves for mild slopes of 1:10, but for gravel beaches milder slopes are less relevant.

Therefore, a slope of 1:10 is chosen. This slope is mild and develops a damage profile corresponding to mild slopes, that is upslope transport of the stones. This slope is also for irregular waves able to develop plunging breakers and to reach the transition zone from plunging to spilling breakers, which is preferred for the research.

C.2.2 Water depth

The water depth is optimized in between a minimum water depth to simulate deep water and a maximum for the workability. The filling and emptying of the flume take a lot of time that increases for a higher water depth.

The maximum wave height that can be generated in the Pacific basin is 0.21 m for irregular waves. The water depth has to be determined for this significant wave height to make it possible to use the basin to its maximum possibilities.

There are multiple criteria to determine if the water depth is deep compared to the wave height or length. Marcel van Gent states that the water depth is deep if: $\frac{h}{H_s} \approx$ 3 to 4 (personal communication, January 21, 2019). The user guide to physical modelling and experimentation gives as criteria: $\frac{H_s}{h} <$ 0.3 (Frostick, McLelland, & Mercer, 2011) and from the Coastal Engineering Manual – Part III follows: $\frac{h}{L} > 0.5$ (USACE, 2015). The maximum wave steepness for irregular waves is 0.05 (Miche, 1944) that determines the deep-water wavelength, L_{0p}. With the significant wave height of 0.21 m, a maximum wave steepness of 0.05 and the maximum significant wavelength of 4.2 m the different criteria are tested for water depths from 0.55 m to 0.85 m. An overview is given in Table C.1.

Table C.1: The water depth determined by the different deep-water criteria. Red numbers mean that the criteria are not met. The green numbers mean that the criteria are met.

h [m]	H_s [m]	s_{max} [-]	ξ_{0p} [-]	L_{0p} [m]	h/H_s = 3-4 [-]	H_s/h < 0.3 [-]	h/L > 0.5 [-]
0.55	0.21	0.05	0.45	4.2	2.62	0.38	0.13
0.6	0.21	0.05	0.45	4.2	2.86	0.35	0.14
0.65	0.21	0.05	0.45	4.2	3.10	0.32	0.15
0.7	0.21	0.05	0.45	4.2	3.33	0.30	0.17
0.75	0.21	0.05	0.45	4.2	3.57	0.28	0.18
0.8	0.21	0.05	0.45	4.2	3.81	0.26	0.19
0.85	0.21	0.05	0.45	4.2	4.05	0.25	0.20

From Table C.1 follows that for a depth of 0.65 m the criteria by Van Gent is met, for a depth of 0.75 m the Frostick criteria is met and that the USACE criteria is not met at all. By these criteria it is decided that the water depth is 0.75 m. This is assumed to be deep water for two of the three criteria. The smallest water depth for the deep-water criteria is chosen to decrease the time needed for filling and emptying the basin. This water depth also makes it possible to walk inside the basin when it is filled.

C.2.3 Stone diameter and weight

The most important parameter with regard to the stones is the nominal median diameter. The stone diameter determines how much damage can be made for a certain wave height. The wave height is limited and therefore the diameter has to enable the wave height to induce start of damage and failure of the slope. To determine the nominal median diameter diameters of 12, 14, 16 and 18 mm have been tested for different Iribarren numbers and wave heights. The Iribarren numbers are determined for the lowest and highest wave steepness and one in between. By Van der Meer (1988) the expected damage is calculated. The expected damage gives an indication if the combination of stone diameter, Iribarren number and wave height can induce start of damage and failure, see Table C.2.

The start of damage with the damage level of Van der Meer (1988) is for a slope of 1:10 equal to S = 7 (Wit, 2015). Failure of the slope is around S = 40. Calculated with the damage levels of Van der Meer (1988) and translating them to the steep slopes with Equation C.1 from Wit (2015). The Van der Meer (1988) damage level is conservative for mild slopes, but it gives an indication for the damage to compare the different diameters.

$$S(\alpha) = S_{start}\frac{\sin(\alpha_{start})}{\sin(\alpha)} \qquad \text{C.1}$$

From the report of Kramer (2016) follows that for a slope of 1:10, a diameter of 16.2 mm and a wave height of 0.094 m the result of the physical test was a damage level of 2.01. The Pacific basin is able to create wave heights of two times the height Kramer used. This leads to a damage level of 64, according to Equation C.2. This equation states that if the wave height is two times higher, the damage level becomes 32 times higher.

$$S \sim \left(\frac{H}{\Delta d}\right)^5 \qquad \text{C.2}$$

To determine the d_{n50} of the stones different stone sizes are tested versus the Iribarren number, the wave height and the expected damage. The constant parameters used are: tan α = 1:10, ρ_s = 2944 kg/m^3, ρ_w = 1000 kg/m^3, Δ = 1.94 and N = 1000 waves. From Table C.2 is concluded that the nominal median diameters of 12 mm and 14 mm give too much damage. For the higher Iribarren numbers the damage levels exceed start of damage for the lower wave heights. For the higher wave heights, the damage is too high. To make a curve of the damage versus the wave height it is preferred that the damage does not develop too fast for a rising wave height.

The nominal median diameter of 16 mm has for the lower two Iribarren numbers a good range for the damage value. The higher Iribarren number of 1.0 gives a damage level for the lowest wave height that already exceeds the start of damage. However, the wave height can be lowered, see

The nominal median diameter of 18 mm does not reach failure for the lower Iribarren number. The wave height cannot be much higher (0.21 m is the maximum) and failure may not be reached with this diameter.

Table C.2: The results of the determination of the nominal stone diameter versus the Iribarren number, the wave height, the wave steepness and the expected damage.

d_{n50} = 0.012 mm	ξ_p = 0.29			ξ_p = 0.50			ξ_p = 1.00		
	H_s [m]	T_p [s]	S [-]	H_s [m]	T_p [s]	S [-]	H_s [m]	T_p [s]	S [-]
	0.08	0.65	1.2	0.08	1.13	4.6	0.08	2.26	0.8
	0.10	0.73	3.6	0.10	1.27	14.1	0.10	2.53	79.9
	0.12	0.80	8.9	0.12	1.39	35.2	0.12	2.77	198.9
	0.14	0.86	19.2	0.14	1.50	76.0	0.14	2.99	429.9
	0.16	0.92	37.5	0.16	1.60	148.2	0.16	3.20	838.1
	0.18	0.98	67.6	0.18	1.70	267.0	0.18	3.40	1510.3
	0.20	1.03	114.5	0.20	1.79	452.1	0.20	3.58	2557.7
d_{n50} = 0.014 mm	ξ_p = 0.29			ξ_p = 0.50			ξ_p = 1.00		
	H_s [m]	T_p [s]	S [-]	H_s [m]	T_p [s]	S [-]	H_s [m]	T_p [s]	S [-]
	0.08	0.65	0.5	0.08	1.13	2.1	0.08	2.26	12.1
	0.10	0.73	1.7	0.10	1.27	6.5	0.10	2.53	37.0
	0.12	0.80	4.1	0.12	1.39	16.3	0.12	2.77	92.0
	0.14	0.86	8.9	0.14	1.50	35.2	0.14	2.99	198.9
	0.16	0.92	17.4	0.16	1.60	68.5	0.16	3.20	387.8
	0.18	0.98	31.3	0.18	1.70	123.5	0.18	3.40	698.8
	0.20	1.03	53.0	0.20	1.79	209.2	0.20	3.58	1183.4
d_{n50} = 0.016 mm	ξ_p = 0.29			ξ_p = 0.50			ξ_p = 1.00		
	H_s [m]	T_p [s]	S [-]	H_s [m]	T_p [s]	S [-]	H_s [m]	T_p [s]	S [-]
	0.08	0.65	0.3	0.08	1.13	1.1	0.08	2.26	6.2
	0.10	0.73	0.8	0.10	1.27	3.4	0.10	2.53	19.0
	0.12	0.80	2.1	0.12	1.39	8.3	0.12	2.77	47.2
	0.14	0.86	4.6	0.14	1.50	18.0	0.14	2.99	102.0
	0.16	0.92	8.9	0.16	1.60	35.2	0.16	3.20	198.9
	0.18	0.98	16.0	0.18	1.70	63.4	0.18	3.40	358.4
	0.20	1.03	27.2	0.20	1.79	107.3	0.20	3.58	607.0
d_{n50} = 0.018 mm	ξ_p = 0.29			ξ_p = 0.50			ξ_p = 1.00		
	H_s [m]	T_p [s]	S [-]	H_s [m]	T_p [s]	S [-]	H_s [m]	T_p [s]	S [-]
	0.08	0.65	0.2	0.08	1.13	0.6	0.08	2.26	3.4
	0.10	0.73	0.5	0.10	1.27	1.9	0.10	2.53	10.5
	0.12	0.80	1.2	0.12	1.39	4.6	0.12	2.77	26.2
	0.14	0.86	2.5	0.14	1.50	10.0	0.14	2.99	56.6
	0.16	0.92	4.9	0.16	1.60	19.5	0.16	3.20	110.4
	0.18	0.98	8.9	0.18	1.70	35.2	0.18	3.40	198.9
	0.20	1.03	15.1	0.20	1.79	59.5	0.20	3.58	336.8

To get a d_{n50} of 16 mm a batch of gravel was ordered with a 15-25 mm gradation. This normally gives a d_{n50} of 16 mm, because the d_{50} then is 20 mm and the d_{n50} is determined by: $d_{n50} = 0.81 d_{50}$ and that gives a d_{n50} of 16.2 mm. However, when the d_{n50} was determined from the batch the diameter appeared to be 14.8 mm after weighing a selection of stones. This was determined with the weighing curve in Figure C.2 and with the density determined to be 2944 kg/m^3.

For stable rock on a slope, the grading should be small, because otherwise all the smaller stones from the wider grading are transported. From the weighing curve can be determined that the d_{85}/d_{15} is 1.4 and that means a narrow gradation which is preferred for mild gravel slopes. For the development of damage without scale effects from the width of the flume is it preferred to have ideally 100 stones per width of the flume or minimal 50. For a nominal median diameter of 16 mm there are 62 stones per width of the flume, which is above the minimum.

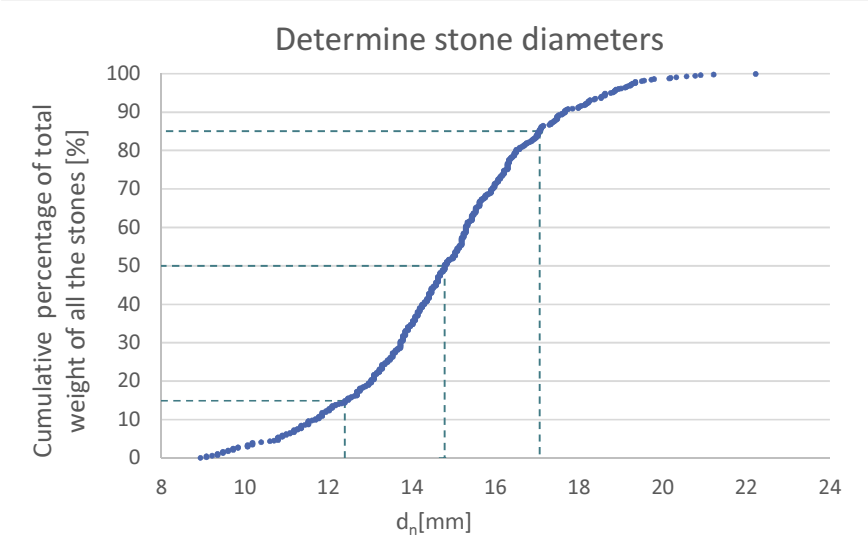

Figure C.2: The cumulative graph of the stone diameter.

The diameter is checked for scale effects with the Reynolds theory, see Equation C.3 in which u is the flow velocity [m/s], d the stone diameter [m] and v the kinematic viscosity [m^2/s]. The velocity is determined by the simplified equation of the linear wave theory (Holthuijsen, 2007).To prevent scale effects the Reynolds number needs to be higher than $3 \cdot 10^4$ according to Dai and Kamel (1969). For the minimal wave height of 0.06 m, the Reynolds number is $1.1 \cdot 10^4$ and for the highest wave height of 0.20 m, the Reynolds number is $2.1 * 10^4$. This means that the Reynolds number for the tests is in the same order of magnitude as the minimal Reynolds number for turbulent flow. The first scale effects are noticed in the core of the structure. In these tests, the core is impermeable and these scale effects do not play a significant role. Due to the mild slope the velocities are higher and this increases the turbulence. It is therefore concluded that the tests are not influenced by viscous scale effects.

$$Re = \frac{ud}{\nu}, \quad u = \sqrt{gH} \qquad \text{C.3}$$

The density of the stones, ρ_s, is assumed to be 2650 kg/m^3 and then the relative density, Δ, is 1.65. This is concluded by taking the densities from similar tests done with gravel (Kramer, 2016) and (Terrile, 2004). These densities fall in the range that the Rock Manual gives for gravel (CIRIA, CUR, & CETMEF, 2007). The exact stone density is determined by weighing a part of the batch. From this stone density the exact relative density follows.

C.2.4 Strip width

The coloured stones are laid down in six strips with six different colours. The colours used are red, blue, yellow, purple, orange and green. The length of the strips is equal to the width of the flume, which is 1.00 m. The width of the strips needs to be determined, because the strip width, W_{strip}, induces an error in the damage measurement. The stones that move within the strip are not measured with this method and therefore cause an error in the damage measurement. A width of one stone diameter induces no error, because the stones are not able to be displaced inside the strip in cross-shore direction. However, a strip width of one diameter is an enormous amount of work to put in place and it gets very hard to determine which stone came from which strip, because there are so many strips with the same colours. Therefore, the strip width needs to be wider. To determine the strip width, executed tests of others are compared. The strip widths of these tests are compared to the nominal median diameters used in the corresponding tests. A factor is determined between the strip widths and the diameters. This is shown in Table C.3.

Table C.3: The strip widths versus the diameters of previous done tests.

Reference	W_{strip} [m]	d_{n50} [m]	Factor
(Hofland, 2005)	0.10	0.0062	16
	0.10	0.0108	9
(Grote, 1994)	0.25	0.0147	17
	0.25	0.0096	26
(Hoan, 2011)	0.10	0.0080	13
(Terrile, 2004)	0.15	0.0071	21
	0.15	0.0092	16
		Average:	**17**

From these tests follow that the average factor between the strip widths and the diameters is 17. If this is translated to the nominal median diameter used in this research of 16 mm the strip width is 0.25 m.

The length for which the strips are laid down over the slope is determined from the physical tests done by Kramer (2016). The part of the slope where the most movement of the stones occurred for the slope of 1:10 is from 3.0 m to 5.5 m, see Figure C.3. The most important is where the stones are removed and a pit develops. In this area the stones are picked up and transported mostly up shore and a bit down shore. The removal of the stones was from 3.5 m to 5.0 m. This means a length of 1.5 m where the stones are removed. With a strip width of 0.25 6 strips are needed to fulfil a length of 1.5 m. If the strips are located where the stones are picked up, it is possible to follow the transport of the coloured stones and where they eventually end up.

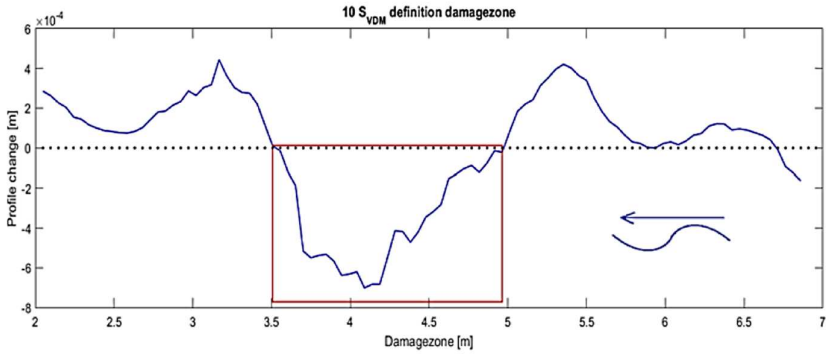

Figure C.3: The damage profile of the 1:10 slope test of Kramer (2016).

During the testing the length of the slope over which the damage occurred was much larger than was expected. The erosion area was around 3 m instead of 1.5 m. For this reason, the strips widths were increased from 0.25 m to 0.5 m after test series 2 and the entire erosion area could be checked for stone transport. If this had not been done, all the coloured strips would have been covered by the black uncoloured stones.

C.2.5 Summary of the constant parameters

An overview of the constant parameters that are used in the physical tests is given in Table C.4. The densities and the specific submerged density are assumed to determine the variable parameters. Before the tests are started, these densities need to be measured for their exact value.

Table C.4: An overview of the constant parameters for the physical tests.

Description	Parameter	Value	Unit
Slope	tan α	1:10	-
Water depth	h	0.75	m
Nominal median diameter	d_{n50}	14.8	mm
Density of stones	ρ_s	2944	kg/m^3
Density of water	ρ_w	1000	kg/m^3
Specific submerged density	Δ	1.94	-
Strip width	W_{strip}	0.5	m

C.3 Variable parameters

The variable parameters change between the tests. The parameters are investigated for their effect on the stability of the stones. An overview of the variable parameters is given in Table C.11 in Paragraph C.3.9.

C.3.1 Layer thickness

The tests are done with a layer thickness of $2.5d_{n50}$. This is the same for the non-coloured and coloured stones. The stones are placed directly on the steel plates. For a layer thickness of $2.5d_{n50}$ the bottommost $0.5d_{n50}$ simulates a permeable filter layer and this total layer thickness gives a permeability of P = 0.1, see Figure C.4. A layer thickness of $2.5d_{n50}$ is the minimum layer thickness to simulate an armour layer and underlayer. Gravel beaches are in real life laid down with higher layer thicknesses. If the layer thickness is very high the gravel layer can be said to be a homogeneous structure with P = 0.6. Therefore, the two extremes are P = 0.1 and 0.6. Of these two the permeability of 0.1 is the most unstable and the most conservative. The wave energy is less decreased if the slope

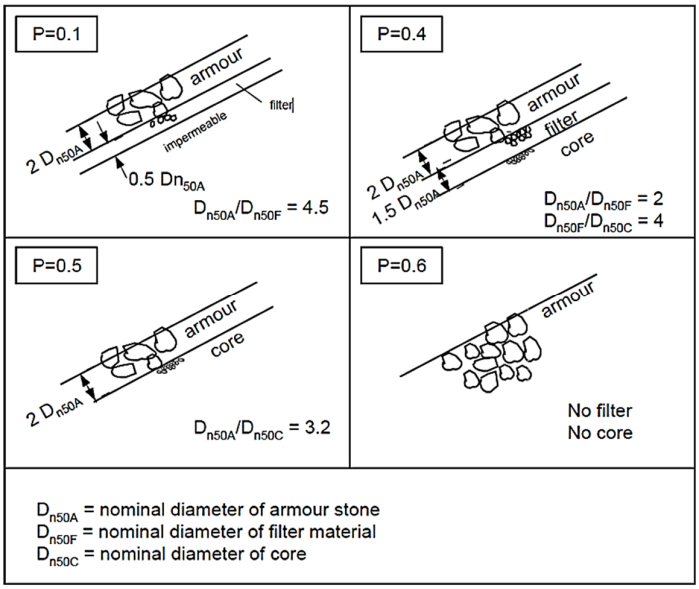

Figure C.4: Permeability of the slope for an armour layer of $2d_{n50}$ and a filter layer of $0.5d_{n50}$ (Jumelet, 2010).

has a lower permeability and is therefore less stable. For a permeability of 0.1 the core of the construction is assumed to be impermeable, for instance a clay or sand core. If the layer thickness increases the influence of the impermeable core on the armour layer decreases and the armour layer stability increases.

In the tests the underlayer consists of the same stones as the armour layer. This decreases the amount of work for laying down the stones and is assumed to be of negligible impact on the stability of the stones.

The thickness of $2.5d_{n50}$ is a thickness for which damage is visible and measurable. The thickness of the layer determines the amount of work. The higher the thickness the more stones have to be placed on the slope. For this reason, the tests to investigate the influence of wave breaking are done for a layer thickness of $2.5d_{n50}$.

According to Van der Meer (1988) the stability of the stones increases for a more permeable core, as can be seen in Figure C.5. These tests were done for a slope angle of tan α = 1:2. The water forces that reach the bottom of the armour layer need to be distributed. For an impermeable core the forces cannot enter the core and dissipate their energy in that direction. Instead the waves flow down in between the underlayer and the core. The run-down forces decrease the stability. For a permeable core the forces can dissipate into the core and the run-down forces are less.

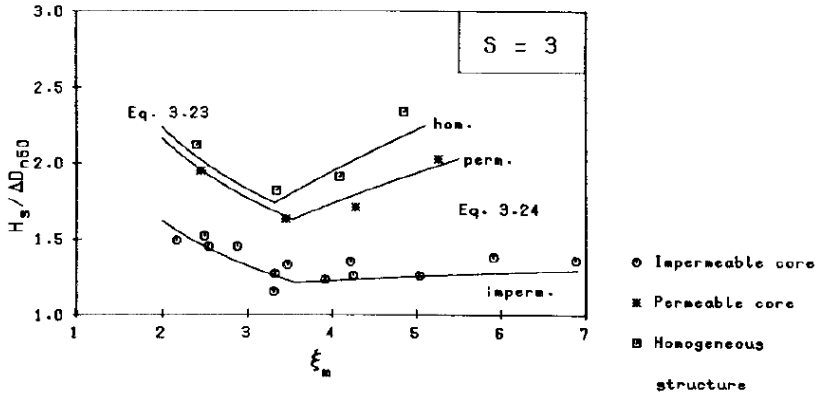

Figure C.5: Stability of the stones versus different core types for a slope angle of tan α of 1:2 (Van der Meer, 1988).

The datapoints in Figure C.5 are all calculated points from the damage curves of the physical tests done by Van der Meer (1988). Of all the datapoints from the physical tests an average damage curve is drawn in between the points for each different test. From these curves are for fixed amounts of damage (e.g. S = 3) and Iribarren numbers the stability numbers calculated. These stability numbers are set out against the Iribarren numbers in a graph for a fixed damage level and slope angle. The curves in Figure 3.9 are lines drawn between the calculated points for the different core structures.

The overall trend from these graphs from Van der Meer (1988) is that the impermeable cores are the least stable, the permeable cores are more stable and the homogeneous structures are the most stable.

Another layer thickness is tested too check the effect on the stability of mild slopes. The layer thickness is set to $5d_{n50}$. The output of this test gives the trend how the slope reacts to a higher layer thickness and a higher permeability. The permeability for this layer thickness is around P = 0.6, see Figure C.5. A layer thickness of $5d_{n50}$ equals a homogeneous structure with no difference between the armour layer, underlayer or the core.

C.3.2 Wave type

The tests can be done with regular or irregular waves. Regular waves induce damage on the slope concentrated at one location. The damage develops just after the point of breaking at H_0/h =1.25-1.4 and around the SWL due to the run-up and run-down velocities. The development of the damage is fast, mostly after 250 waves. The fast development is due to the fact that all the waves break at the same location with the same type of wave breaking. The irregular waves induce damage more spread over the slope than for regular waves. The most damage is located around the SWL. Larger run-up velocities develop for irregular waves. If a few small waves reach the slope one after the other, the SWL is a bit lowered. If these small waves are followed by a large wave the run-up of this wave causes a lot of damage to the slope due to its high energy level and run-up velocity.

The regular waves can vary in wave steepness from 0.01 up to 0.14 (Holthuijsen, 2007). Due to the regularity the waves all have the same height, length and period and therefore higher steepnesses can be developed. Irregular waves can only develop steepnesses from 0.01 up to 0.05 (Van der Meer, 1988). These waves are all different and it is therefore much harder to develop high steepnesses.

The tests need to be as close to the real situation as possible. Therefore, irregular waves are used, because their effects on the stability are the most realistic. The spectrum used for the irregular waves is the JONSWAP spectrum. This spectrum is representative for the real-life spectrum on the Dutch coast. The damage induced by the regular waves gives a different profile and location of the damage and these effects are very hard to translate to the effects the irregular waves would have on the slope. Regular waves are therefore disregarded in this research.

C.3.3 Wave steepness

The wave steepness determines the Iribarren number together with the slope angle. The slope angle is constant during the tests. The wave steepness has to change during the tests to develop plunging and spilling breakers. The wave steepness is defined as the wave height over the wavelength, see Equation C.4. The wavelength is determined at the deep water, so the wave steepness is the fictious wave steepness.

$$s_{0p} = \frac{H_s}{L_0} = \frac{2\pi H_s}{g T_p^2} \qquad \text{C.4}$$

The wave steepness has a maximum for the irregular waves. As discussed in Paragraph C.3.2 the irregular waves have wave steepnesses in the range from 0.01 up to 0.05. It is preferred to test the wave breaking from plunging towards the transition with the spilling breaker. To achieve this the wave steepness has to vary between 0.01 and 0.05 to reach all these types of breakers, see Paragraph 0. It is therefore chosen to test with 0.01, 0.02, 0.03, 0.04 and 0.05 for the irregular waves. This gives the plunging breaker and the transition zone between the plunging and spilling breaker. The overview of the wave steepnesses that are used in the tests is given in Table C.5.

Table C.5: The wave steepnesses that are going to be tested for the irregular waves.

	Irregular waves
s_{0p} [-]	0.01
	0.02
	0.03
	0.04
	0.05

C.3.4 Iribarren number

The Iribarren number determines the type of wave breaking on the slope. The type of wave breaking influences the damage on the slope and therefore the tests are done with different values of the Iribarren number. On a mild slope of 1:10 plunging breakers and spilling breakers occur. The spilling breakers occur only in combination with plunging breakers, because for irregular waves not only spilling breakers develop for the lower wave steepnesses in combination with a slope of 1:10. If a plunging wave breaks, the overturning part of the wave reaches the underlying water layer with a jet-like force, see the right image in Figure C.6. This induces a high local damage and a relatively low run-up of the wave. The energy dissipation is more concentrated on one location. For spilling waves, the jet-like force is a lot smaller and the underlying water layer has a larger depth. The waves also break multiple times if the water depth decreases. The local effect is therefore a lot less than for the plunging wave. The energy dissipation is more spread over the slope and therefore the damage is also more spread over the slope, see Figure C.6. The run-up of the wave is higher than for the plunging wave.

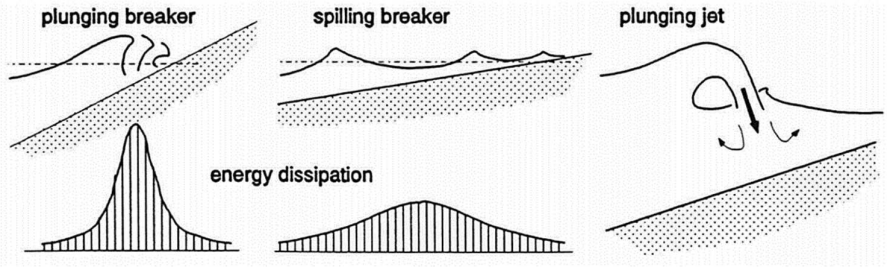

Figure C.6: The energy dissipation for the plunging and spilling breaker on the left. A schematization of the plunging breaker on the right (Schiereck & Verhagen, 2016).

The Iribarren number is defined by Equation C.5. It is the slope angle divided by the square root of the wave steepness. The Iribarren number determines how the waves break. The Iribarren number is determined with the deep-water wave parameters, that are the significant wave height and the deep-water wavelength. For the mild slopes there are two wave breaking types that occur: spilling and plunging.

$$\xi_p = \frac{\tan \alpha}{\sqrt{s_{0p}}} \qquad \text{C.5}$$

The plunging breaker determined by the deep-water conditions is in the range of $0.5 < \xi_m < 3.3$. Spilling occurs if $\xi_m < 0.5$. These values are determined by Battjes (1974) for regular waves. These Iribarren numbers do vary between different research. In Table C.6 the Iribarren numbers are given from different research. The transition from plunging to spilling is not a direct change, but a gradual transition in the breaking type. The Iribarren number of 0.5 is thus an indication. To make good plunging waves, the Iribarren number needs to be a lot higher than 0.5. For spilling the Iribarren number needs to be a lot lower than 0.5. For the transition the Iribarren needs to be close to 0.5. There is a slight variation in these numbers between the regular and irregular waves. For the irregular waves the peak period is used instead of the mean period of the waves. This gives for the irregular waves slightly lower Iribarren numbers, because $T_m = 0.8T_p$ (Schiereck & Verhagen, Introduction to bed, bank and shore protection (2nd edition), 2016).

The irregular waves are all different and do all have a slightly different wave steepness and Iribarren number. For the irregular waves with the Iribarren numbers around the transition zone plunging and spilling waves can alternate each other. The higher waves give a more spilling breaker and the lower waves more plunging breakers. The transition zone is therefore not a hard boundary, but a range. The roughness of the bed also influences the breaker types.

Table C.6: An overview of the different ranges of Iribarren numbers for the plunging and spilling breaker and the transition zone in between taken from various research. The values for the irregular waves are calculated from the values of the regular waves with $T_m = 0.8T_p$.

Reference	Regular			Irregular		
	Spilling	Transition	Plunging	Spilling	Transition	Plunging
(Battjes, 1974)	$\xi_m < 0.4$	$\xi_m = 0.4 - 0.6$	$\xi_m = 0.6 - 3.3$	$\xi_p < 0.3$	$\xi_p = 0.3 - 0.5$	$\xi_p = 0.5 – 2.6$
(Schiereck & Verhagen, 2016)	$\xi_m < 0.3$	$\xi_m = 0.3 - 0.6$	$\xi_m = 0.6 - 3.0$	$\xi_p < 0.2$	$\xi_p = 0.2 - 0.5$	$\xi_p = 0.5 - 2.4$
(Jennings & Shulmeister, 2001)			$\xi_m = 0.5 - 1.8$			$\xi_p = 0.4 - 1.5$
(Iglesias, et al., 2006)			$\xi_m < 2.5$			$\xi_p < 2.0$

Van der Meer (1988) concluded that the stability also depends on the slope angle. Figure C.7 shows the graph produced by Van der Meer (1988) by which the datapoints follow from the damage curves of the physical tests as explained in Paragraph C.3.1. The graph confirms that the stability is influenced by the slope angle. The stability increases for a milder slope for the same Iribarren number. The stability curves have a minimum value that is related to the collapsing breakers.

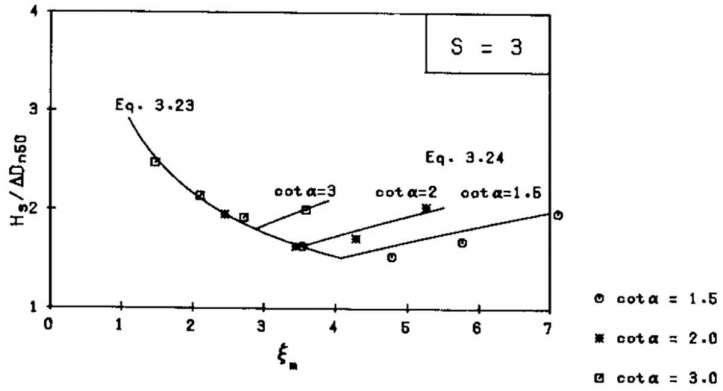

Figure C.7: Stability number versus the Iribarren numbers for different slope angles (Van der Meer, 1988).

The slope angle is constant in the tests, being tan α = 1:10. Therefore, the only parameter that causes the variation in the Iribarren number is the wave steepness. In Table C.7 the Iribarren numbers are shown for the wave steepnesses that can be developed for irregular waves. The Iribarren numbers that are possible to produce are varying from the plunging breaker type to the transition zone. With wave steepnesses of 0.01 to 0.05, the Iribarren numbers are good into the plunging range (ξ_p = 1.00) and just into the transition zone (ξ_p = 0.45).

Table C.7: The wave steepness versus the Iribarren number.

Irregular					
s_{0p} [-]	0.01	0.02	0.03	0.04	0.05
ξ_p [-]	1.00	0.71	0.58	0.50	0.45

C.3.5 Number of waves

The number of waves determines the storm duration. At the Holland coast, a representative storm has a storm duration of about 5 hours. The average wave period in this storm is 6 seconds, which gives 3000 waves in a standard representative storm duration (Vellinga, 1982). The number of waves determines the amount of damage that develops until the equilibrium profile is reached. This equilibrium profile is not reached in the case of the static stability, because the profile has to remain the same as the initial slope. Only the armour layer is allowed to be damaged, but the total profile should stay the same.

Thompson and Shuttler (1975) performed more than 100 tests to determine the effect of the storm duration on the damage development for steep slopes with tan α < 1:6. They performed also a few long duration tests up to 15000 waves. The tests were stopped in between to measure the damage after each 1000 waves. The first 500-1000 waves cause the most damage and have therefore an almost linear relation with the damage. After this the relation between the damage and the number of waves is a square root function. For the long duration tests to 15000 waves the damage goes towards a maximum damage related to the damage at 5000 waves, see the results of the tests of Thompson and Shuttler (1975) in Figure C.8.

For a storm duration that has less than 10000 waves there is no maximum or equilibrium for the damage. This means that for a test below this number of waves there is no equilibrium damage for static stability.

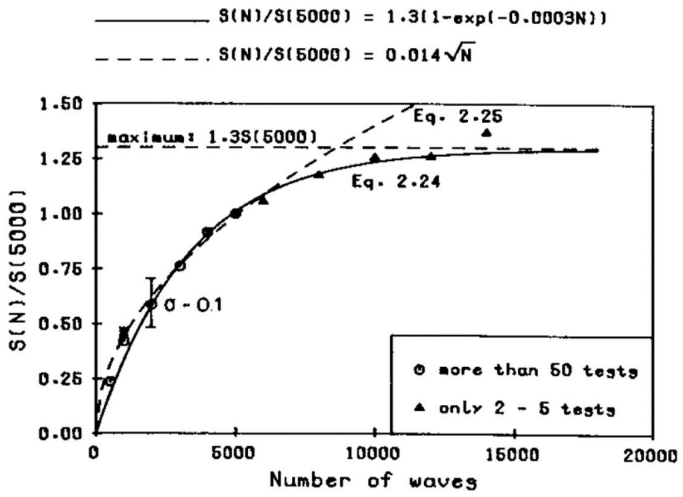

Figure C.8: The influence of the number of waves on the damage (Van der Meer, 1988).

The damage level is proportional to the square root of the storm duration, $S \sim \sqrt{N}$ (Van der Meer, 1988). This means that the damage increases if the storm duration is longer for steep slopes. This relation is checked during the tests by one test where the damage is measured in between. The expected damages combined to the number of waves are shown in Table C.8. This gives an indication of how much waves are needed for the damage per wave steepness. For all the Iribarren numbers 1000 waves are enough to cause failure within the maximum wave height of the basin. It is therefore chosen to take for the irregular wave tests 1000 waves per test, for which failure can be reached.

Table C.8: The number of waves related to the damages.

N [-]	s_{0p} [-]	ξ_p [-]	$H_{s,min}$ [m]	$H_{s,max}$ [m]	S_{min} [-]	S_{max} [-]
500	0.01	1.00	0.08	0.18	3.3	187.7
1000	0.01	1.00	0.08	0.18	4.6	265.5
2000	0.01	1.00	0.08	0.18	6.5	375.5
3000	0.01	1.00	0.08	0.18	8.0	459.9
500	0.02	0.71	0.08	0.18	1.4	78.9
1000	0.02	0.71	0.08	0.18	1.9	111.6
2000	0.02	0.71	0.08	0.18	2.7	157.9
3000	0.02	0.71	0.08	0.18	3.4	193.4
500	0.03	0.58	0.08	0.18	0.8	47.6
1000	0.03	0.58	0.08	0.18	1.2	67.2
2000	0.03	0.58	0.08	0.18	1.6	95.1
3000	0.03	0.58	0.08	0.18	2.0	116.5
500	0.04	0.50	0.08	0.18	0.6	33.2
1000	0.04	0.50	0.08	0.18	0.8	46.9
2000	0.04	0.50	0.08	0.18	1.2	66.4
3000	0.04	0.50	0.08	0.18	1.4	81.3
500	0.05	0.45	0.08	0.18	0.4	25.1
1000	0.05	0.45	0.08	0.18	0.6	35.5
2000	0.05	0.45	0.08	0.18	0.9	50.2
3000	0.05	0.45	0.08	0.18	1.1	61.5

The influence of the number of waves on the damage is tested for one test. From this test a relation follows between the damage and the storm duration. This is done by measuring the damage in between. The damage is measured after 300, 700, 1000, 2000, 3000 and 4000 waves. The cumulative number of waves is than 11000 waves in total, see Table C.9. The wave numbers differ all to see the effect of the different number of waves following each other up. From these points the relation can be determined whether the damage level is proportional to the linear relationship for the small number of waves or to the square root of the number of waves for the large number of waves.

Table C.9: The number of waves after which the test is stopped to measure the damage in between with the cumulative number of waves.

N_per test	N_cummulative [-]
300	300
700	1000
1000	2000
2000	4000
3000	7000
4000	11000

C.3.6 Wave height

The wave height is determined with the already determined parameters being the stone diameter, the wave steepness, the Iribarren number and the number of waves. The wave height needed for a certain damage level depends on each of these parameters. This follows from the damage level formula of Van der Meer (1988). This damage is an underestimation, because Van der Meer (1988) is developed for steep slopes. Mild slopes are more stable. The damage level calculated with Van der Meer (1988) still gives an estimation if the wave height ranges can give start of damage and failure. Per wave steepness the wave heights are given coupled to the expected damage level, see Table C.10.

Table C.10: Result of the determination of the wave heights per Iribarren number.

s_{0p} = 0.01	ξ_p = 1.00			s_{0p} = 0.02	ξ_p = 0.71		
H_s [m]	L_0 [m]	T_p [s]	S [-]	H_s [m]	L_0 [m]	T_p [s]	S [-]
0.07	7.00	2.1	2.3	0.08	4.00	1.6	1.9
0.09	9.00	2.4	8.2	0.10	5.00	1.8	5.8
0.11	11.00	2.7	22.4	0.12	6.00	2.0	14.6
0.13	13.00	2.9	51.6	0.14	7.00	2.1	31.4
				0.16	8.00	2.3	61.3
				0.18	9.00	2.4	110.5
s_{0p} = 0.03	ξ_p = 0.58			s_{0p} = 0.04	ξ_p = 0.50		
H_s [m]	L_0 [m]	T_p [s]	S [-]	H_s [m]	L_0 [m]	T_p [s]	S [-]
0.09	3.00	1.4	2.1	0.10	2.50	1.3	2.5
0.11	3.67	1.5	5.7	0.12	3.00	1.4	6.1
0.13	4.33	1.7	13.1	0.14	3.50	1.5	13.2
0.15	5.00	1.8	26.7	0.16	4.00	1.6	25.8
0.17	5.67	1.9	50.0	0.18	4.50	1.7	46.5
0.19	6.33	2.0	87.2	0.20	5.00	1.8	78.7
0.21	7.00	2.1	143.9				
0.23	7.67	2.2	226.7				
s_{0p} = 0.05	ξ_p = 0.45						
H_s [m]	L_0 [m]	T_p [s]	S [-]				
0.10	2.00	1.1	1.9				
0.12	2.40	1.2	4.6				
0.14	2.80	1.3	10.0				
0.16	3.20	1.4	19.5				
0.18	3.60	1.5	35.1				
0.20	4.00	1.6	59.5				

The wave heights are chosen to have the damage levels in the right range from start of damage to failure. All the wave heights are below the maximum significant wave height of the basin, which is 0.21 m. If failure is not reached for the maximum wave heights chosen, these can still be increased to get failure.

C.3.7 Wave length

The wavelength is coupled to the wave height by the wave steepness according to Equation C.6. The wavelength is the deep-water wavelength. The wave lengths belonging to the wave heights are shown in Table C.10.

$$s_{0p} = \frac{H_s}{L_0} \quad \rightarrow \quad L_0 = \frac{H_s}{s_{0p}} \tag{C.6}$$

C.3.8 Wave period

The wave period is coupled to the deep-water wavelength according to Equation C.7. The wave period belonging to the significant wave height is the peak period. The wave periods belonging to the wave heights and lengths are shown Table C.10.

$$L_0 = \frac{gT_p^2}{2\pi} \quad \rightarrow \quad T_p = \sqrt{\frac{2\pi L_0}{g}} \approx 0.8\sqrt{L_0} \tag{C.7}$$

C.3.9 Summary of the variable parameters

An overview of the variable parameters that are used in the physical tests is given in Table C.11. These parameters are determined by the theory. It is possible that the parameters need to be different in the tests, because the theory of the steep slopes is not completely correct for mild slopes.

Table C.11: An overview of the variable parameters for the physical tests.

s_{0p} [-]	ξ_p [-]	N [-]	H_s [m]	L_0 [-]	T_p [s]	S [-]
0.01	1.00	1000	0.05-0.13	7.0-13.0	2.1-2.9	2.3-51.6
0.02	0.71	1000	0.08-0.18	4.0-9.0	1.6-2.4	1.9-110.5
0.03	0.58	1000	0.09-0.23	3.0-7.7	1.4-2.2	2.1-226.7
0.04	0.50	1000	0.10-0.22	2.5-5.0	1.3-1.8	2.5-78.7
0.05	0.45	1000	0.10-0.20	2.0-4.0	1.1-1.6	1.9-59.5

Appendix D: Pictures of the flume/basin

This appendix gives an overview of the basin and the flume used for the physical tests. Firstly, an outline of the Pacific basin is given in which all the elements are named and placed in the basin (Figure D.1). A small impression of the paining of the stones is given next (Figure D.2 and Figure D.3). This was done at the back of the building of Civil Engineering. After that the flume is shown before and after the placement of the stones (Figure D.4 and Figure D.5). The side of the flume is shown with the enclosure for the camera (Figure D.6) and next to that also the window through which the slope can be seen (Figure D.7). Then a picture of the support construction is given from which the measurements are taken (Figure D.8). At last two pictures that show the (breaking) waves inside the flume and the basin (Figure D.9 and Figure D.10).

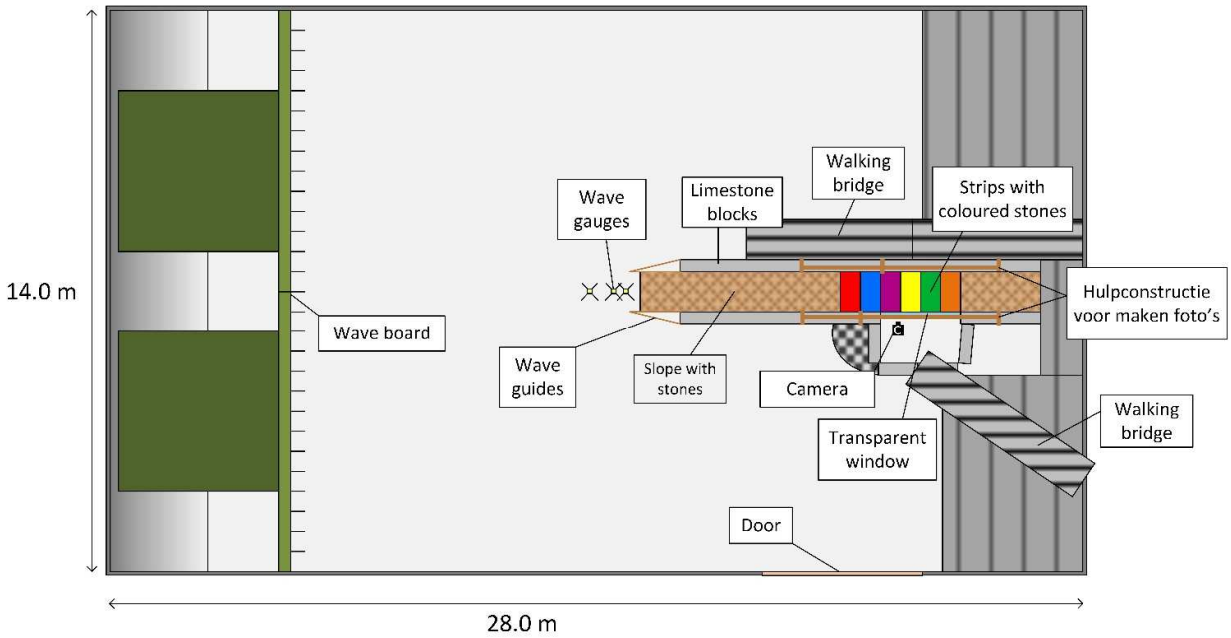

Figure D.1: An overview of the Pacific basin in Deltares with the wave generators on the left and the small flume built inside on the right. A detailed overview of the flume with all the dimensions is given in Figure 4.3.

Figure D.2: The painted stones drying behind the building of Civil Engineering.

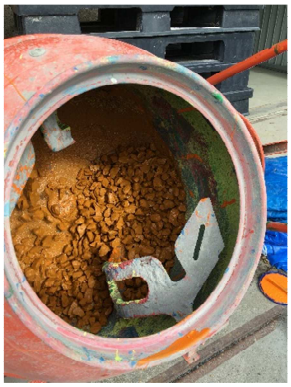

Figure D.3: The stones being painted in a concrete mixer.

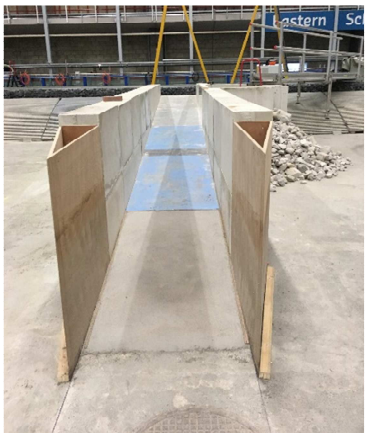

Figure D.4: The flume inside the basin with the concrete and steel slope.

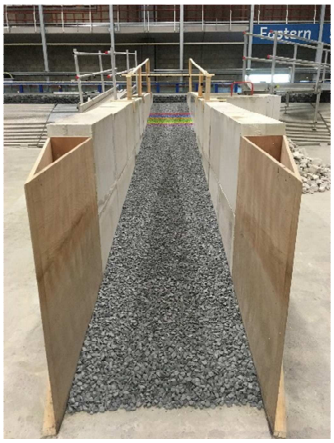

Figure D.5: The flume with the stone laid down on the slope.

Figure D.6: The flume from the side with on the right the enclosure for the camera.

Figure D.7: The window inside the enclosure.

Figure D.8: The support construction for the measuring the slope.

Figure D.9: A breaking wave inside the flume.

Figure D.10: Waves inside the basin.

Appendix E: Measuring techniques

The most important measurement is the measuring of the slope profile. The slope profile can be measured with multiple techniques. The processes concerning the breaking of the waves need to be observed together with the transport of the stones. These observed processes can connect the transport of the stones to the different breaking processes. The measurement techniques are elaborated in the next paragraphs. In paragraph E.1 the measurement techniques for the profile are explained and in paragraph E.2 for the processes. At the end of each paragraph a conclusion is given for the technique used in the tests.

E.1 Profile measurements

There are multiple techniques available to measure the profile changes of a slope with stones. In this paragraph the techniques are explained, an overview is given with the different (dis)advantages and a conclusion is given for the technique used in the tests. There are two preferred outputs. First, the location from which the stones are being transported from their strips and secondly the profile of the slope after the test. The damage can be measured from the profile output directly by comparing the post-profile with the pre-profile. Measuring of the profile is done before and after every single test.

E.1.1 Counting displaced stones

A part of the stones on the slope is laid down in strips with different colours. The coloured stones are laid down for the whole layer thickness. The displacements are measured by taking a photo with the camera on the ceiling from a height of about 15 m before and after the test and then counting the displacements. Because the stones are laid down in coloured strips it can be checked from which strip the stone moved where. With this technique the output is the displacement of the stones from a certain strip to its final location or the number of stones transported from one strip. This can be expressed in the local damage level percentage: $S = \frac{n}{A} d_{n50}^2$. In which A is the area of the strip [m^2] and n being the number of displaced stones [-] (Schiereck G. J., Fontijn, Grote, & Sistermans, 1994).

The number of displaced stones depends on the local number of stones available for movement. The local available stones are all the stones that can be fitted into an area of d_{n50}^2 in the armour layer of the strip. The strips are laid down around the still water level, because the most transport occurs at that location.

The stones are coloured before they are laid down on the slope. Between the different colours are placed separation plates to be able to lay the right colours over the whole depth. After all the stones are laid down the plates are removed. It has to be prevented that after the removal of the plates little holes are present in the profile where the plates were located first. These holes should be as small as possible to prevent influence of this on the development of the damage.

The local damage depends largely on the strip width. A used strip width in earlier research is 25 cm. The ideal strip width would be a strip width of one stone diameter, because in this way there is no transport possible within the strip. This is however not executable, because this would mean too much colours and too much strips to make. A balance has to be found between the width of the strip and the error, induced by a wider strip width. The stones that moved within a strip are not measured, because they still have the same colour as the strip. In this way these stones are not taken into account for the total damage and induce an error in this value. If tests need to be done for different stone diameters, the amount of stones in a strip should be the same to compare the damages for the different tests. Damage level should be independent of the total amount of stones in a strip. Therefore, a minimum amount is necessary. S_n is the total damage and is the total visible number of displaced stones per unit width of d_{n50}. $S_{\%}$ is the visible number of stones displaced from a strip compared to the

total number of stones in the top layer of the strip. This total number is the area of the strip divided by d_{n50}^2. The length of the strip is of big influence on $S_{\%}$. According to Hofland (2005), there is a relation between the damage in one place on the slope and the damage in another place. There is also a relation between the number of displaced stones and the local number of stones available.

E.1.2 Stereo photogrammetry

Stereo photography (DSP) is a tool to measure a structure in 3D. Two cameras are set up on a fixed location connected to a laptop. Markers and a marker base plate are placed on and around the structure to calibrate the cameras. The markers have to overlap between the pictures for the software to put to the pictures together and form a 3D-image. The base plate is used as the origin in the pictures. The images are processed with software that can create a 3D-model, e.g. Autodesk ReCap. From the before and after 3D-models the profile changes can be measured (Hofland, Raaijmakers, Van Gent, & Liefhebber, 2013).

For the measurements, first the markers are placed in such positions that each photo contains multiple markers. The photos are taken in sets (one photo with each camera). The photos are processed by software that can detect the symbols on the markers. By detecting the markers, the positions of the cameras and the markers can be reconstructed in the axial system. Then the photos from the set are warped. This means that the photos are shifted in horizontal direction only. After the warping a 3D-image can be developed with more than a million points per photo. Each point contains an xyz-coordinate (Hofland et al., 2013).

The (dis)advantages of measuring the slope with DSP are listed below.

- The measurement accuracy of this method is in between the 1 mm and 9 mm. This follows from previous done tests with the same method (Hofland et al., 2013) and (Bertin, Friedrich, Delmas, Chan, & Gimel'farb, 2014). The accuracy depends mostly on the conditions and the used cameras.
- The method is low in costs, due to the fact that only two standard cameras are necessary.
- The method is not time consuming, because for every measurement only two pictures have to be taken and processed.
- For stereo photogrammetry the markers are read in automatically by the software.
- A minor construction is needed to make sure the cameras are for every measurement in the exact same location.
- The equipment is low in availability and it is not guaranteed that the equipment is available during the complete test time. If the cameras are displaced in between the tests an error can occur due to shifting of the camera location.

E.1.3 Photogrammetry

Instead of DSP another photogrammetry method can be applied. Photogrammetry literally means “light drawing measurement”. By photogrammetry photographs of objects are processed to get metric information of the object. This metric information is received from overlapping photographs. The photographs have to be taken from at least two different locations with an overlap of about sixty percent. From the camera positions to the objects are the so-called lines-of-sight. The 3D-coordinates of the object are produced by intersecting the lines-of-sight mathematically. The more lines-of-sights the more accurately the coordinates are (GIS Resources, 2019).

There are three types of photogrammetry if they are divided by the location/axis of the camera: aerial, terrestrial and space photogrammetry. Aerial photogrammetry is done by vertically taken photos towards the object, mostly done by airplanes. Terrestrial photogrammetry has a fixed location for the camera near the ground, mostly on a horizontal axis that takes overlapping photos. Space photogrammetry has photos taken from out of space directed to the earth from e.g. a satellite. In this research aerial photogrammetry is used to get an accurate 3D-profile of the bed, because the photos have to be taken from a vertical axis.

Photogrammetry can also be divided by how the output is used: interpretative and metric photogrammetry. Interpretative photogrammetry is used for identifying objects from the photos. These photos are received from satellites or remote sensing. Metric photogrammetry is used to do exact measurements from photos and receive the point locations with distances and elevations. In this research the metric photogrammetry is used to receive the exact locations and elevations of the stones in the bed and make a 3D-profile (GIS Resources, 2019).

Summing up, for this research the photos are taken from a vertical axis facing the bed. The photos overlap by about sixty percent to get a good accuracy. Ground control points (GCP) are needed to get the locations of the points in an xyz-plane. These GCPs are located on the limestone blocks above the bed.

The photos are taken with one camera from different locations and angles spread over the slope. Markers are placed over the slope to calibrate the photos to each other. The pictures are processed by Agisoft to make a 3D-image with all the 3D-points. With the xyz-coordinates of the points the profile can be rebuilt and the damage can be determined when comparing the pre and post profile.

The (dis)advantages of measuring the slope with photogrammetry are listed below.

- The equipment and software are always available and free in costs.
- High measurement of 3 mm achieved by Van den Berg (2018). Van den Berg (2018) tested on large XBlockPlus elements and the large gaps in between these elements caused a relatively large error. This resulted in an accuracy of 3 mm. In this research, small angular stones are used that only have minor gaps in between the stones. This gives a smaller error and a higher accuracy.
- There is a minor construction needed for the equipment to photograph from almost the same location in between the tests.
- The method is more time consuming than DSP, because more pictures have to be taken and processed.

E.1.4 3D laser scanner

The profile of the slope can be measured by a 3D terrestrial laser scanner, like the Leica p30 or the Riegl VZ-2000. For a 3D laser scanner, it is preferred to scan from the top of the slope and to make scans from both sides of the flume. In this way, the scans overlap and the error is decreased. Scan the profile if the slope is dry, to prevent scattering of the laser light. Scanning the profile when the stones are wet, gives a negative result on the intensity (Shen, 2017). The scans can be processed by e.g. the software package Tie Control Point or Leica Cyclone.

The (dis)advantages of measuring the slope with a 3D laser scanner are listed below.

- The accuracy of a 3D laser scanner for the measuring of a slope is very high. The slope is relatively close to the scanner. This gives an accuracy higher than 2 mm for the Leica scanner (Leica Geosystems AG, 2017) and 1.5 mm for the Riegl scanner (Riegl, 2017).
- The entire slope is measured in one scan.
- A large construction has to be made in the basin to locate the scanner to make it possible to scan the slope from the top.
- The flume has to be sealed off completely to prevent the laser light from scattering into someone's eyes.
- The equipment is very expensive and the availability is low.
- Scattering of laser light due to the wet slope can decrease the intensity and increases the error.

E.1.5 Conclusion profile measuring techniques

The different methods are compared to each other by their (dis)advantages. These are translated to a trade-off system with plusses and minuses by which the methods can be easily compared. The methods and their ratings to four requirements are stated in Table E.1. The requirements include costs, time, accuracy and construction.

From Table E.1 is concluded that the photogrammetry method is the best option. This method is the lowest in costs and still has a high accuracy. The construction for this method is relatively small and doesn't have to stay exactly in the same place. The only disadvantage is the time it takes to measure and to process the photos.

Table E.1: A trade-off of the (dis)advantages of the different methods to measure the profile of the slope expressed in plusses and minuses for four requirements.

Method	Costs	Time	Accuracy	Construction	Total
Counting displaced coloured stones	++	--	+	0	+
Stereo photogrammetry	+	+	+	-	++
Photogrammetry	++	-	+	+	+++
3D laser scan	-	+	++	--	0

Next to photogrammetry, the other method going to be used is the counting of the displaced coloured stones. This gives extra information that cannot be extracted from the 3D profiles of the photogrammetry. This extra information is the knowledge from which strip the stones are picked up and at which location they end up.

The check of the measurement equipment for the photogrammetry method is done by a practice test set-up. It is tested if with a constant slope the output of two individual measurements is equal. The markers have to stay in the exact same place to make an equal output possible.

E.2 Process measurements

To describe the breaking process and to couple the stone displacements to this process it is necessary to record this with a camera. There are two possibilities for recording the breaking process. First, making a video of the waves and moving stones and secondly, making a video to track particles in the water for the velocity and acceleration. Both options are elaborated further in this paragraph and at the end it is concluded what method is used.

E.2.1 Camera

The recording of the wave breaking can be done with a camera. The camera can be placed behind a translucent window. A protection screen has to be made to protect the camera from influences of the waves next to the flume. The breaking waves and the transport of the stones have to be visible in the video. In this way, both processes can be linked together. It can amongst others be checked at which moment of the wave breaking the stones start to move.

E.2.2 Particle image velocimetry

The velocity and acceleration of the water near the bed can be measured with particle image velocimetry (PIV). The particles are traced by a camera. By comparing the frames taken by the camera the velocities and their directions can be determined. PIV is used by adding small particles into the water. It gives results for a small region of interest. This region of interest is smaller than that of the video method, because it needs to be focused on capturing the tracer particles in the images. PIV needs to be supported by powerful lights to light up the particles, so the processing program can detect them. A laser light is placed above the channel to create a vertical light-sheet orientated parallel to the channel centreline. The concentration of the particles should be large enough to have high resolution PIV images, but low enough so the light-sheet is not attenuated due to particle scattering. Processing of the PIV images can be done by PIVlab, according to Kramer (2016) and Wendt (2017). The accelerations are found by differentiating the velocities in time.

A PIV construction gets very complicated in the case of a large basin like the Pacific basin. The PIV-camera and the electricity have to stay sealed off from water to prevent damage or dangerous situations. The laser has to be close to the water inside the flume. For this a large construction has to be built to make this work. The flume around the laser needs to be completely sealed off from light with wood to prevent the laser light from being scattered around into the open. Even after reflection it is still harmful for someone's eyes. The tracer particles do have to be removed from the flume before the water flows out of the basin. This is almost impossible for a basin like the Pacific basin. Another disadvantage is that calibration of a PIV set-up is very time-consuming. Above information follows from Wout Bakker (personal communication, January 15, 2019).

E.2.3 Conclusion process measurements

There are two possibilities to map the processes around wave breaking and transport. The video method gives visual information about the breaking of the waves and the connection with the transport of the stones. The PIV method gives the same visual information as the video method only in a smaller region of interest. It also gives the velocities and accelerations in the water. The PIV method is very complicated to construct and calibrate in a flume like the Pacific basin. Due to this the video method is chosen for the process measurements. The used camera is an Olympus Tough TG-4. This camera is able to film in wet conditions and under water.

E.3 Wave gauges

Wave gauges are needed to measure the incoming wave height. Wave gauges measure the water surface elevation compared to the SWL. They do this by the electrical resistance in the wire. The change in the voltage output can be translated to a wave signal. The wave signal includes the wave height, length and period. Three wave gauges are placed in front of the slope. By placing three wave gauges the incoming wave height can be extracted from the wave signal, because the reflected wave height influences the wave signal.

For the distances in between the probes several recommendations and prohibitions are stated by Funke and Mansard (1980) shown inTable E.2. The distances may not be equal to halve the wavelength,

because this leads to indeterminate reflection calculations. The distances may not be a multiple of each other, because the reflection calculations can in that case not be solved for both the wave signals. The minimal distance in between the probes is 0.2 m. If the probes are too close the gauges electronically influence each other's signals (Terrile, 2004). The best ratio between the distances is 2:1 according to Wenneker and Hofland (2014).The distance between the first and second probe in the direction of the wave propagation is X_{12}. The distance between the second and third probe is X_{23}, see Figure E.1. The wave lengths differ widely, because the waves are irregular and wave steepnesses and heights vary too. Because of this, it is impossible to determine distances that comply with all the recommendations and prohibitions. The distances chosen are X_{12} = 0.6 m and X_{23} = 0.3. For the wavelength ranges these comply mostly with the recommendations and are outside the above described prohibitions.

Table E.2: The recommendations and prohibitions stated by Funke and Mansard (1980) for the determination of the distances.

Prohibited		Recommended	
$X_{12} = \frac{nL}{2}$	$X_{13} = mX_{12}$	$X_{12} = \frac{L}{10}$	$\frac{L}{6} < X_{13} < \frac{L}{3}$
	$X_{13} = \frac{L}{5}$	$X_{12,23} > 0.20$ m	
	$X_{13} = \frac{3L}{10}$	$X_{23} = \frac{1}{2}X_{12}$	

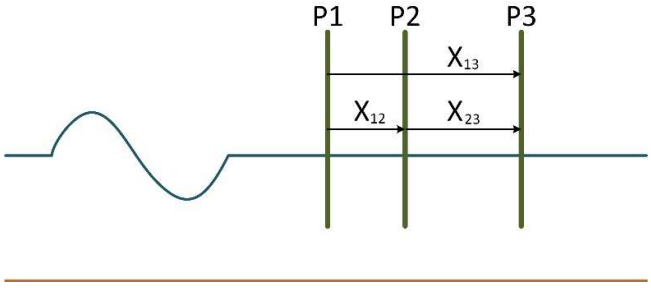

Figure E.1: Definitions of the distances in between the probes.

Appendix F: Plots of the profile changes per test

In this paragraph all the plots of the averaged profile changes in y-direction are shown. They are clustered together per test series and shown in Figure F.1 till F.7.

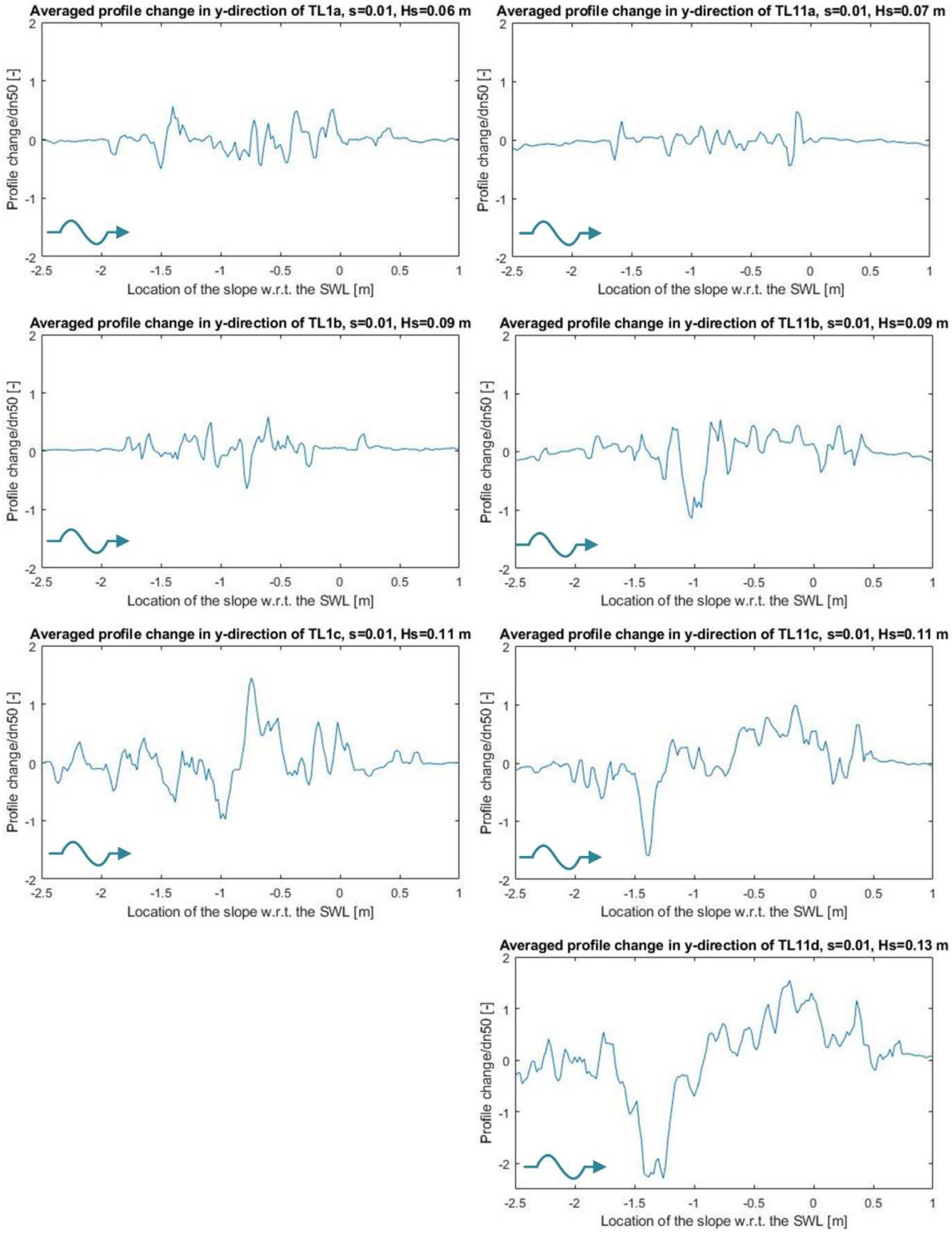

Figure F.1: The averaged profile changes in y-direction for test series TL1 and TL11.

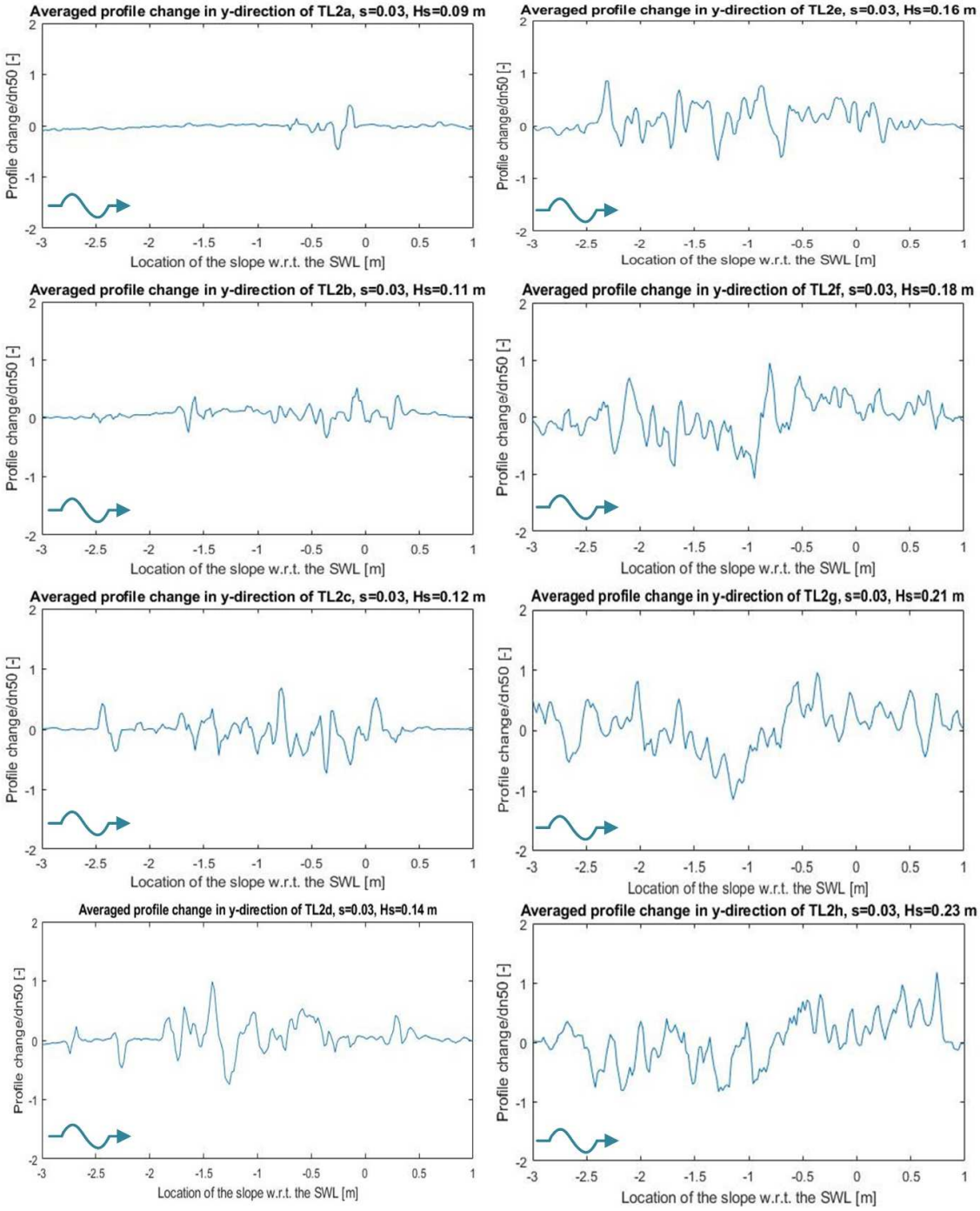

Figure F.2: The averaged profile changes in y-direction for test series TL2.

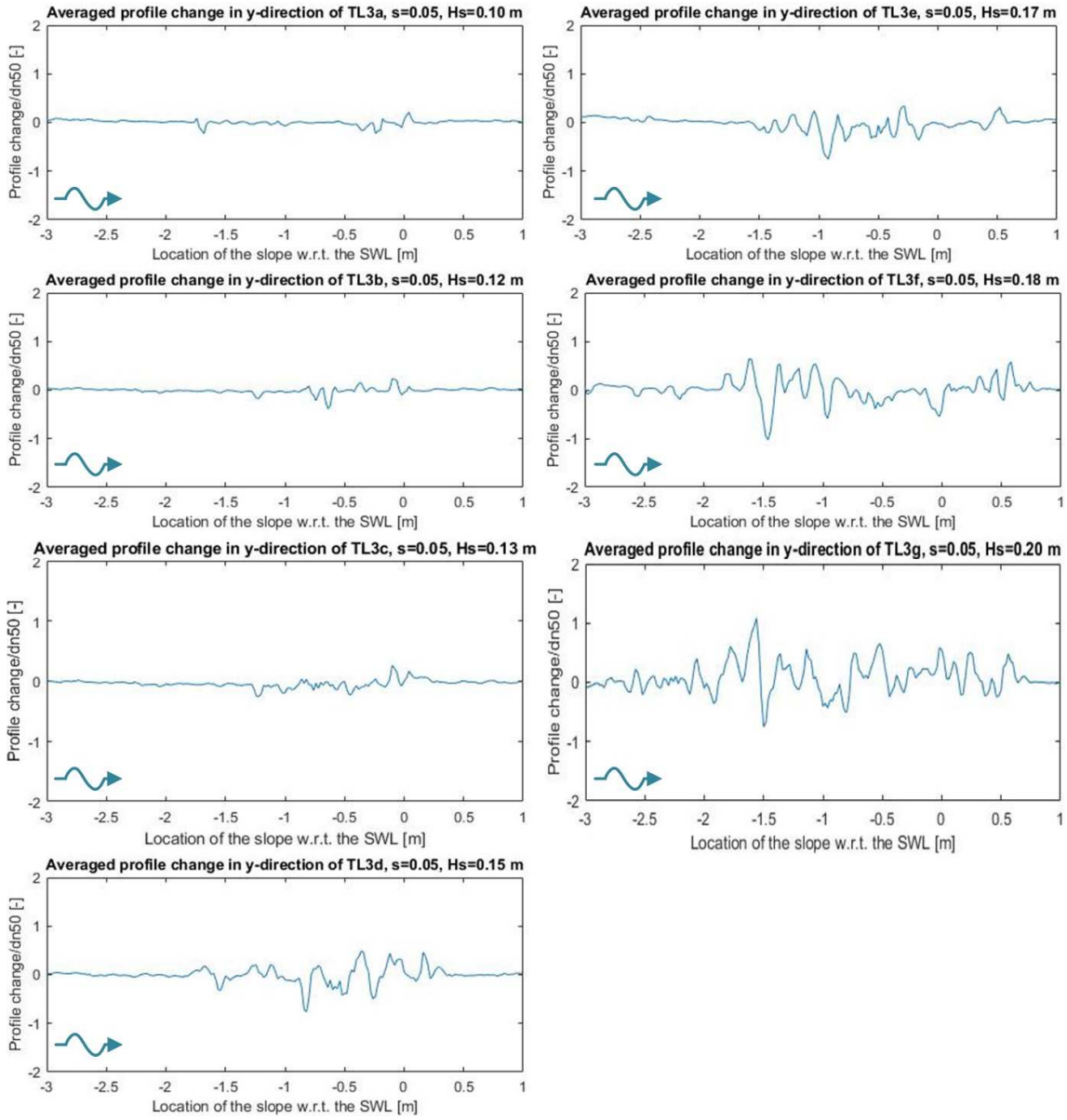

Figure F.3: The averaged profile changes in y-direction for test series TL3.

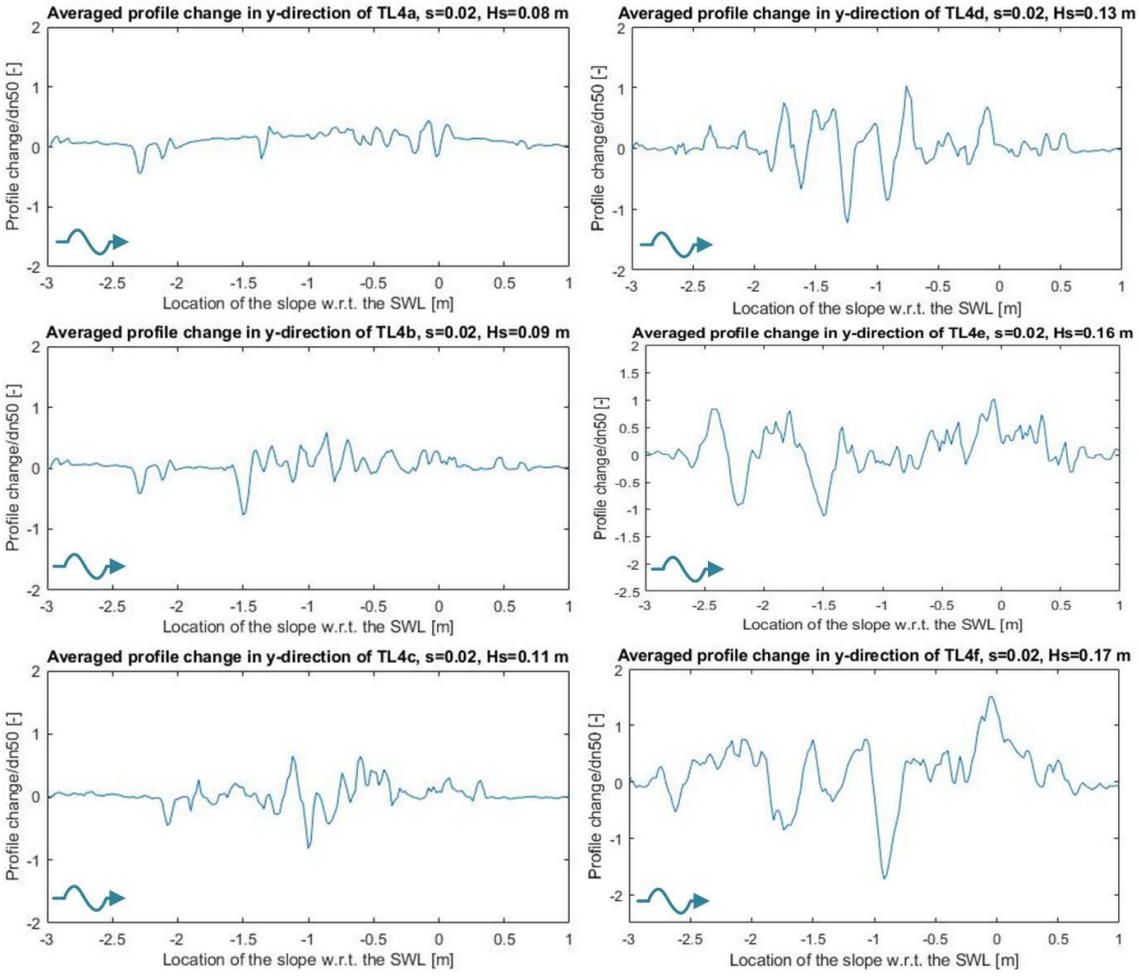

Figure F.4: The averaged profile changes in y-direction for test series TL4.

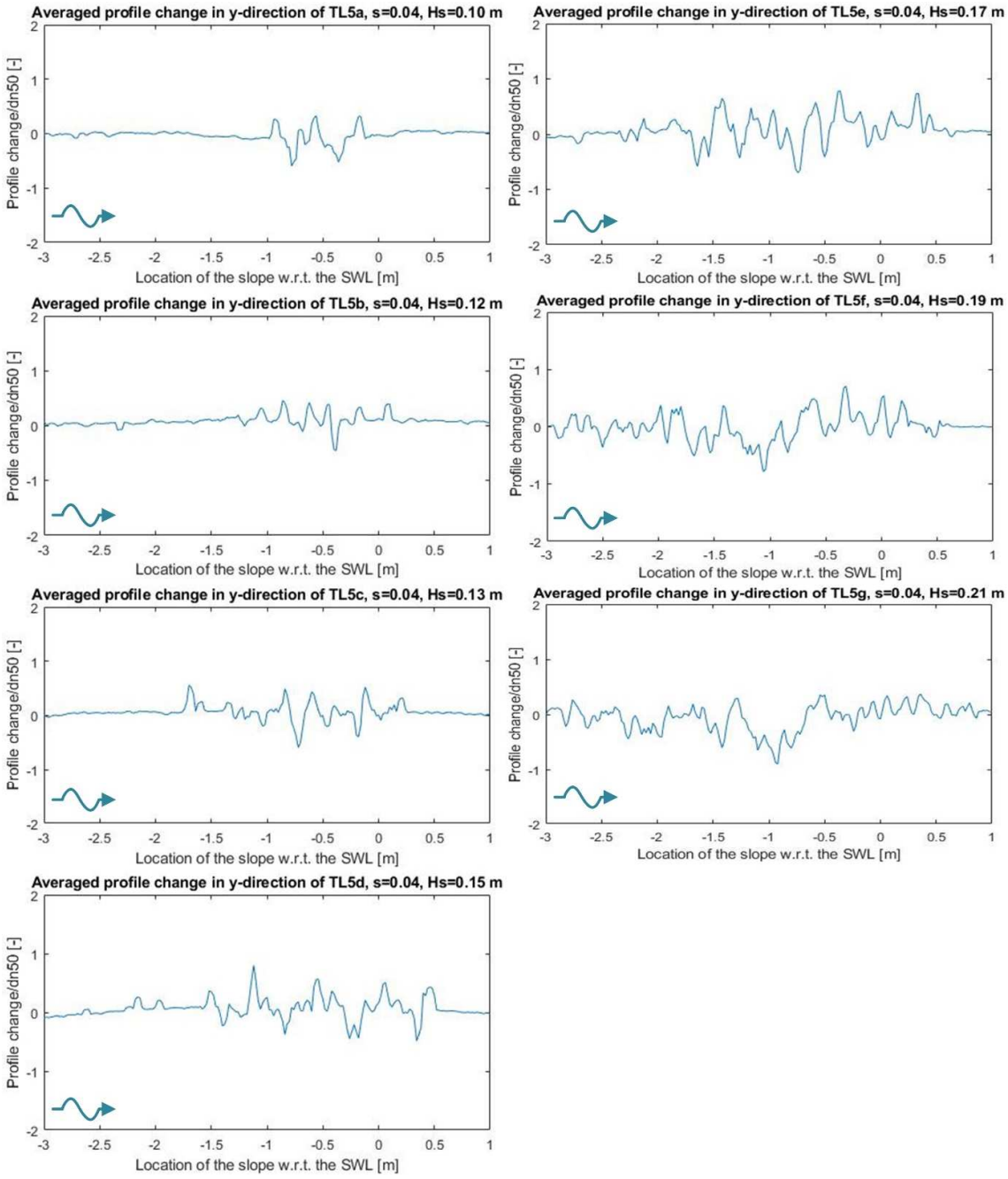

Figure F.5: The averaged profile changes in y-direction for test series TL5.

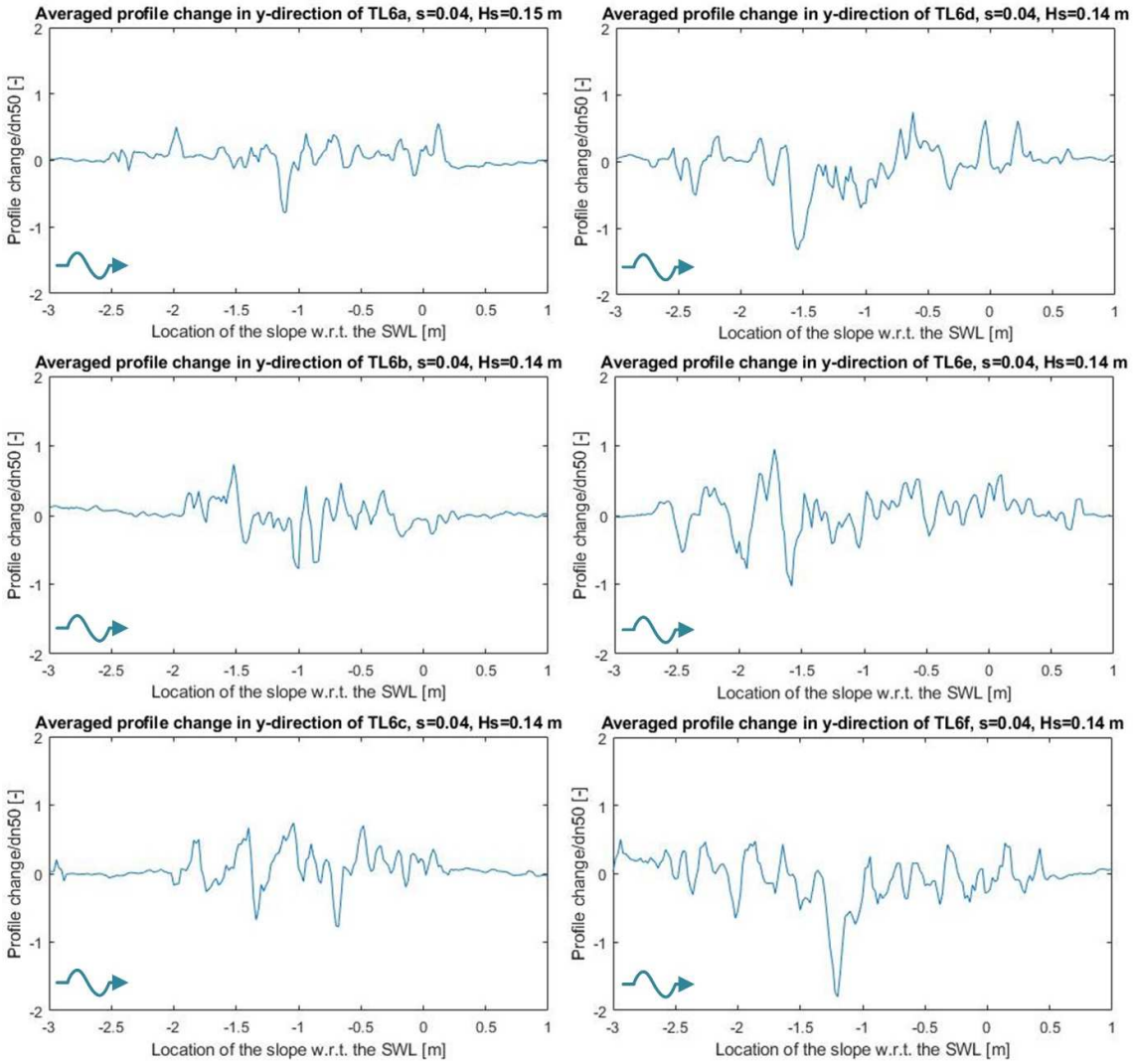

Figure F.6: The averaged profile changes in y-direction for test series TL6.

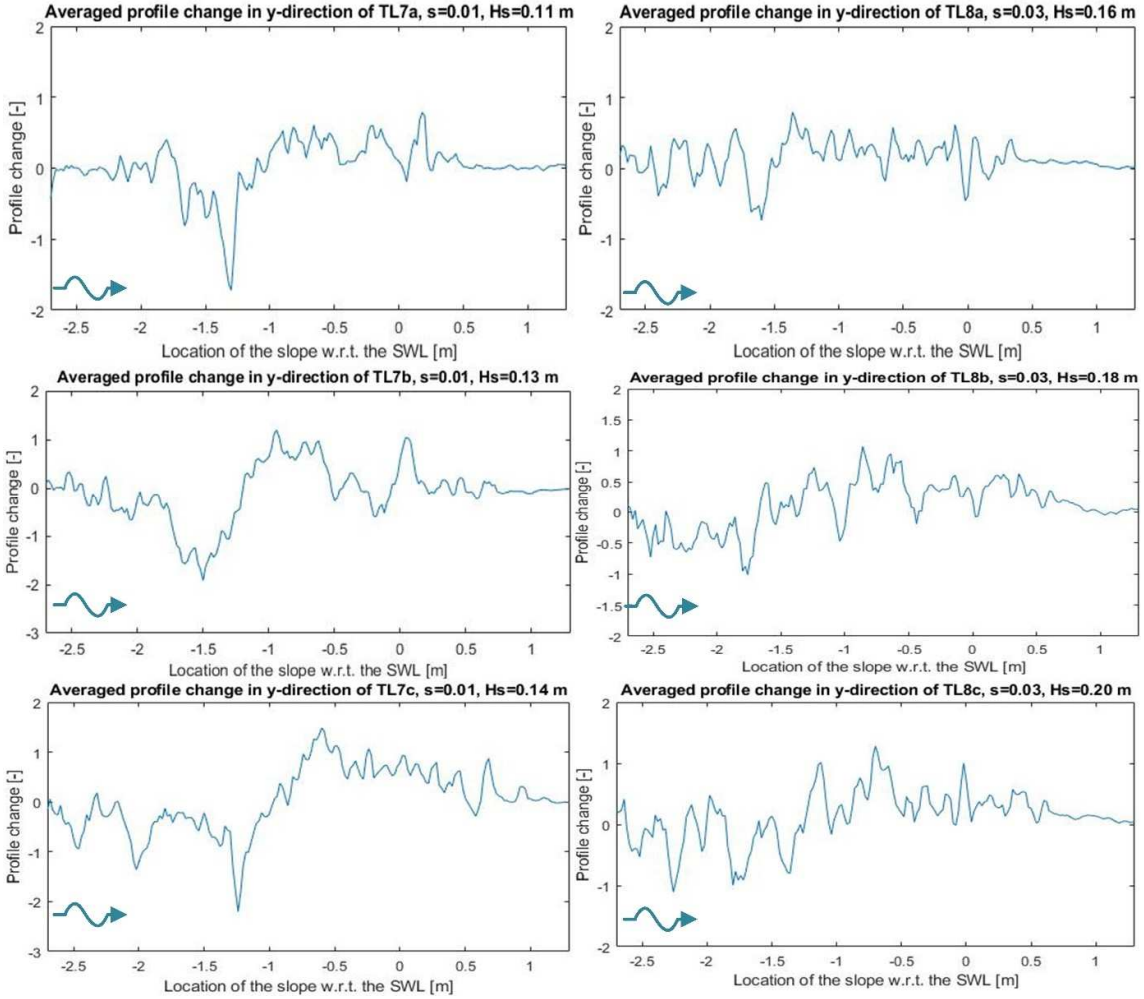

Figure F.7: The averaged profile changes in y-direction for test series TL7 and TL8.

Appendix G: Determine trendlines per given damage level

From the data gathered of the tests the stability curves have to be determined in which the stability number, $H_s/\Delta d_{n50}$, is plotted against the Iribarren number. First, for each wave steepness (for test series 1-5) are all the stability numbers calculated with the wave height (from the output), the notional permeability and the stone diameter. These stability parameters are plotted against the damage parameters that belong to the same test (in this appendix is the damage level used as example). Per test series is a trendline interpolated between the data points, see Figure G.1. With the trendlines can for the wanted damage level values (like S = 2 or S = 17) the stability number be determined. These stability numbers can be plotted against the Iribarren number used in the corresponding test series. Through these data points can also a trendline be fitted. This trendline is the stability curve which can be used for the design of mild slopes for the specific conditions of these tests. The stability curves are shown in Figure G.1.

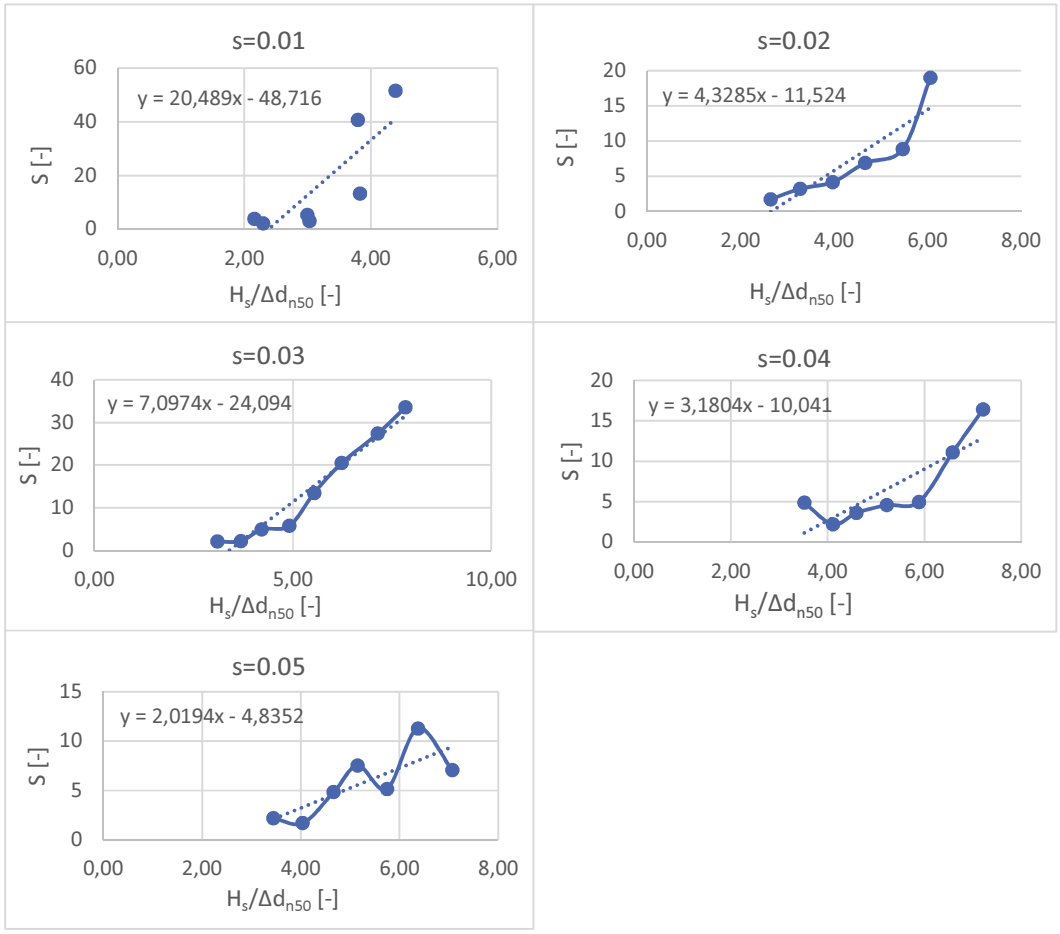

Figure G.1: The graphs for the test series 1-5 where the calculated stability curve is plotted against the damage level per test. For each test series is the trendline plotted. This trendline gives the relation between the damage level and the stability number.

Appendix H: Stability curve

The stability curve made in Appendix G is displayed here in Figure H.1 with the profile changes and overlay photos to show how start of damage, intermediate damage and failure look like.

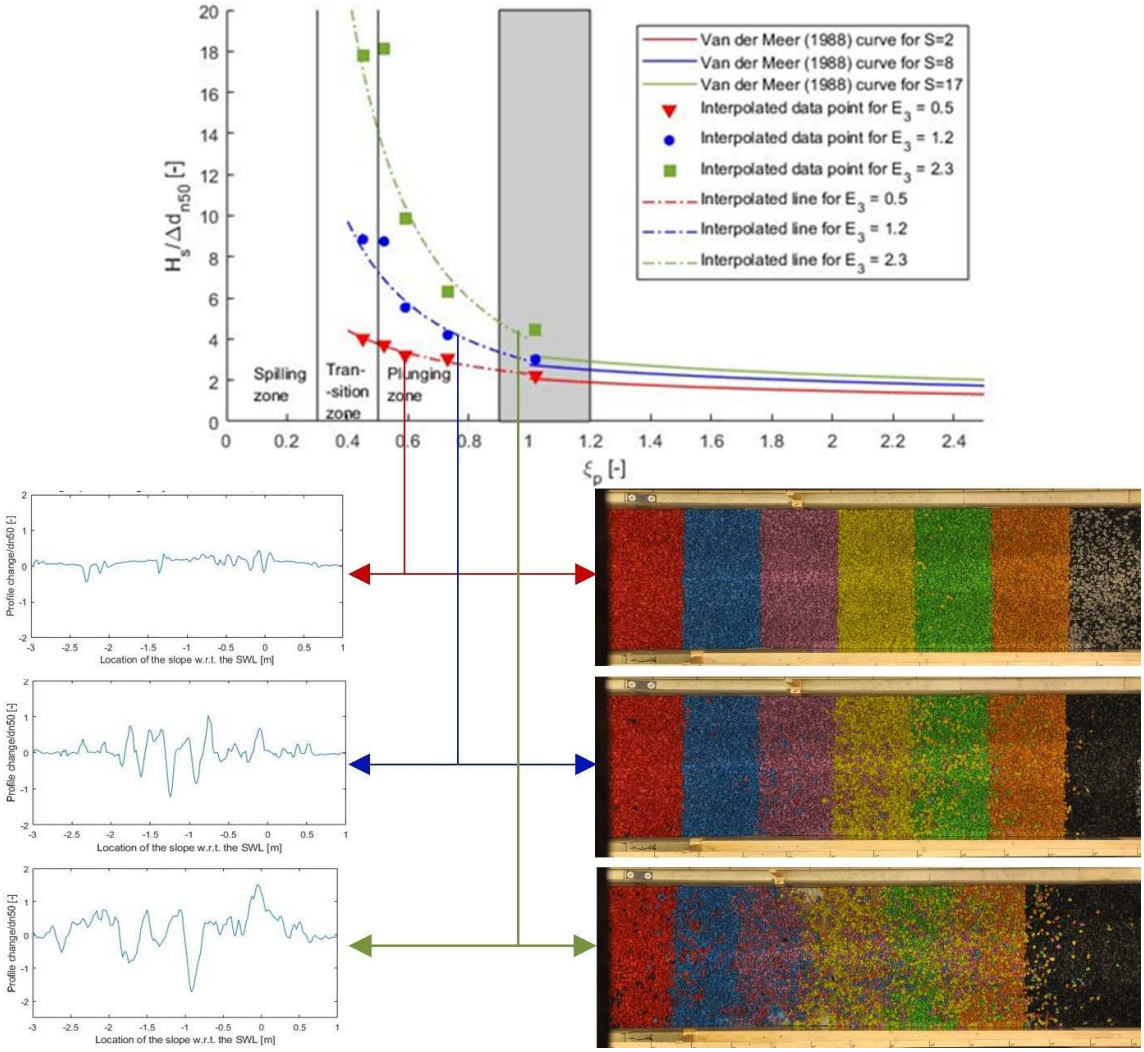

Figure H.1: The stability curve together with the profile changes and overlay photos to show how start of damage, intermediate damage and failure look like.

Appendix I: Determine stability curve with E_3

The stability curves were tested for their agreement per Iribarren number for the damage depth (in Figure I.1) and the stability number (in Figure I.2). In Figure I.3 is the new stability curve displayed for the damage depth against the data points of the physical tests.

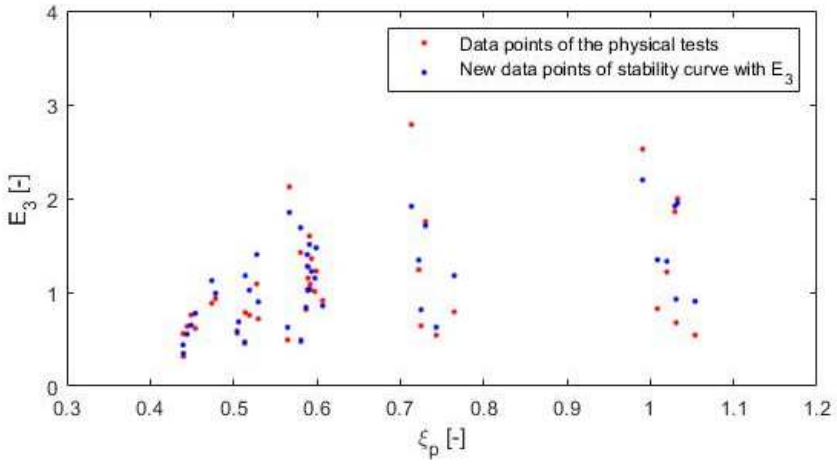

Figure I.1: The new stability curve compared to the data points of the physical tests per Iribarren number for the damage depth.

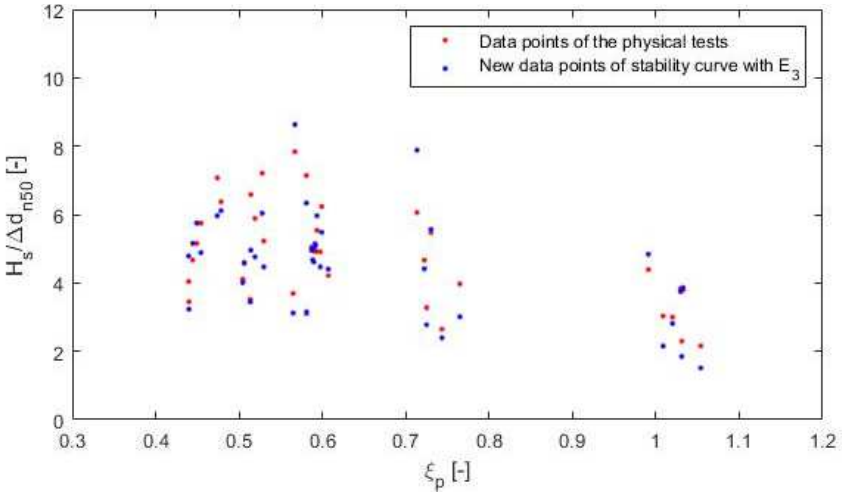

Figure I.2: The new stability curve compared to the data points of the physical tests per Iribarren number for the stability number.

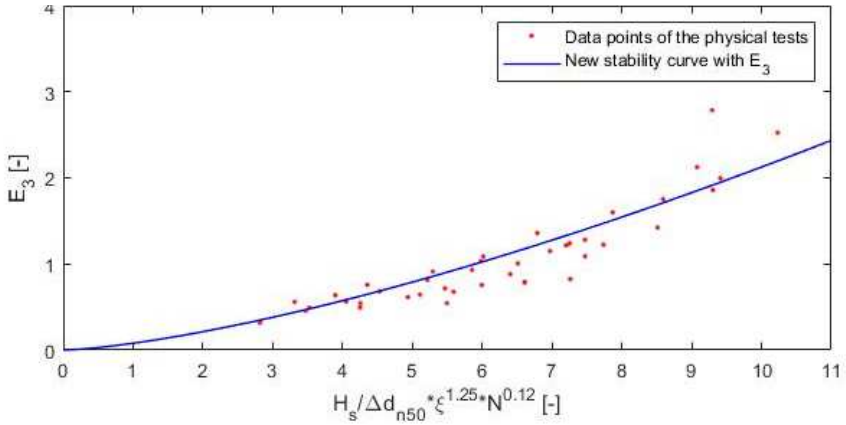

Figure I.3: The new stability curve compared to the data points of the physical tests.

Appendix J: Stone counting results

In Table J.1 are the results shown of the counting of the coloured stones. A difference is made between the upward and downward transport. The column names, like RY, give the strip colour the stone is taken from by the first letter (R from red) and where the stone ended up by the second letter (Y from yellow), see Figure J.1.

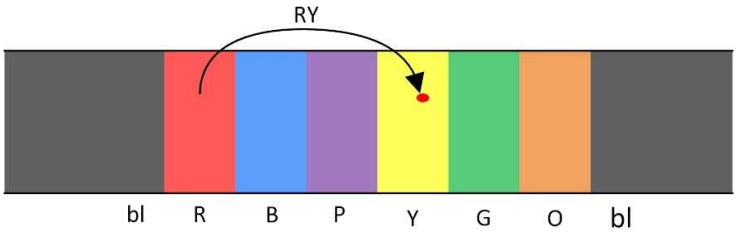

Figure J.1: Here is explained how the abbreviations of the transport paths are called.

Table J.1: The results of the counting of the stones with the upslope and downslope transport separated.

Upward moving stones/strip																										
Test	blR	blB	blP	blY	blG	blO	RB	RP	RY	RG	RO	Rbl	BP	BY	BG	BO	Bbl	PY	PG	PO	Pbl	YG	YO	Ybl	GO	Gbl	Obl
1.2a																		6				29			9		
1.2b							2						7					205	7	1		173	6	1	22		5
1.2c	6						18	5					173	29	7	2		612	167	39		320	47	2	39	1	14
2a							1						3					3							3		
2b	3						2						11					13				1			7		
2c	21	1					55	5					31	3	1			20	4	3		20			11	1	1
2d	45	7	2				69	21	5		1		64	11	5	1		28	7	5		24	4		16	2	3
2e	111	37	14				95	40	14	2	3		92	23	8	5	2	37	16	7	1	37	6	2	19	5	13
2f	189	93	35	14	4	4	138	63	29	10	5	3	84	35	19	9	4	41	22	13	5	37	13	9	23	14	22
3a																						1			1		
3b																						2			5		
3c																						7	1		9		
3d													2					2				19	2		20		
3e													2					8	1			43	3	1	35		6
4a																		3				25			5		
4b							1											15				45			15		
4c	1						5						15					80	4			132	6	1	31		3
4d	6						17	1	1				51	1	1			251	137	3		238	30	4	39	1	13
5a																						3			1		
5b																						22			2		
5c													1									35	1		13		
5d													3					16				73	5		34		3
6a							11						8					52		1		39	1		16		9
6b							11						19					76	4	1		71	5		44		7
6c							13						26	2				137	14	1		102	21		82		8
6d							15						44	9	1			215	26	2	1	169	37	2	105		13
6e							31						57	7	3	4		284	72	11	1	229	67	5	125	1	12
7a	5	1					74	14	4				374	71	8			195	39	6		132	3		30		
8a	5						35	2					104	7	3			120	13	2		48			34		
8b	17	2					85	14	1	2			250	30	11	2		196	48	11	1	91	19		51	1	

Downward moving stones/strip						
Test	Rbl	BR	PB	YP	GY	OG
1.2a				2		
1.2b			1	27	10	
1.2c		2	52	51	4	
2a						
2b						
2c		13		2		
2d	11	19	3			
2e	70	37	6	3	1	
2f	131	65	12	4		
3a						
3b					1	
3c			1	1	1	
3d			2	3	2	
3e			5	4	1	1
4a						
4b					2	
4c		2	3	12	7	
4d		2	21	41	10	
5a						
5b					1	
5c				4	6	
5d		4	2	11	4	
6a			2	10	1	
6b		3	23	16	2	
6c		3	22	11	3	
6d		3	27	21	4	
6e		15	31	32	5	
7a		3	4	2		
8a		9	6	2		
8b		35	9	2		

In Table J.1 is the transport of the stones given per strip in the erosion or deposition of the stones and the total transport. The results of Table J.1 are used to determine the total erosion and deposition per strip. These added up give the total transport of the stones.

he graphs where the stone transport is plotted per single test are given below. In Figure J.2 is shown the transport of the stones that are removed per strip and where these stones have ended up. The total transportation graphs for each countable test are given in Figure J.3.

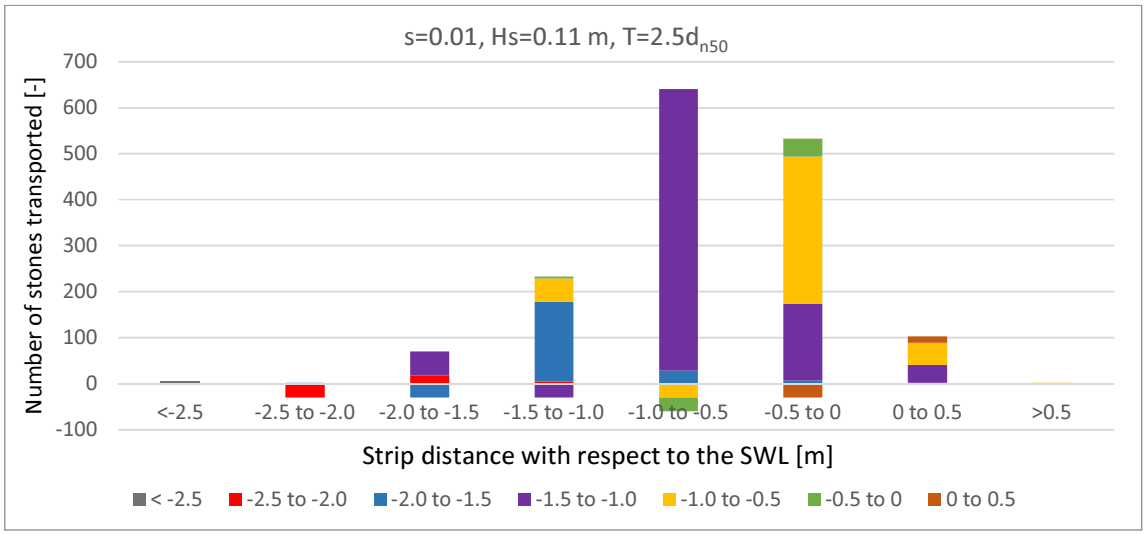

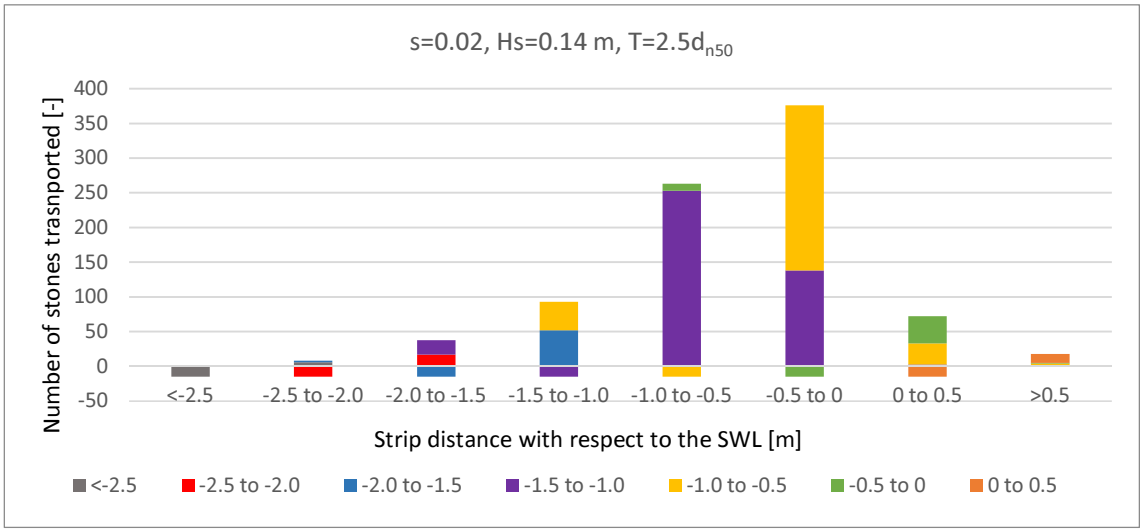

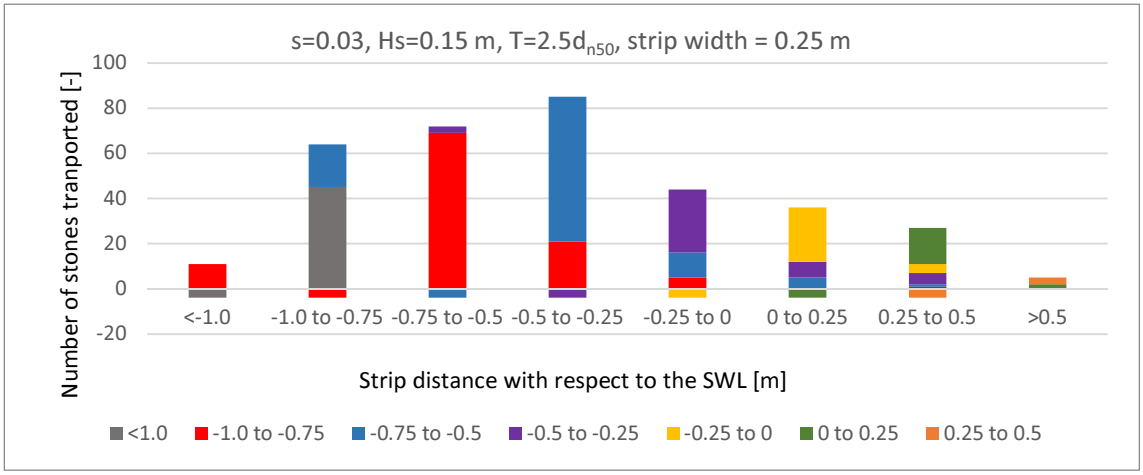

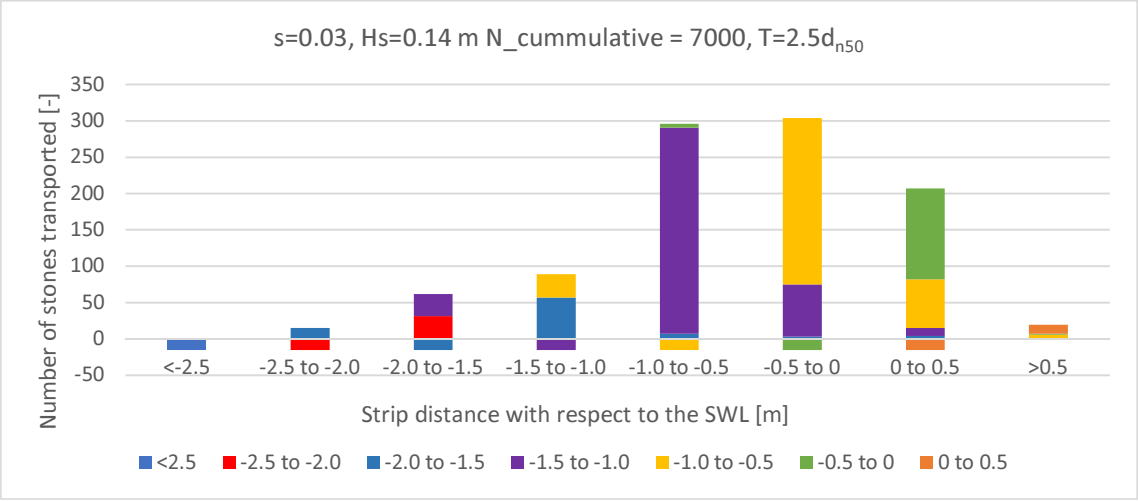

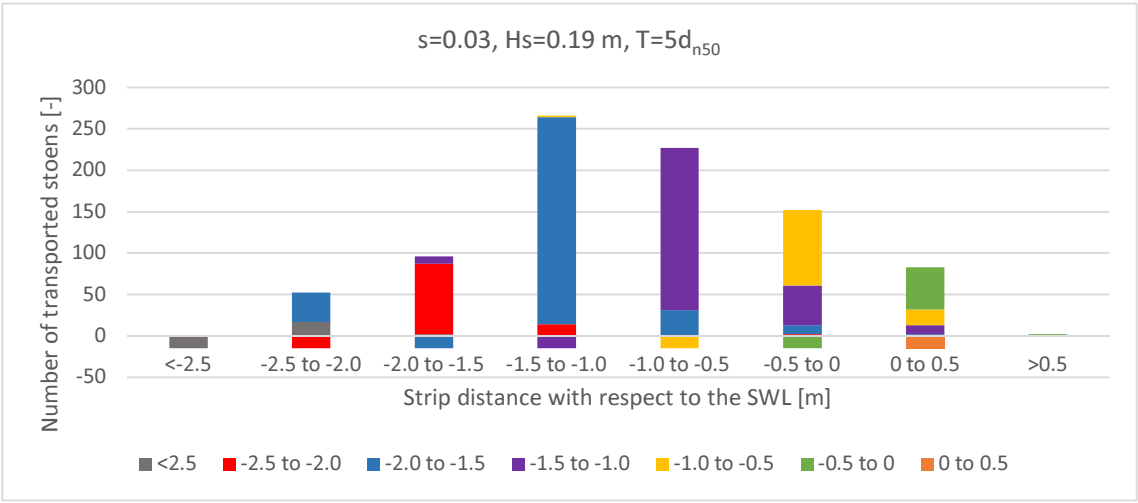

Figure J.2: The transportations of the stones inside the strips are shown in the graphs above. On the x-axis are given the locations of the strips with the colour of this strip displayed as a block in the negative part under the x-axis. The histograms are filled with different colours. Each colour belongs to the strip from which the stones are transported.

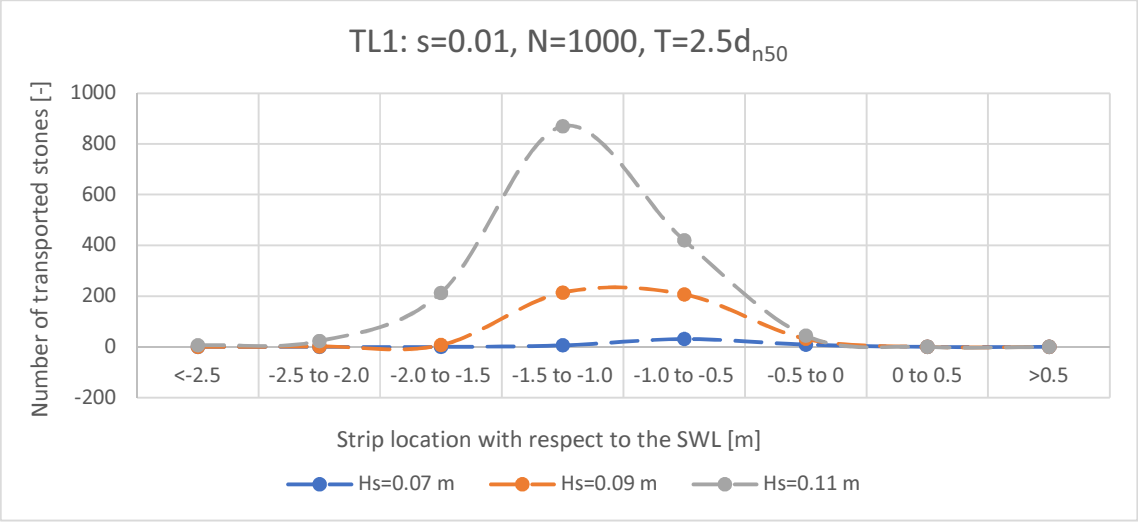

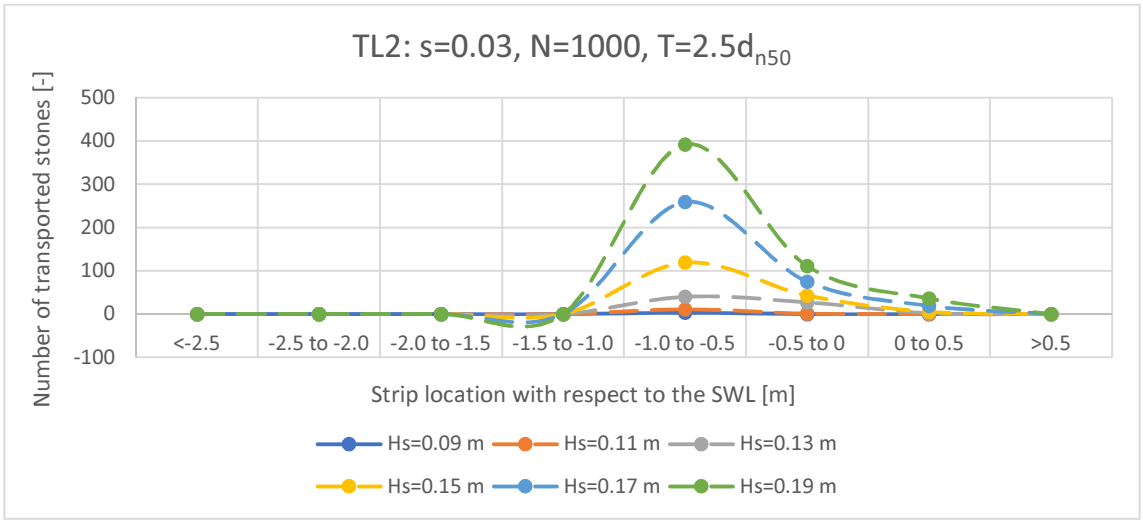
TL2: s=0.03, N=1000, T=2.5d$_{n50}$
Number of transported stones [-]
500
400
300
200
100
0
-100
<-2.5
-2.5 to -2.0
-2.0 to -1.5
-1.5 to -1.0
-1.0 to -0.5
-0.5 to 0
0 to 0.5
>0.5
Strip location with respect to the SWL [m]
Hs=0.09 m
Hs=0.11 m
Hs=0.13 m
Hs=0.15 m
Hs=0.17 m
Hs=0.19 m

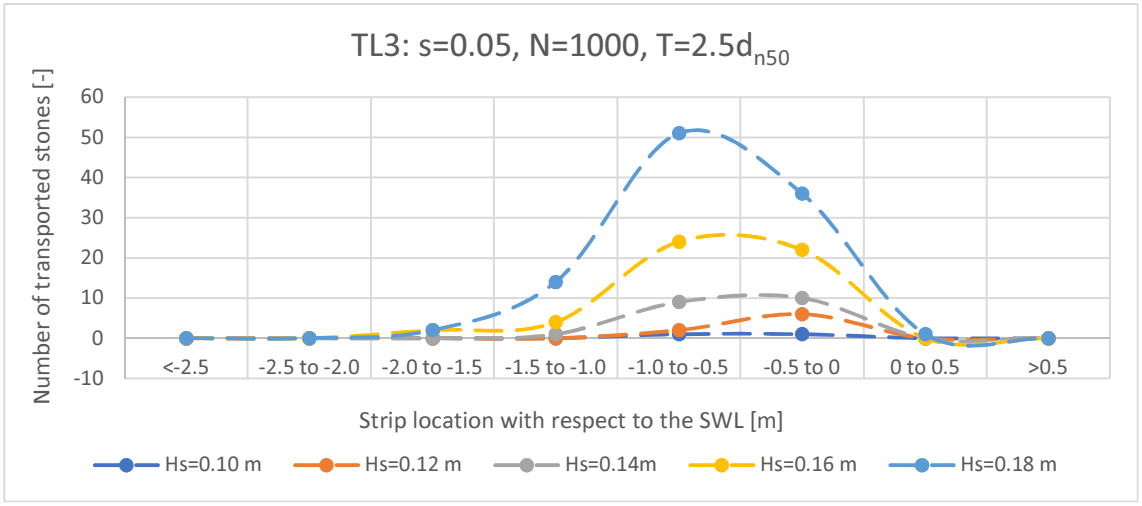
TL3: s=0.05, N=1000, T=2.5d$_{n50}$
Number of transported stones [-]
60
50
40
30
20
10
0
-10
<-2.5
-2.5 to -2.0
-2.0 to -1.5
-1.5 to -1.0
-1.0 to -0.5
-0.5 to 0
0 to 0.5
>0.5
Strip location with respect to the SWL [m]
Hs=0.10 m
Hs=0.12 m
Hs=0.14m
Hs=0.16 m
Hs=0.18 m

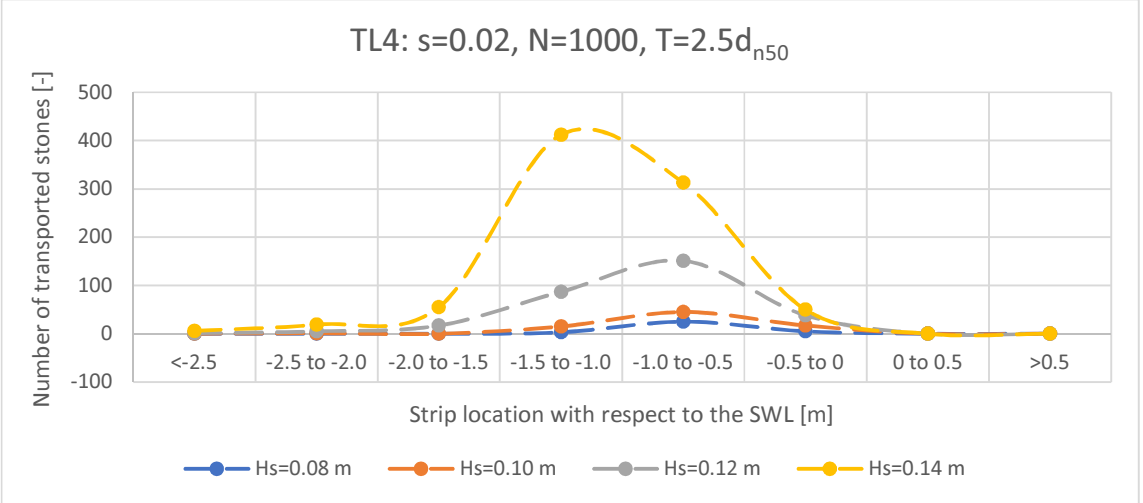
TL4: s=0.02, N=1000, T=2.5d$_{n50}$
Number of transported stones [-]
500
400
300
200
100
0
-100
<-2.5
-2.5 to -2.0
-2.0 to -1.5
-1.5 to -1.0
-1.0 to -0.5
-0.5 to 0
0 to 0.5
>0.5
Strip location with respect to the SWL [m]
Hs=0.08 m
Hs=0.10 m
Hs=0.12 m
Hs=0.14 m

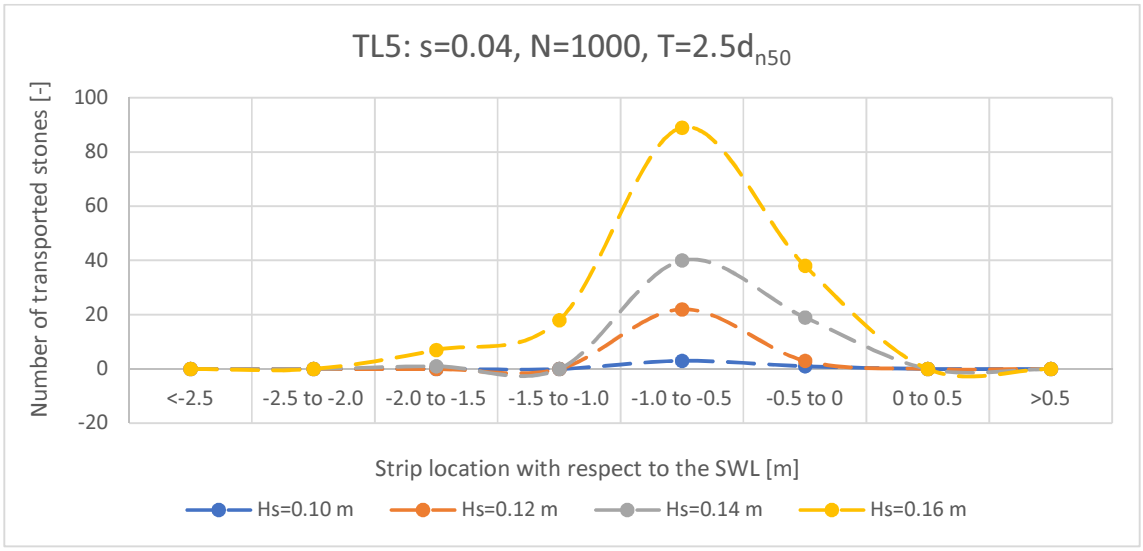
TL5: s=0.04, N=1000, T=2.5dn50
Number of transported stones [-]
100
80
60
40
20
0
-20
<-2.5
-2.5 to -2.0
-2.0 to -1.5
-1.5 to -1.0
-1.0 to -0.5
-0.5 to 0
0 to 0.5
>0.5
Strip location with respect to the SWL [m]
Hs=0.10 m
Hs=0.12 m
Hs=0.14 m
Hs=0.16 m

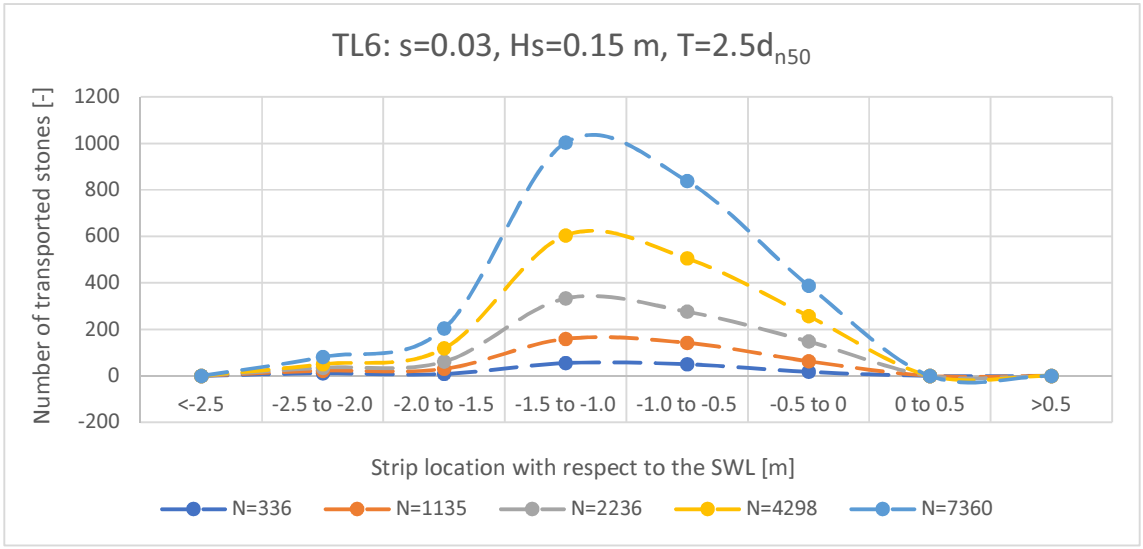
TL6: s=0.03, Hs=0.15 m, T=2.5dn50
Number of transported stones [-]
1200
1000
800
600
400
200
0
-200
<-2.5
-2.5 to -2.0
-2.0 to -1.5
-1.5 to -1.0
-1.0 to -0.5
-0.5 to 0
0 to 0.5
>0.5
Strip location with respect to the SWL [m]
N=336
N=1135
N=2236
N=4298
N=7360

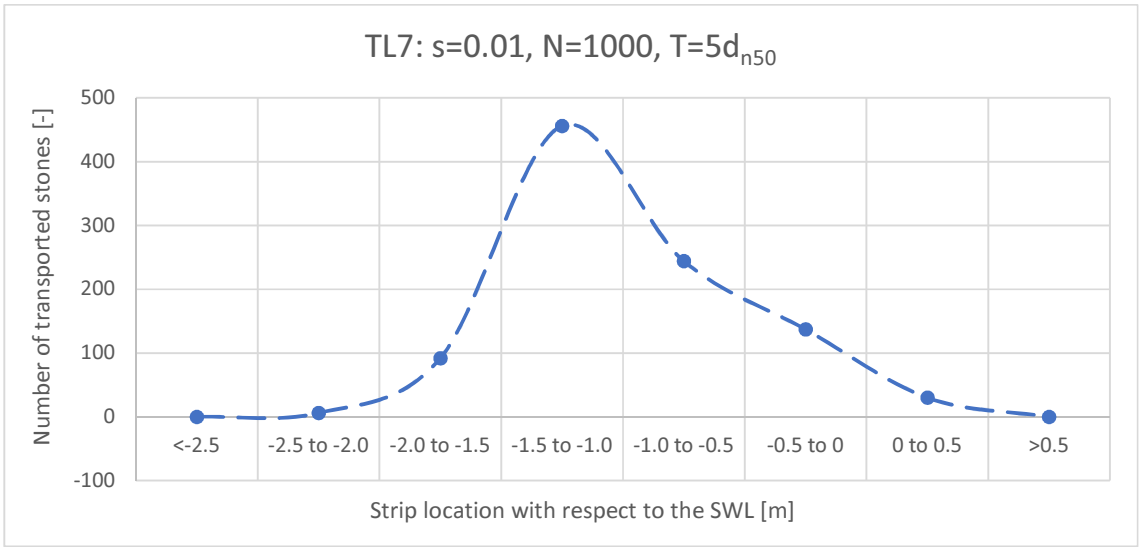
TL7: s=0.01, N=1000, T=5dn50
Number of transported stones [-]
500
400
300
200
100
0
-100
<-2.5
-2.5 to -2.0
-2.0 to -1.5
-1.5 to -1.0
-1.0 to -0.5
-0.5 to 0
0 to 0.5
>0.5
Strip location with respect to the SWL [m]

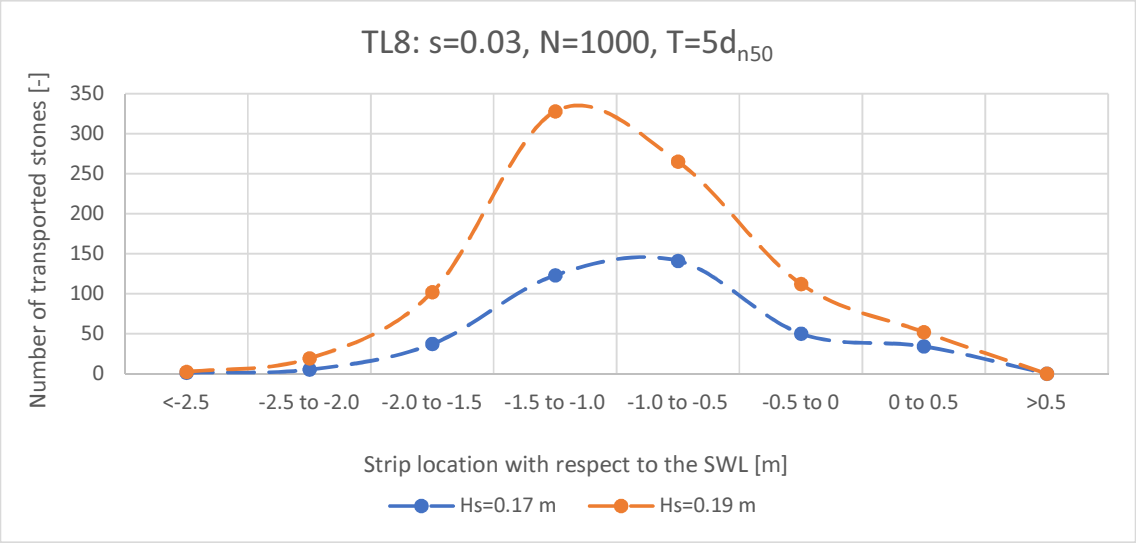

Figure J.3: The above graphs show the total transport of all the tests that were countable. If the damage become too much the stones where so mixed and up/under each other that counting became impossible.

Appendix K: Damage zone locations

In this appendix the damage zone locations are presented. The damage zones are obtained by giving the total area in which damage occurs, the area of the maximum damage area and the location of the maximum erosion for every test. The damage depths are also given. These results are given in Table K.1. The results are given by the boundaries between which the total or maximum damages are present or by the location where the maximum damage occurred. In Figure 5.33 is shown how the boundaries and locations are determined. The total damage area is set to the total area where damage occurred. The boundaries are set to the most down- or upslope location where the erosion profile goes from erosion back to the zero line. The maximum damage area is determined in the same way for the erosion hole with the maximum erosion. The location of the maximum damage is set to the location of the maximum erosion.

Table K.1: The damage zone boundaries/locations for the total and maximum damage together with the damage depth value per test.

	Total damage area		Max damage area		Maximum damage	
Test	Downslope boundary [m]	Upslope boundary [m]	Downslope boundary [m]	Upslope boundary [m]	Location [m]	E_3 [-]
1a	-0.20	-0.02	-	-	0.07	0.54
1b	-0.16	-0.03	-0.08	-0.08	-0.08	0.82
1c	-0.24	0.03	-0.12	-0.09	-0.10	2.00
11a	-0.17	-0.02	-0.03	-0.02	-0.02	0.68
11b	-0.18	0.03	-0.12	-0.09	-0.11	1.22
11c	-0.21	0.03	-0.17	-0.13	-0.14	1.86
11d	-0.25	-0.09	-0.17	-0.09	-0.13	2.52
2a	-0.03	-0.02	-0.03	-0.02	-0.03	0.49
2b	-0.17	0.02	-0.04	-0.03	-0.05	0.49
2c	-0.24	0.03	-0.05	-0.04	-0.04	0.91
2d	-0.24	-0.07	-0.14	-0.13	-0.14	1.09
2e	-0.23	0.02	-0.14	-0.13	-0.13	1.36
2f	-0.30	-0.06	-0.15	-0.09	-0.10	1.22
2g	-0.27	0.07	-0.16	-0.09	-0.12	1.42
2h	-0.25	-0.08	-0.14	-0.12	-0.13	2.12
3a	-0.17	-0.02	-0.17	-0.16	-0.18	0.32
3b	-0.08	-0.06	-0.08	-0.06	-0.07	0.56
3c	-0.13	-0.05	-0.13	-0.12	-0.13	0.64
3d	-0.16	-0.02	-0.09	-0.08	-0.08	0.76
3e	-0.16	-0.02	-0.11	-0.09	-0.09	0.62
3f	-0.17	0.01	-0.17	-0.14	-0.15	0.93
3g	-0.20	0.05	-0.16	-0.14	-0.15	0.88
4a	-0.24	0.00	-0.24	-0.23	-0.24	0.54
4b	-0.24	-0.02	-0.16	-0.15	-0.15	0.64
4c	-0.22	-0.08	-0.11	-0.10	-0.11	0.79
4d	-0.18	-0.02	-0.13	-0.12	-0.13	1.24
4e	-0.23	-0.07	-0.17	-0.13	-0.15	1.75
4f	-0.26	-0.08	-0.11	-0.07	-0.09	2.79

	Total damage area		Max damage area		Maximum damage	
Test	Downslope boundary [m]	Upslope boundary [m]	Downslope boundary [m]	Upslope boundary [m]	Location [m]	E_3 [-]
5a	-0.10	-0.04	-0.10	-0.08	-0.08	0.46
5b	-0.09	-0.04	-0.05	-0.04	-0.05	0.56
5c	-0.13	-0.02	-0.08	-0.06	-0.07	0.68
5d	-0.15	0.04	-0.04	-0.02	-0.03	0.72
5e	-0.17	0.02	-0.09	-0.07	-0.07	0.76
5f	-0.25	-0.05	-0.13	-0.09	-0.11	0.78
5g	-0.28	-0.03	-0.13	-0.07	-0.09	1.09
6a	-0.12	0.00	-0.12	-0.10	-0.11	0.82
6b	-0.15	0.01	-0.13	-0.10	-0.11	1.03
6c	-0.20	-0.02	-0.08	-0.07	-0.07	1.01
6d	-0.26	-0.03	-0.17	-0.13	-0.16	1.15
6e	-0.26	-0.06	-0.17	-0.14	-0.16	1.28
6f	-0.26	-0.03	-0.14	-0.10	-0.12	1.60
7a	-0.24	-0.01	-0.18	-0.12	-0.13	1.64
7b	-0.24	-0.01	-0.22	-0.12	-0.15	2.36
7c	-0.27	-0.10	-0.17	-0.10	-0.13	2.09
8a	-0.25	0.02	-0.19	-0.15	-0.16	0.91
8b	-0.27	0.00	-0.19	-0.18	-0.18	1.81
8c	-0.26	-0.12	-0.24	-0.21	-0.23	1.84

In the graphs displayed below are the boxplots given per level of the damage depth. The boxplots are made for the down- and upslope boundary for the damage area, for the down- and upslope boundary for the maximum damage area and for the location of the maximum damage. Before the boxplots are made the boundary/location units are transferred from meters to H_s. This is done by per test dividing the number of meters by the wave height used in that test. The wave heights per test are given in Appendix B.

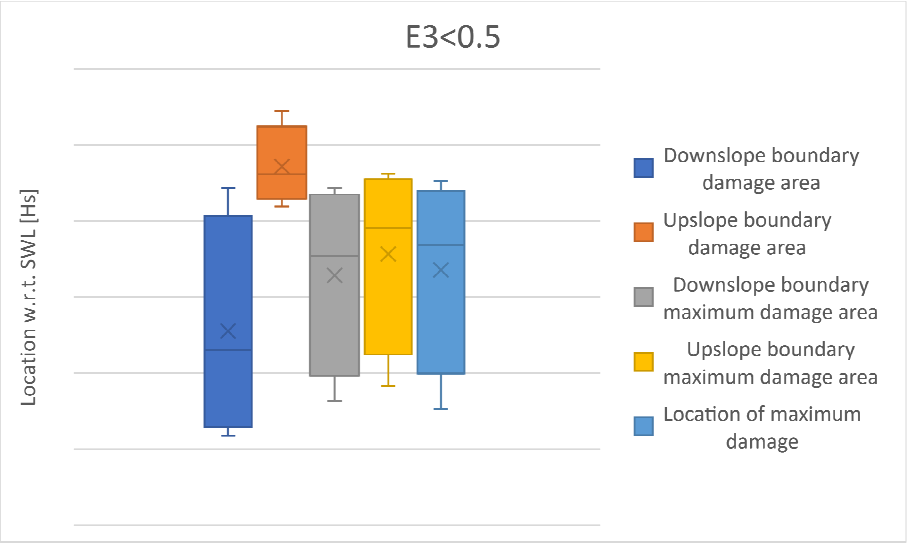

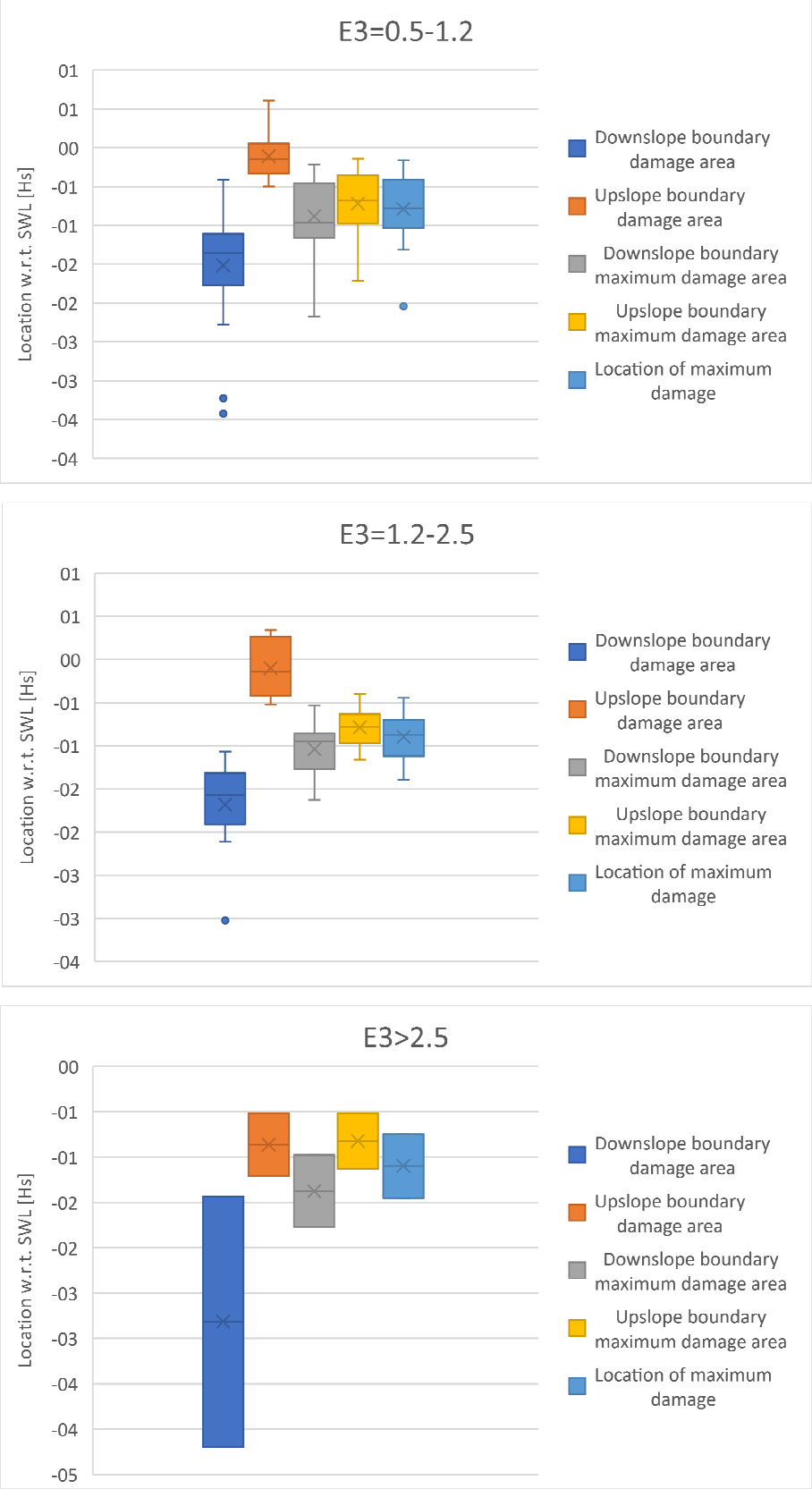

Figure K.1: The boxplots of the damage boundaries/locations for the total and maximum damage. They are divided per value of the damage depth.

In the two graphs below are the boxplots given of all the boundaries/locations per layer thickness. The boxplots are made for the down- and upslope boundary for the damage area, for the down- and upslope boundary for the maximum damage area and for the location of the maximum damage.

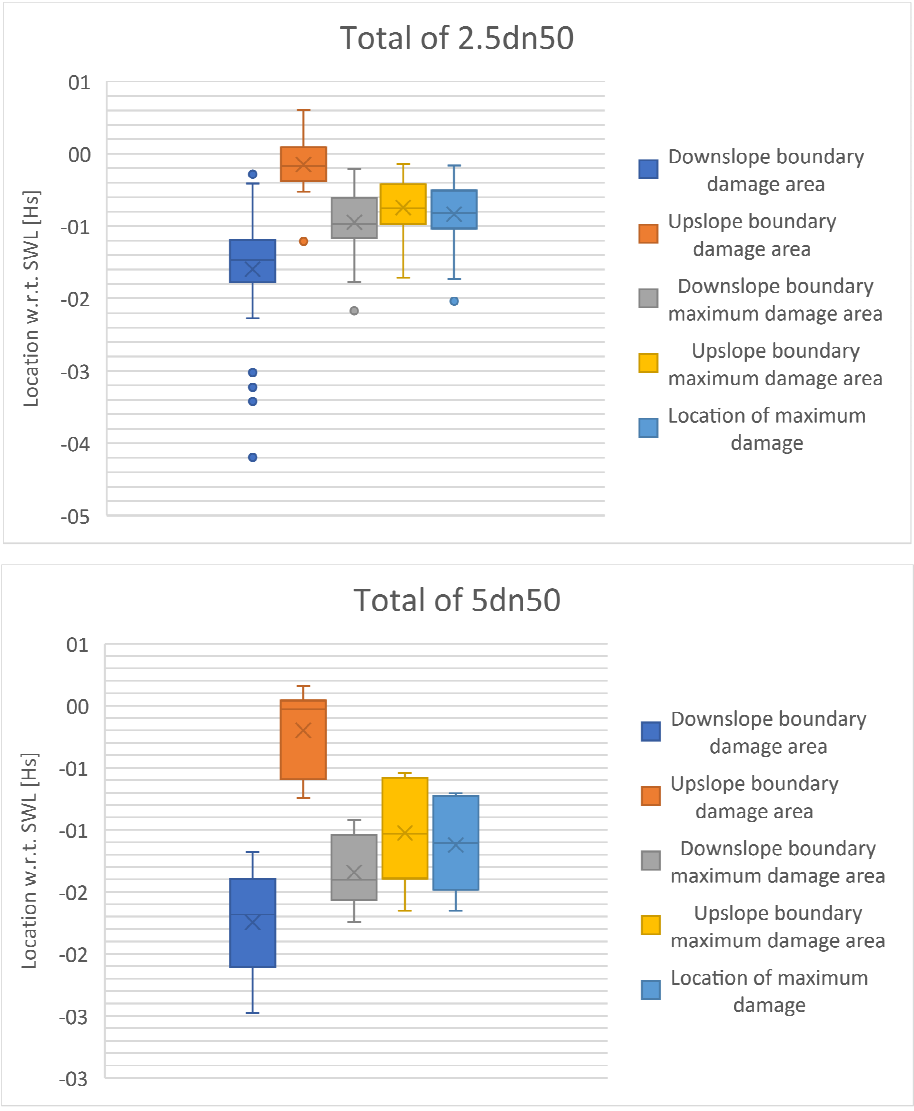

Figure K.2: The boxplots of the damage boundaries/locations for the total and maximum damage. They are divided per height of the layer thickness.